The Dissertation Committee for Sai Sriharsha Manoj Varma Konda certifies that this is the approved version of the following dissertation:

Theory and Computational Studies of Mechanochemical Phenomena

Committee:

Dmitrii E. Makarov, Supervisor

Christopher W. Bielawski

Peter J. Rossky

Issac C. Sanchez

Graeme Henkelman

Theory and Computational Studies of Mechanochemical Phenomena

by

Sai Sriharsha Manoj Varma Konda, B.S.; M.S.; M.S.

Dissertation

Presented to the Faculty of the Graduate School of

The University of Texas at Austin

in Partial Fulfillment

of the Requirements

for the Degree of

Doctor of Philosophy

The University of Texas at Austin

May 2014

To my grandfather

Acknowledgements

First and foremost, I would like to thank my supervisor, Dr. Dmitrii Makarov for his support, patience, enthusiasm and remarkable scientific intuition. It has been a great learning experience and I could not have asked for a better mentor when it came to developing as a scientific professional. I am also grateful to Dr. Christopher Bielawski for his collaboration and support, without whom, this work would have not been possible. I would like to thank Dr. Peter Rossky, Dr. Isaac Sanchez and Dr. Graeme Henkelman for agreeing to be on the thesis committee. I also would like to specially thank my former supervisor, Dr. Scott Kirkby, for his guidance, advice and help in the initial stages of my graduate studies at ETSU.

I have been really fortunate to work and share the graduate school experience with many close friends. I would like to thank Penny Kile, Brooke Graham, Betsy Hamblen and Rachel Walker at the Graduate Office for their continuous support and for putting up with my endless queries and questions. My sincere thanks to John Brantley, for having introduced me to the topic of mechanochemistry and without whose collaboration this work would not be complete. I have been very lucky to have officemates in Dr. Alex Hawk and Dr. Ryan Cheng for the majority of my stay at UT-Austin. I will always cherish the wonderful memories, whether it was discussing science or playing numerous tennis and “office ping-pong” matches. Similarly, thanks to Dr. Stas Avdoshenko, Dr. Atanu Das and Rachel Craigmile, current Makarov group members, for

being such great friends and keeping the workplace ever lively. Finally, to all the wonderful friends (too numerous to name everyone) at Austin, Johnson City, India and elsewhere, thank you for the hikes, bike rides, great parties, smiles and support at all times.

Last but not the least, to my wonderful family: Thanks to mom, dad, sister, aunt and my grandparents for making me what I am today. Even though I have been away for a long time, you have always provided me the strength, support and encouragement for accomplishing my dreams in life. The final word of thanks to my wife, for being my best friend and companion for life.

Theory and Computational Studies of Mechanochemical Phenomena

Sai Sriharsha Manoj Varma Konda, Ph.D.

The University of Texas at Austin, 2014

Supervisor: Dmitrii E. Makarov

Mechanochemistry, or the modulation of chemical reactivity through the application of mechanical forces, has shown to facilitate a number of otherwise prohibitive chemical transformations. Computational approaches employing electronic structure calculations have explained a number of mechanochemically activated processes such as thermally inaccessible isomerizations and cycloreversions, symmetry-forbidden electrocyclic ring openings or activation of latent catalysts and, more recently, have been successfully used to design novel mechanosensitive systems. A significant limitation of such approaches, however, is their high computational cost, as finding force-dependent transition states requires multiple saddle searches and consequently, multiple energy evaluations. To circumvent this problem, an approximation has been proposed, extending the well know "Bell formula", which estimates the force-dependent reaction barrier based on zero-force transition state properties. We demonstrate the numerical efficiency of this approximation termed as extended Bell theory (EBT) by comparing to existing theories and experiments. We also apply this method to suggest the unexplored,

yet potentially useful possibility of suppressing chemical reactions through mechanical perturbation. Furthermore, in sharp contrast to simple, one-dimensional theories, our analysis reveals that the anti-Hammond effect is dominant in the mechanical activation of polyatomic molecules. Finally, we propose a numerical scheme to address the drawback of the EBT approximation, which is the failure to account for force-induced instabilities. Our approach provides a computationally efficient recipe to track the instabilities and follow the evolution of the reactant or transition states at any explicit force. We provide a classification of the different instability scenarios, and provide an illustrative example for each case.

Table of Contents

List of Figures

Chapter 1: Introduction

MECHANOCHEMISTRY

A simple view of a chemical reaction $A \rightarrow B$, consists of a transformation of molecules labeled as reactants (A) to products (B). Typically the reactants and products are stable molecules, which means that an activation energy barrier must be overcome for the progress of a reaction. Given a sufficient time span, the familiar Maxwell-Boltzmann distribution[1, 2] predicts the statistical probability for conversion of reactants into products as $\sim \exp[-\Delta V^{\neq}/k_B T]$. However, this phenomenon is a rare event with the probability decreasing exponentially with increasing barrier height $\Delta V^{\neq}$. Experimentalists often resort to thermal or photochemical activation to accelerate desired chemical reactions. Unfortunately, thermal activation often leads to undesirable side reactions such as decomposition. As such, an external perturbation through which a reaction is not only accelerated but also directed in a selective manner holds significant importance. While commonly used thermodynamic parameters such as temperature or pressure are scalar quantities, mechanical force is a vector that enables it's use to direct chemical transformations along selected pathways. Such a methodology wherein mechanical forces are harnessed to control chemical reactivity is termed as mechanochemistry[3-17]. The first known theoretical model to understand mechanochemistry was proposed by Eyring, who predicted that a mechanical force could alter the potential energy surface (PES) along the mechanical coordinate (x) by lowering the activation energy barrier (Fig. 1.1)[18, 19].

Consequently, increased reaction rate accompanied by selective bond scission could potentially minimize unwanted reactivity and lead to the development of novel materials.

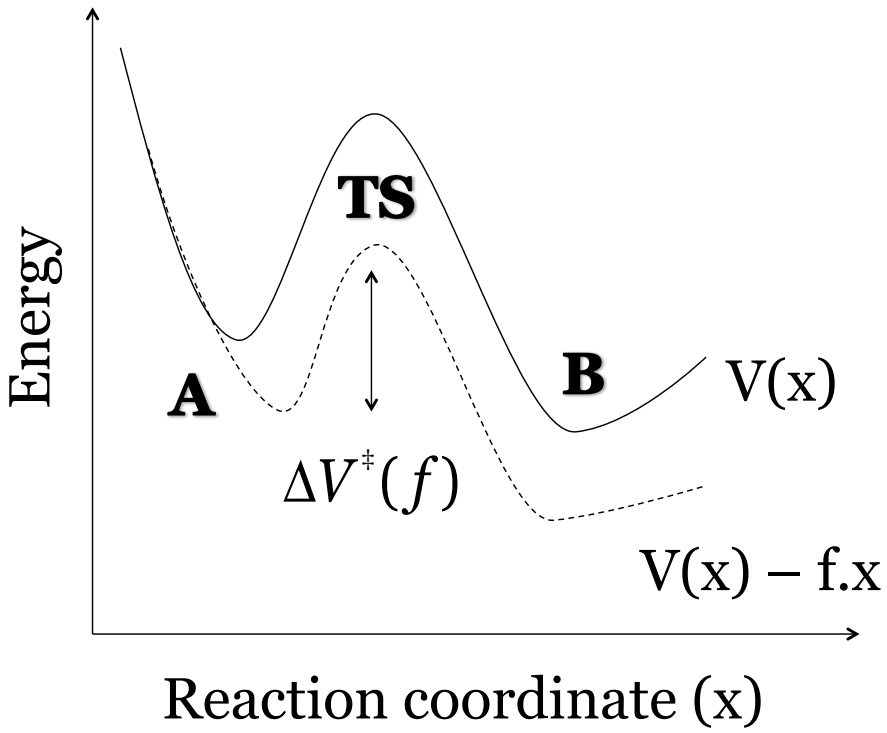

Figure 1.1: Cartoon representation of a one-dimensional model of a force-modified PES.

Recent advances in the nascent field of mechanochemistry involve experimental techniques exploiting mechanical forces from high molecular weight polymers that are covalently attached to chemical entities termed as mechanophores[3-17]. A specific example is the "unclicking of the click" reaction (Figure 1.2), wherein the unfavorable cycloreversion of the highly inert triazole to the constituent azide and alkyne was readily achieved through the application of mechanical forces[8]. The coupling between chemical

and mechanical processes has long been recognized as an important component of biological activity. This includes phenomena such as mechanical unfolding of proteins, which is believed to account for viscoelasticity of muscle fiber[20] and for high toughness and strength of natural materials[21-23]. Moreover, processes such as protein degradation[24-29] and control of enzymatic activity[30] are known to proceed through mechanically induced conformational changes. In a broader context, mechanical forces are involved in studies such as single-molecule pulling of biomolecules[20, 30-64], molecular motors[65-67], molecular force-probes[68-70], DNA and protein translocation through biological and solid-state pores[25, 71-79] and materials chemistry[3, 5-8, 11, 13-15, 80-89].

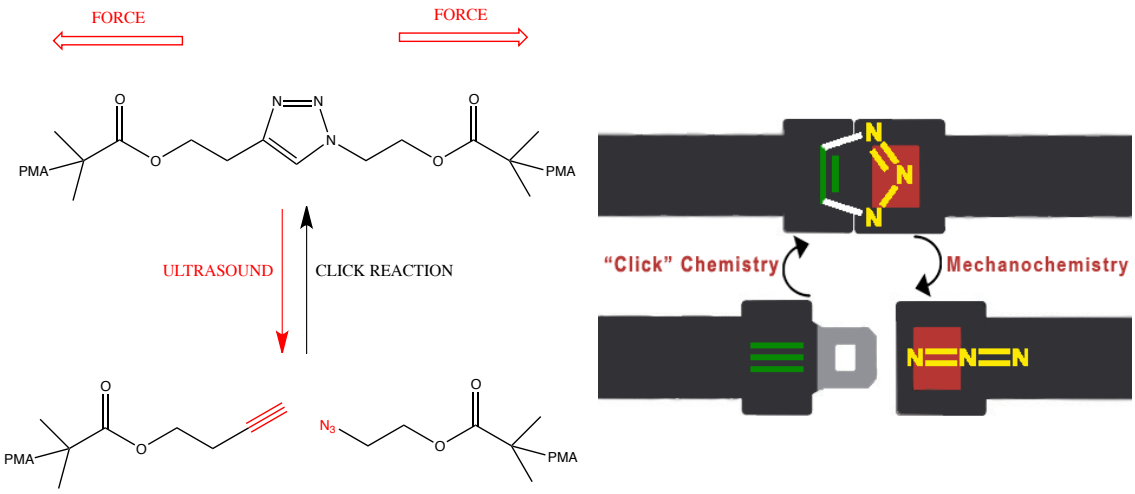

Figure 1.2: "Unclicking the click". The application of ultrasound to a triazole embedded within a polymer chain (PMA) yields a cycloreversion process (red). The resulting azide and alkyne substrates undergo a click reaction to generate the triazole (black)[8].

ADVANCES IN FORCE MANIPULATION TECHNIQUES

Experimental work employing mechanical forces can be broadly classified under two categories: (a) Solution-based studies of mechanoresponsive polymers (b) Single-molecule studies. Mechanical activation by ultrasound is the most popular solution-based method as it offers great selectivity[3, 15, 16, 90-92]. The forces and the strain rates generated by sonication are often higher as compared to flow fields that enables its use to mechanically facilitate a number of novel reactions. The observed signal in these bulk experiments is the ensemble average over Avogadro number of molecules. Consequently, the signal is dominated by major contributors and the fluctuations arising from transient process is often averaged out. While these techniques are often robust, they cannot track individual trajectories in real time, an advantage offered by single-molecule techniques.

Single-molecule manipulation methods such as atomic force microscopy (AFM) and optical tweezers offer high spatio-temporal resolution and have become the popular choice for investigating the dynamics of biopolymers such as DNA and proteins[20, 30-64]. While bulk methods provide a mean value of a given ensemble measurement, single-molecule experiments report the distribution of these values. This approach is useful in identifying transient processes; for example, monitoring molecular fluctuations, alternate reaction mechanisms and even the detection of non-equilibrium states of the molecule found far from the average of the population[93-97]. In what follows, a brief overview of the popular force manipulation techniques is provided.

Atomic force microscopy (AFM)

In an AFM experiment, a single biopolymer such as a polyprotein or DNA is attached between a cantilever with a sharp tip and a substrate surface mounted on a piezoelectric positioner (Fig. 1.3). The tip and the surface are functionalized to hold the molecule of interest. As the distance between the cantilever and the piezoelectric actuator is increased, the molecule is stretched resulting in a signal as a function of the tip position. Any resistance in the conformational change of the biomolecule is provided by the deflection of the laser beam from the cantilever to a sensitive photodetector. This allows one to measure the force exerted by the molecule attached to the tip. Depending on the shape and the material properties of the cantilever, the range of force offered by AFM are typically in the 10^1 - 10^3 pN range[98].

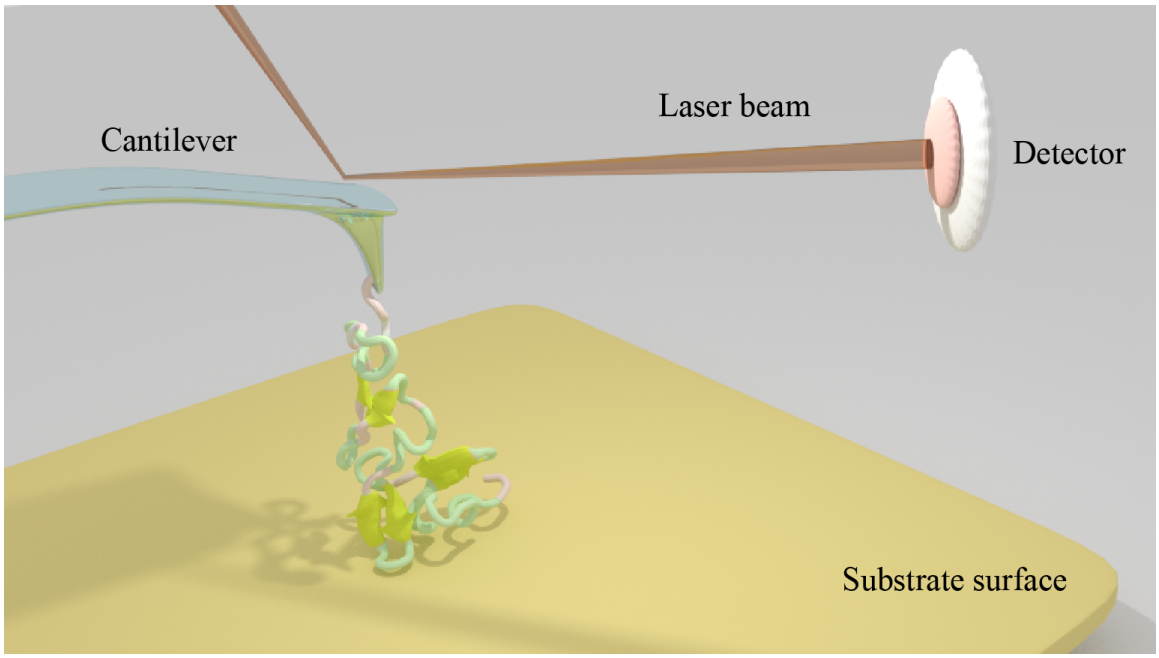

Figure 1.3: A simplified AFM set-up consisting of the biopolymer that is held in between the cantilever tip and the substrate surface. The displacement of the cantilever is measured by the reflection of the laser beam on the detector.

Optical tweezers (OT)

Optical trapping offers another effective way to study biopolymers. Experiments involving OT utilize micrometer-sized beads that are attached to the molecule of interest. The other end is either attached to a surface or a second bead, hence forming a single-molecule tether (Fig. 1.4). A highly focused laser beam from a microscope objective is then used to optically trap the beads. The equilibrium position of the bead is near the middle of the laser beam. As a result, any shift in the position of the bead from the center of the optical trap generates a restoring force that is linearly proportional to the magnitude of the displacement. OT setups offer a sub-nanometer resolution for the

measurement of the position of the trapped beads and the forces are in the order of 0.1 – 100 pN[99].

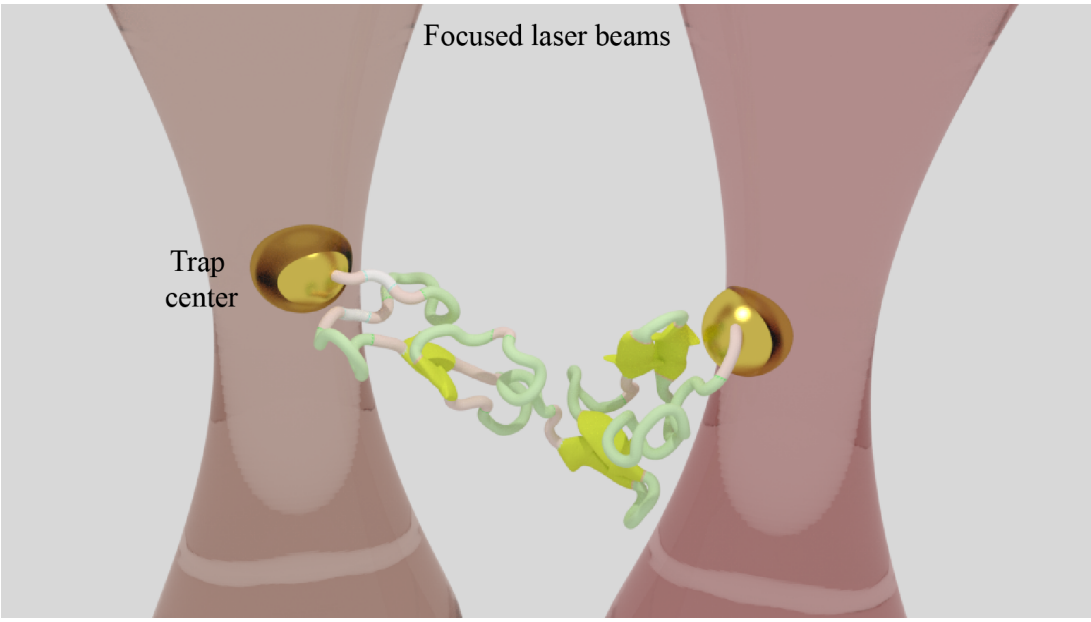

Figure 1.4: A general representation of an OT setup that utilizes radiation pressure to exert mechanical forces.

While the use of AFM and OT allows a precise control of mechanical force, they are however not suitable for practical synthetic efforts. Recent advances in sonication and the development of molecular force probes has led to the application of mechanical forces to a large number of molecules in solution.

Sonication

Sonochemistry, or the study of chemical effects using ultrasound has seen a rapid growth in its application to synthesis and design of novel organic materials in recent years[90-92]. As shown in Figure 1.5, acoustic fields created by ultrasound pull the ends of the polymer chain in opposing directions, generating a mechanical force on the molecular

entity (termed as mechanophore) embedded within these chains[17]. The velocity gradients are not created by the direct interaction with the acoustic field, rather, from the solvent cavitation process. This involves the formation, growth and subsequent collapse of solvent bubbles. The polymer chains in the vicinity of the collapsing bubble are pulled towards them at higher velocities than the chains that are farther away from the cavitation process. Consequently, a mechanical force is transmitted to the mechanophore near the midpoint of the polymer chain. The magnitude of these forces, which is of the order of 10 – 10^3 pN, is dependent on the molecular weight of the polymer, as mechanical activation is not seen beneath a certain threshold.

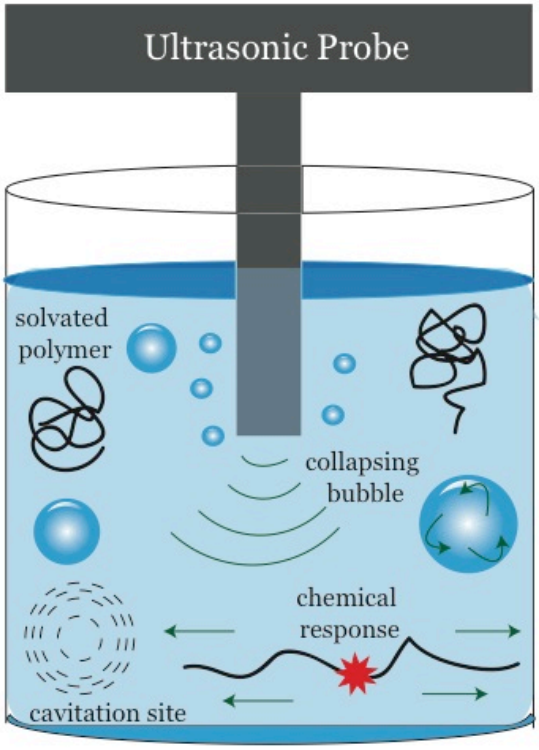

Figure 1.5: Different stages in the process of solvent cavitation that generates shear forces responsible for the elongation of the polymer chain resulting in a chemical reaction[17].

OBJECTIVE AND OVERVIEW OF THESIS

The concept central to the above mentioned experimental procedures is the determination of the force dependence of the reaction rate. Electronic structure calculations have been employed to great effect to investigate the force effects on the reaction rate[3-7, 13, 14, 69, 81-89]. The main goal of the thesis is to formulate a theoretical view and develop predictive computational models of the diverse mechanochemical phenomena. The motivation for the work comes from advances in experiments that

demand a better understanding of these phenomena. Existing one-dimensional models are often inaccurate to explain mechanical activation processes[46, 100, 101]. The approach presented in this work establishes a direct connection between intrinsic chemical reactivity and mechanical behavior, by proposing higher-dimensional theories. We further show that the differences between low- and high-dimensional views are not merely a quantitative one, but new emergent behaviors are expected instead[7, 83, 84, 102]. Each of the following chapters are self-contained stories and a brief overview is as follows:

In Chapter 2, we propose a computationally cheap and efficient model termed as extended Bell theory (EBT) to understand and predict the force dependence of the reaction barrier[83]. We show that EBT is quantified by two parameters ΔR and $\Delta\chi$ that determine the mechanical susceptibility of any reaction pathway. Electronic structure calculations were performed on well-studied mechanophores to demonstrate the numerical efficiency of this model. As an extension, Chapter 3 discusses a case study where results from EBT compliment and provide a mechanistic understanding of the experimental work performed in Prof. Christopher Bielawski's lab at UT-Austin[7].

Chapter 4 describes a survey of mechanophoricity, which is the identification and characterization of novel mechanochemical systems. We show that EBT based theoretical analysis can guide rational design of new mechanophores. We present an argument that the novel trends predicted in this work are a direct consequence of the multidimensional nature of the mechanochemical processes; a fact that is not accounted by commonly used one-dimensional models[46, 100, 101]. Our computational results also demonstrate the first instance of reaction suppression arising from the application of mechanical forces[84].

While EBT approximation is shown to work remarkably well for a variety of cases, it is not without limitations. The most obvious of them is that it is an approximation. Most notably, EBT fails to account for force-induced instabilities in the reaction mechanisms at high forces. For example, there may be a switch in reaction mechanism at high forces that is triggered by the disappearance of the transition state. Chapter 5 introduces an exact approach that follows the evolution of critical points (reactant or transition states) on the molecule's PES as a function of an external force. By drawing parallels from catastrophe theory, we provide a robust framework supported by electronic structure calculations to classify these instabilities as the PES topology varies with force[102].

Chapter 2: Chemical Reactions Modulated by Mechanical Stress: Extended Bell Theory

ABSTRACT

A number of recent studies have shown that mechanical stress can significantly lower or raise the activation barrier of a chemical reaction. Within a common approximation due to Bell [Science, 1978. **200**, 618-627], this barrier is linearly dependent on the applied force. A simple extension of Bell's theory that includes higher order corrections in the force predicts that the force-induced change in the activation energy will be given by $-F\Delta R - \Delta\chi F^2/2$. Here ΔR is the change of the distance between the atoms, at which the force F is applied, from the reactant to the transition state, and $\Delta\chi$ is the corresponding change in the mechanical compliance of the molecule. Application of this formula to the electrocyclic ring-opening of *cis* and *trans* 1,2-dimethylbenzocyclobutene shows that this extension of Bell's theory essentially recovers the force dependence of the barrier, while the original Bell formula exhibits significant errors. Because the extended Bell theory avoids explicit inclusion of the mechanical stress or strain in electronic structure calculations, it allows a computationally efficient characterization of the effect of mechanical forces on chemical processes. That is, the mechanical susceptibility of any reaction pathway is described in terms of two parameters, ΔR and $\Delta\chi$, both readily computable at zero force.

INTRODUCTION

Mechanochemistry, an emerging field that deals with the coupling between mechanical and chemical phenomena, holds great promise for precise control of chemical reactivity. Unlike scalar quantities such as pressure or temperature, the vectorial character of an applied mechanical force allows one to precisely guide molecular systems along desired reaction pathways, which may be unique from common thermal or photochemically driven processes[3, 6]. Recent developments in mechanochemistry include experimental techniques allowing application of mechanical forces to molecular entities covalently attached to high molecular weight polymers[3, 5] and single-molecule methods (AFM and optical tweezers) to stretch individual proteins and RNA[45]. In addition, it is possible to design molecular machines that utilize energy of chemical reactions to exert mechanical forces and perform work[63, 64].

Rational control of chemical reactivity through application of mechanical stress requires an understanding of the effect of the force on the rate of a chemical reaction as well as on the stability of the respective reactants and/or reactive intermediates. Consider, for example, the reaction shown in Fig. 2.1: If a stretching force is applied to an arbitrarily selected pair of atoms, will that force speed up or suppress the reaction? What is the magnitude of this effect? Which pair of atoms should be selected in order to achieve the maximum rate enhancement? As electronic structure or molecular dynamics calculations are arguably less expensive than the design of an appropriate experimental system, computational predictions are of obvious value for answering these questions.

Mechanical pulling processes can be incorporated in electronic structure calculations in a number of ways. Suppose, for example, that one pulls on a pair of atoms, *i* and *j*, as illustrated in Fig. 2.1. This can be achieved, computationally, by imposing strain via a constraint on the distance R_{ij} between the two atoms [4, 6, 86, 87]. Alternatively, one can impose a stress via an additional energy term of the form $-FR_{ij}$ (where F is the pulling force) added to the molecule's potential energy[86]. By computing how stress or strain affects the energies of the stable-state and transition-state structures of the molecule(s) in the reaction of interest, it is then possible to estimate the force dependence of the reaction rate. This procedure is costly, however, as it requires multiple transition-state searches (and, consequently, multiple energy evaluations) that must be performed for each value of the force or constraint. If one desires to know how the pulling depends on the positions *i* and *j* at which the forces are applied, this further increases the computational cost by a factor of $N(N-1)/2$, where N is the total number of atoms in the system.

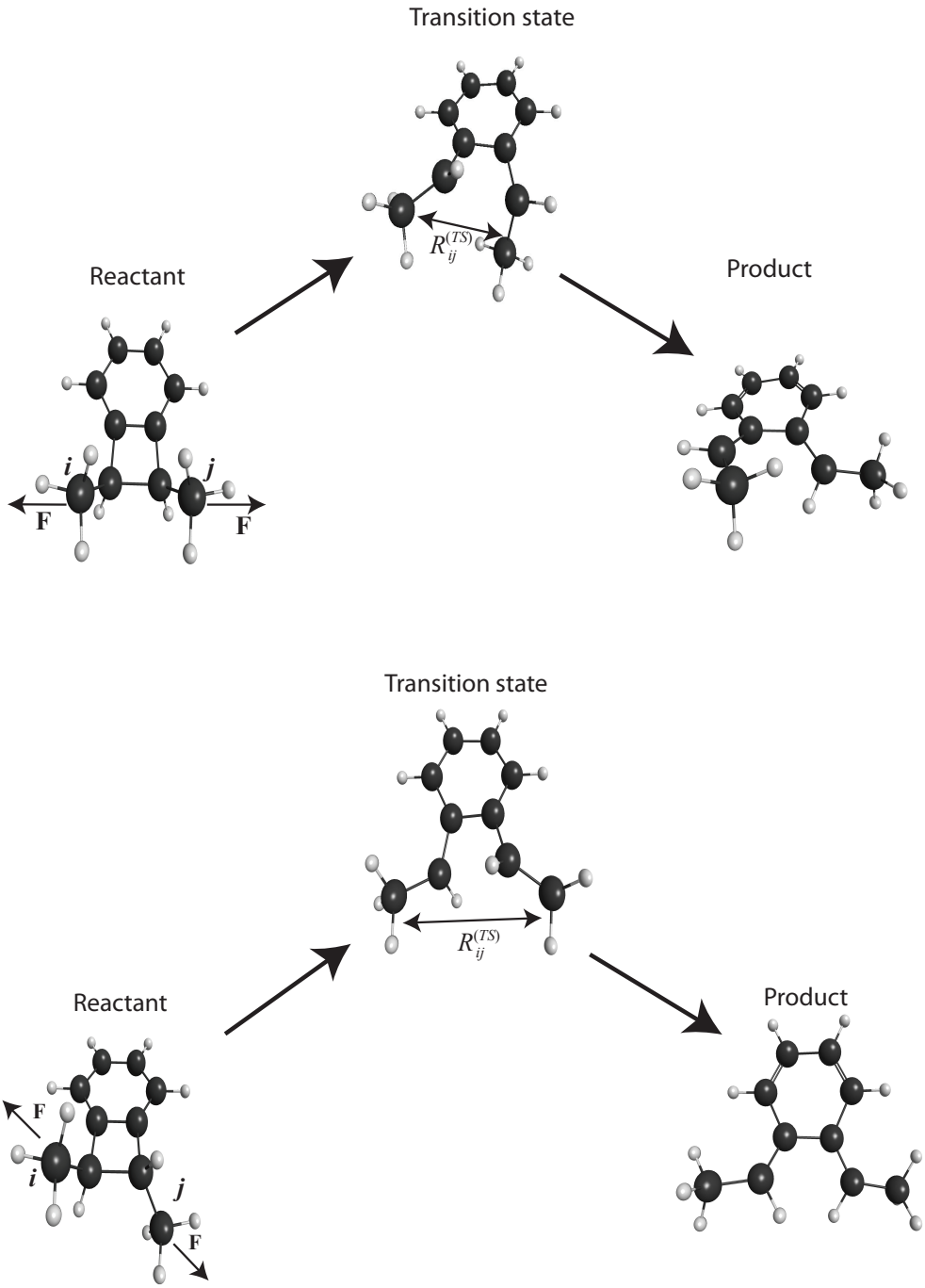

Figure 2.1: Conrotatory pathway for electrocyclic ring-opening of (a) *cis* and (b) *trans* 1,2-dimethylbenzocyclobutene. The force applied to two carbons lowers the reaction barrier if the distance R_{ij} between these atoms is longer in the transition state than it is in the reactant state.

To avoid high computational cost, simple, approximate theories have been widely used. Perhaps the most widespread approximation is the one introduced by Bell[100, 101], which states that upon the application of a force F, the barrier of chemical reaction is changed by an amount equal to $-F\Delta R_{ij}$, where ΔR_{ij} is the change in the distance between the atoms (to which the force is applied) from the stable (reactant) state to the transition state. Bell's theory thus predicts a linear relationship between the logarithm of the rate and the force. As ΔR_{ij} can be estimated from the stable- and transition-state geometries at *zero* force, Bell's formula offers tremendous computational savings, providing the force dependence of the reaction rate, at any force, without having to actually impose such a force (or a constraint) in the electronic structure calculations. Unfortunately, in practice this linear relationship is commonly violated because the distance change ΔR_{ij} is itself force-dependent[6, 48, 51, 53, 56, 71, 86]. Other approaches, which approximately account for the force-induced changes in the molecular geometry, have also been proposed[86]. Somewhat surprisingly, however, one straightforward refinement of Bell's formula, although pointed out in the literature[13, 14], has not been commonly used to improve the accuracy of the calculations. Specifically, Bell's formula, predicting the linear force dependence of the reaction barrier, is nothing but a Taylor series truncated to first order in the force. The second order term is, however, also readily obtained. Moreover, evaluation of this second-order term does not require any additional information other than the Hessian matrices of the molecule in the reactant and the transition states. The latter comes at no additional cost as they are readily evaluated by

most electronic structure codes. The purpose of this chapter is to derive such an improved approximation in terms of electronic structure data and to evaluate its performance. We call this approximation extended Bell theory (EBT). In what follows, we show that EBT accounts, rather accurately, for the nonlinearity of the force dependence of the reaction barrier observed in the more expensive calculations that explicitly include mechanical forces. We further expose certain mathematical peculiarities of EBT arising from the multidimensional character of the underlying potential energy surface and make connection to other approaches used in the literature.

EBT is related to the harmonic transition theory[103] in that both approximations assume quadratic potential energy surfaces in the vicinity of the reactant and transition states. We further show that the same approximation readily yields other useful mechanical properties of the molecule, such as its effective compliance in response to the mechanical stress.

The remainder of this chapter is organized as follows: In Section 2 we derive the EBT approximation. In Section 3 we examine the accuracy of the method by studying numerical examples. Section 4 derives and tests relationships describing the mechanical compliance of a molecule in the harmonic approximation. Section 5 concludes with a discussion of extensions and limitations of the method.

THEORY

We start with illustrating EBT in a simple one-dimensional model of a reaction governed by a potential $V(s)$, which is a function of a single reaction coordinate s (Fig.

2.2). The minimum of the potential is located at $s = s^{(0)}$ and the maximum is at $s^{(TS)}$, where the superscripts (0) and (TS) refer, respectively, to the stable, reactant conformation and to the transition state.

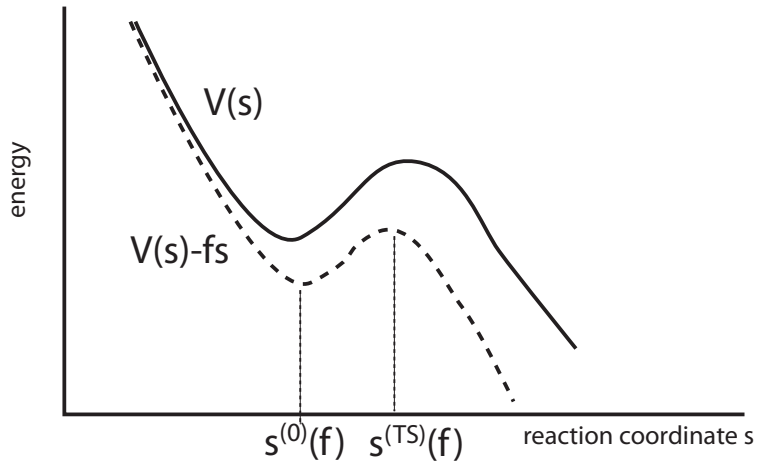

Figure 2.2: Simple one-dimensional model of a chemical reaction modulated by a mechanical force. The force lowers the reaction barrier and shifts the reactant and transition-state conformations toward one another.

When a force f is exerted along the reaction coordinate, the system feels the potential $V(s) - fs$, with a modified activation energy barrier[46, 47]:

$$V^{\neq}(f) = V^{(TS)} - V^{(0)} = V[s^{(TS)}(f)] - V[s^{(0)}(f)] - f[s^{(TS)}(f) - s^{(0)}(f)] .$$

(2.1)

The force-dependent rate is estimated using transition-state theory as

$$k(f) = \nu(f) \exp\left[-\frac{V^{\neq}(f)}{k_B T} \right] , \qquad (2.2)$$

where the prefactor ν depends on the vibrational frequency in the stable state. For condensed-phase reactions, the prefactor also contains an appropriate transmission factor that accounts for the recrossings of the transition state[103]. Because $k(f)$ is exponentially dependent on the force, it is reasonable to neglect the much weaker force dependence of the prefactor itself, i.e., $\nu(f) \approx \nu(0)$.

The locations $s^{(0),(TS)}(f)$ of the potential minimum and maximum satisfy the equation

$$V'(s) - f = 0 \tag{2.3}$$

Expanding Eq. 2.3 in a Taylor series, we get, to first order in f:

$$s^{(TS),(0)}(f) \approx s^{(TS),(0)}(0) + \frac{f}{V''[s^{(TS),(0)}(0)]}. \tag{2.4}$$

That is, the potential minimum shifts to the right (since $V'' > 0$) and the transition state is shifted to the left. Substituting this into Eq. 2.1, we find, to second order in the force[13, 14]:

$$V^{\neq}(f) = V^{\neq}(0) - f\left[s^{(TS)}(0) - s^{(0)}(0)\right] - \frac{f^2}{2}\left\{\frac{1}{V''\left[s^{(TS)}(0)\right]} - \frac{1}{V''\left[s^{(0)}(0)\right]}\right\} \tag{2.5}$$

The first term in Eq. 2.5 corresponds to Bell's theory[101], in which the activation barrier is linearly dependent on the force. The second term describes the "Hammond" effect[48, 53, 56, 71], i.e. the force-induced shift of the positions of the transition and reactant states. Notice that the second term is always positive since $V''[s^{(0)}(0)] > 0$ and $V''[s^{(TS)}(0)] < 0$.

Eq. 2.5 is obviously an approximation that is valid only for a sufficiently low force. As f is increased, there is a critical value $f = f_c$, after which the barrier disappears

altogether and Eq. 2.5 becomes meaningless. At $f < f_c$, Eq. 2.5 is exact for a cusp-shaped parabolic potential[56, 104], provided that one sets $V''\left[s^{(TS)}(0)\right] = \infty$. For more realistic potentials, Eq. 2.5 often still remains a reasonable approximation as long as the applied force is considerably smaller than f_c. For example, if $V(s)$ is a cubic parabola[56], the relative error in the barrier introduced by this approximation is less than 3% for $f < 0.5 f_c$. The quadratic approximation of Eq. 2.5, however, breaks down in the vicinity of f_c, where the activation barrier vanishes with a power law dependence on $(f\text{-}f_c)$ (see, e.g., refs.[105-107]).

To conclude our discussion of the 1D case, we point out a useful relationship derived by Suzuki and Dudko [108], which is true for any force (as long as a barrier is still present):

$$dV^{\neq} / df = s^{(0)}(f) - s^{(TS)}(f) \tag{2.6}$$

This follows immediately from Eqs. 2.1 and 2.3.

We now turn to the general case and describe the configuration of a molecule consisting of N atoms by a 3N-dimensional vector: $\mathbf{r} = (x_1, y_1, z_1, ..., x_N, y_N, z_N)$. Conjugate to it is a $3N$-dimensional force vector $\mathbf{f} = (f_{x1}, f_{y1}, f_{z1}, ..., f_{xN}, f_{yN}, f_{zN})$, where $\mathbf{F}_i = (f_{xi}, f_{yi}, f_{zi})$ is a three-dimensional force vector acting on the i-th atom. The energetics of the system is described by the Born-Oppenheimer potential energy surface $V=V(\mathbf{r})$. The generalization of the above equations to many dimensions is straightforward. In particular, to first order in the force we find that the stable and the transition state

configurations undergo force-induced shifts according to an equation analogous to Eq. 2.4:

$$\mathbf{r}^{(0),(TS)}(\mathbf{f}) = \mathbf{r}^{(0),(TS)}(0) + \left(\mathbf{h}^{(0),(TS)}\right)^{-1}\mathbf{f}\,, \tag{2.7}$$

where

$$\mathbf{h}^{(0),(TS)} = \left.\frac{\partial^2 V}{\partial r_\alpha \partial r_\beta}\right|_{\mathbf{r}=\mathbf{r}^{(0),(TS)}(0)} \tag{2.8}$$

is the Hessian matrix computed for the reactant/transition state at zero force. For the reaction barrier, we obtain an equivalent of Eq. 2.5:

$$\begin{aligned} V^{\neq}(\mathbf{f}) &= V^{\neq}(0) - \mathbf{f}\left[\mathbf{r}^{(TS)}(0) - \mathbf{r}^{(0)}(0)\right] - \frac{1}{2}\mathbf{f}^T\left[\left(\mathbf{h}^{(TS)}\right)^{-1} - \left(\mathbf{h}^{(0)}\right)^{-1}\right]\mathbf{f}\,, \\ &\equiv V^{\neq}(0) + \Delta V_1^{\neq}(\mathbf{f}) + \Delta V_2^{\neq}(\mathbf{f}) \end{aligned} \tag{2.9}$$

where $\mathbf{f}^T$ denotes the transposed force vector.

If the molecule is free to rotate and translate in space, its Hessian matrix **h** is generally singular (with six zero eigenvalues corresponding to rigid-body motion) and therefore not invertible. Eqs. (2.7) and (2.9), then, appear to be ill-defined. This predicament is easily surmounted, however, by noting that the only physically meaningful force vectors **f** are those orthogonal to the null space of the Hessian matrix. Indeed, only such vectors can ensure that the system is in mechanical equilibrium such that the total force and the torque acting on the molecule are both zero. As a consequence, all the inverses in Eqs. 2.7 and 2.9 should be understood as generalized inverses (pseudoinverses), with the 6 zero eigenmodes suppressed in their spectral expansion.

An important difference between the multidimensional case and the 1D example described above is that, unlike the 1D case, $\Delta V_2^{\neq}$ can be either positive or negative. Indeed, while the compliance matrix in the stable state, $\left(\mathbf{h}^{(0)}\right)^{-1}$, is non-negative definite and so $\mathbf{f}^T\left[\left(\mathbf{h}^{(0)}\right)^{-1}\right]\mathbf{f}$ is nonnegative, nothing can be said in advance about the sign of $\mathbf{f}^T\left[\left(\mathbf{h}^{(TS)}\right)^{-1}\right]\mathbf{f}$. Indeed, the transition-state Hessian has one negative and several non-negative eigenvalues, except in one dimension, where it is negative-definite. Therefore, the second-order term can make the force dependence either stronger or weaker.

Our theory so far is general in that it allows forces to be simultaneously applied to several atoms. Most experimental scenarios are limited to pulling on one pair of atoms, *i* and *j* (Fig. 2.1). Let **F** be the three-dimensional vector representing such a force. From here on, we will use upper-case bold symbols for *three-dimensional* vectors representing positions of and forces on individual atoms. We will continue to use lower-case boldface symbols to represent *3N-dimensional* vectors and (3*N*) × (3*N*) matrices corresponding to the configuration of the entire molecule. The mechanical equilibrium of the system requires that **F** always act along the line connecting the atoms. Let **E**=**F**/|**F**| be the unit vector along the force direction. Therefore, the following condition must hold at any point of the pulling process:

$$\frac{\mathbf{R}_j - \mathbf{R}_i}{\left|\mathbf{R}_j - \mathbf{R}_i\right|} = \mathbf{E}, \tag{2.10}$$

where $\mathbf{R}_i$ is the three-dimensional vector describing the position of atom *i*. To evaluate Eq. 2.9, we note that the 3*N*-dimensional force vector has the following components:

$$\begin{aligned} &f_{xi} = -FE_x, f_{yi} = -FE_y, f_{zi} = -FE_z, \\ &f_{xj} = FE_x, f_{yj} = FE_y, f_{zj} = FE_z, \\ &f_{xk} = f_{yk} = f_{zk} = 0, \text{ for } k \neq i, j \end{aligned} \tag{2.11}$$

In particular, the expression for the first order correction to the barrier height can be simplified to give:

$$\begin{aligned} &\Delta V_1^{\neq}(F) = -\mathbf{f}\left[\mathbf{r}^{(TS)}(0) - \mathbf{r}^{(0)}(0)\right] = -F\left\{\mathbf{E}\left[\mathbf{R}_j^{(TS)}(0) - \mathbf{R}_j^{(0)}(0)\right] - \mathbf{E}\left[\mathbf{R}_i^{(TS)}(0) - \mathbf{R}_i^{(0)}(0)\right]\right\} \\ &= -F\left[\left|\mathbf{R}_j^{(TS)}(0) - \mathbf{R}_i^{(TS)}(0)\right| - \left|\mathbf{R}_j^{(0)}(0) - \mathbf{R}_i^{(0)}(0)\right|\right] \equiv -F\left(R_{ij}^{(TS)} - R_{ij}^{(0)}\right) \end{aligned} \tag{2.12}$$

This shows that (weakly) pulling on a pair of atoms, *i* and *j*, will lower the reaction barrier by an amount that is proportional to the difference between the (zero-force) inter-atomic distances R_{ij} in the transition and the reactant states. If the distance R_{ij} between the two atoms is longer in the transition state than it is in the stable configuration then application of a force between these two atoms will accelerate the reaction. In the opposite case, application of the force will slow the reaction down.

The quadratic correction to the barrier, $\Delta V_2^{\neq}$, is, likewise, easily evaluated using Eqs. 2.9 and 2.11, given the Hessian matrices corresponding to the stable and the transition-state configurations.

Finally, an analog of the Suzuki-Dudko formula [108] can be derived for an arbitrary force (for which the barrier still exists):

$$dV^{\neq} / dF = -\left(R_{ij}^{(TS)} - R_{ij}^{(0)}\right) \tag{2.13}$$

In accord with other predictions[108], pulling on a pair of atoms that are further apart in the transition state than in the stable conformation will speed up the reaction. In contrast, pulling on the atoms that approach one another when going from the stable state to the transition state will slow the reaction down. In the biophysics literature, the latter case is known as the catch-bond behavior[55, 61]. As previously pointed out[58, 109], multidimensionality of the energy landscape is essential for the catch-bond behavior. More generally, a one-dimensional picture is often insufficient to describe the effect of a mechanical force on many processes involving biomolecules [39, 110, 111], and obviously the dependence of the mechanical response on the choice of the atoms at which the force is applied [112, 113].

The first-order term (Eq. 2.12) corresponds to the standard approximation due to Bell[101]. When supplemented with the second-order term as in Eq. 2.9, we call the result extended Bell theory (EBT).

NUMERICAL TESTS OF EBT

The electrocyclic ring-openings of the *cis* and *trans* substituted benzocyclobutenes are pericyclic transformations that are governed by orbital symmetry, as predicted by the Woodward-Hoffman rules[11, 114]. For example, as shown in Figure 2.3, the C_1-C_2 σ-bond orbitals open in a conrotatory manner (rotation in the same direction) in order to constructively overlap with the LUMO of the π-system associated with the fused arene. Depending on the stereochemistry of the benzocyclobutene starting material, this process affords either a *cis*, *trans* diene (**A**) or a *trans*, *trans* diene (**B**) as the product[11]. It

should be noted that these are the expected products of thermal activation; photochemical excitation induces disrotatory ring opening (orbital rotation in the opposite direction) and affords the opposite outcomes (i.e., *cis* 1,2-dimethylbenzocyclobutene is converted to **B** and *trans* 1,2-dimethylbenzocyclobutene is converted to **A**)[11]. The mechanically facilitated ring opening is unique, however, in that, regardless of the stereochemistry of the benzocyclobutene starting material, application of vectorially opposed forces across the methyl substituents generates only the *trans*, *trans* diene product[11]. Such reactivity necessitates that both formally allowed and disallowed electrocyclic processes can be promoted under stress. As such, the coupling of mechanical forces to chemical systems creates opportunities for accessing otherwise prohibitive transformations. EBT offers a simple, fast, and effective computational method that can aid in the understanding of mechanically induced chemical processes as well as the development of reactions that are altogether new.

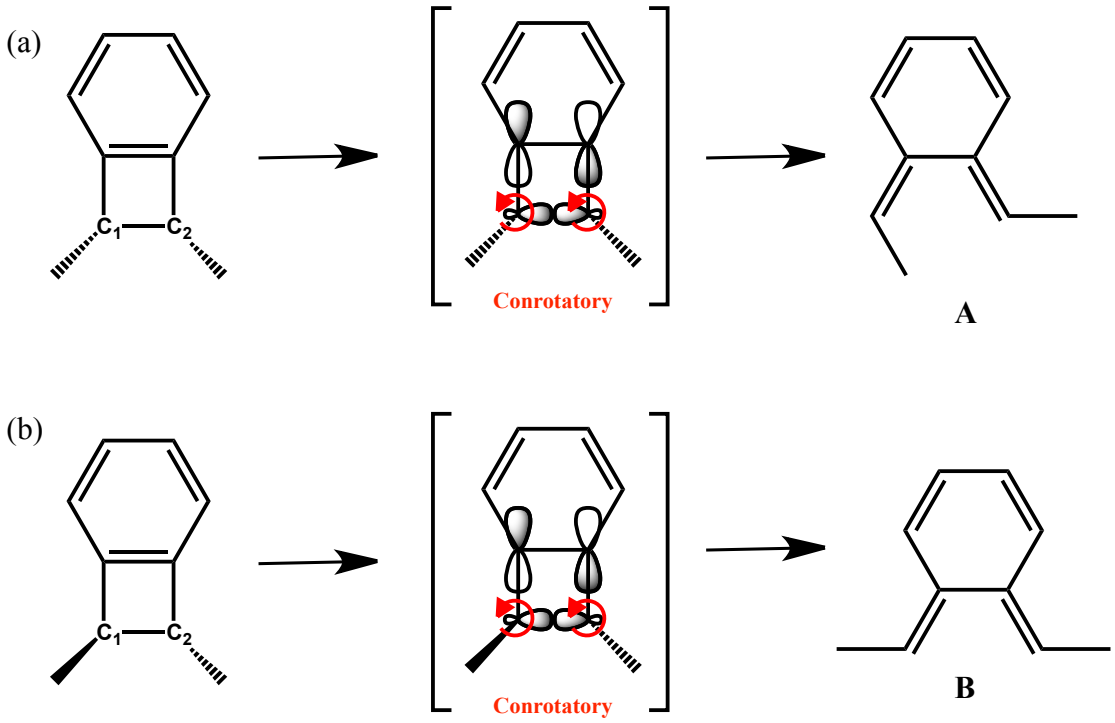

Figure 2.3: The conrotatory electrocyclic ring-opening of (a) *cis* 1,2-dimethylbenzocyclobutene leads to the *cis*, *trans* diene **A** and (b) *trans* 1,2-dimethylbenzocyclobutene leads to the *trans*, *trans* diene **B**. The curved arrows indicate the direction in which the orbitals associated with the C_1-C_2 σ-bond open. Hydrogen atoms are implicit in the structure, including at the atoms C_1 and C_1.

To test EBT, we have used it to estimate the force effect on the barrier for the conrotatory electrocyclic ring-opening of *cis* and *trans* 1,2-dimethylbenzocyclobutene[86]. As in an earlier study by Ribas-Arino *et al*[86], the pulling force was assumed to act between the substituent carbon atoms, as shown in Fig. 2.1 (atoms *i* and *j*). In our study, calculations were performed with the NWChem package[115] using density functional theory[116], employing the 6-31G* basis set[117] and the B3LYP exchange-correlation energy functional[118]. EBT calculation involves computing the reactant and transition state structures in the absence of the force, which are shown in Figure 2.1 (MacMolPlt

software[119] was used to generate the plots). The EBT force dependence of the reaction barrier was then computed using Eqs. 9 and 11.

To compare EBT with the "exact" (inasmuch as the underlying potential energy surface is deemed exact) result, we have computed the activation barriers for a series of constraints imposed on the distance between the two atoms. It is important, however, to realize that such a "constant extension" calculation does not directly correspond to a constant force scenario assumed above. Indeed, when a constant force is imposed on a pair of atoms, the extension (i.e., the distance between those atoms) is different in the reactant and the transition state. As a result, the barrier encountered by the system is different from that measured under the conditions where the extension is fixed. The observation that controlling stress or strain leads to different mechanical responses underscores the importance of knowing exactly how the pulling process is executed[46, 47].

Assuming one pulls on the atoms *i* and *j*, the correspondence between the constant force and the constant extension scenarios is established by the formula:

$$V^{\neq}(F) = U^{(TS)}[R_{ij}^{(TS)}(F)] - U^{(0)}[R_{ij}^{(0)}(F)] - F\left[R_{ij}^{(TS)}(F) - R_{ij}^{(0)}(F)\right] \qquad (2.14)$$

Here $U^{(0,TS)}(R_{ij})$ is the energy of the molecule in the reactant or transition state computed with the distance between the atoms fixed at R_{ij}, and $R_{ij}^{(0,TS)}(F)$ is the distance between the atoms (in the reactant or transition state) as a function of the applied force. That is, to simulate the force through a constraint, one should apply different constraints in the transition and stable states, so as to impose the same stretching force in each case. The dependence $R_{ij}^{(0,TS)}(F)$ can be computed by inverting the obvious relationship:

$$F = dU^{(0,TS)}(R_{ij}) / dR_{ij} \tag{2.15}$$

A comparison between Bell's theory, EBT, and "exact" force dependence obtained through Eqs. 2.14 and 2.15, is shown in Figure 2.4. Consistent with earlier observations[6, 86], Bell's formula performs rather poorly for the *cis*-isomer except at very low forces while EBT remains practically exact throughout the entire range of forces of ~1 nN and lower, where the specific reaction channel considered here exists (Fig. 2.4a). Moreover, the force dependence of the barrier found here is nearly identical to that estimated in ref.[86]. Also note that the second-order correction to the activation barrier is negative in this case, making the force dependence stronger. As discussed in Section 2, this behavior cannot be predicted by one-dimensional models, for which the second-order correction is always positive.

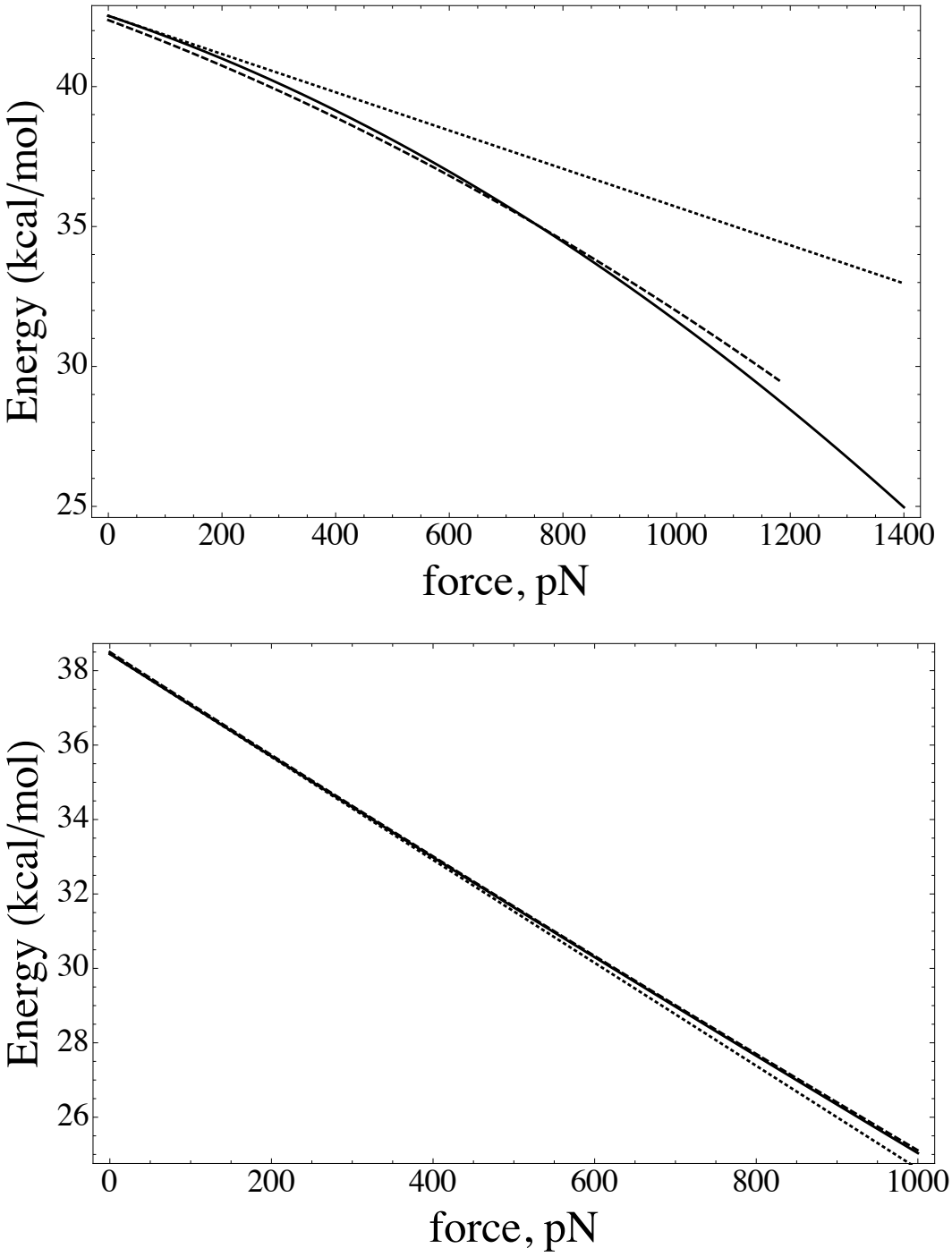

Figure 2.4: Comparison of the force dependence of the reaction barrier obtained by different methods for (a) *cis* and (b) *trans* 1,2-dimethylbenzocyclobutene. Solid line: EBT. Dotted line: Bell's formula. Dashed line: "exact" result obtained from constrained structure optimization.

In the *trans*-case (Fig. 2.4b) Bell's formula is already nearly exact and the second-order correction provided by EBT is relatively small. The origins of this difference between the mechanical responses of the *cis*- and *trans*-isomers are further discussed in the next Section.

MECHANICAL COMPLIANCE OF A MOLECULE WITHIN EBT

The harmonic approximation employed in EBT also allows one to readily obtain another important parameter, the effective mechanical compliance of the molecule, in its reactant configuration, with respect to pulling on any pair of atoms. That is, it allows one to estimate the energy $U^{(0)}(R_{ij})$ as a function of the distance R_{ij} between the atoms one pulls on. Because the underlying potential assumed by EBT is harmonic, one expects that, when stretched between a pair of atoms, the molecule will effectively behave as a Hookean spring with a potential of the form

$$U^{(0)}(R_{ij}) = U^{(0)}[R_{ij}^{(0)}(0)] + k_{ij}^{(0)}[R_{ij} - R_{ij}^{(0)}(0)]^2 / 2 , \qquad (2.16)$$

where $R_{ij}^{(0)}(0)$ is the equilibrium distance between the atoms. When the distance between a pair of atoms is increased, other atoms, of course, also become displaced. Since no external forces act on those atoms, their positions are determined from the condition that they are in mechanical equilibrium. One can view the finding of $U^{(0)}(R_{ij})$ as a coarse-graining procedure in which all of the atomic coordinates, except for the coordinates of the atoms *i* and *j*, are eliminated based on the above mechanical equilibrium condition. As the atoms of the molecule can be arbitrarily relabeled, it is convenient to assume that

one always pulls on the first two atoms. We then write the molecule's Hessian matrix in the block-diagonal form:

$$\mathbf{h}^{(0)} = \begin{pmatrix} \mathbf{h}_{11}^{(0)} & \mathbf{h}_{12}^{(0)} \\ \mathbf{h}_{21}^{(0)} & \mathbf{h}_{22}^{(0)} \end{pmatrix} \tag{2.17}$$

Here $\mathbf{h}_{11}^{(0)}$, $\mathbf{h}_{12}^{(0)}$, $\mathbf{h}_{21}^{(0)}$, and $\mathbf{h}_{22}^{(0)}$ are, respectively, 6×6, 6×(3N-6), (3N-6)×6, and (3N-6)×(3N-6) matrices. The (3N-6) degrees of freedom of the unconstrained atoms are eliminated through the standard coarse graining procedure[120-122], to obtain an effective 6×6 Hessian matrix that describes the mechanical response of the pair of atoms one is pulling on. This matrix is given by the Schur complement:

$$\bar{\mathbf{h}}_{11}^{(0)} = \mathbf{h}_{11}^{(0)} - \mathbf{h}_{12}^{(0)} \left(\mathbf{h}_{22}^{(0)} \right)^{-1} \mathbf{h}_{21}^{(0)} \tag{2.18}$$

This matrix should, of course, coincide with the Hessian matrix computed from Eq. 2.16. This, in particular, means that is has five zero eigenvalues and one nonzero eigenvalue equal to $2k_{ij}^{(0)}$. Thus, starting with the full hessian matrix $\mathbf{h}^{(0)}$, performing coarse-graining via Eq. 2.18 and, finally, diagonalizing the resulting 6×6 Hessian matrix, one can find the effective spring constant $k_{ij}^{(0)}$ with respect to pulling on any pair of atoms.

One can also formally define the effective stiffness $k_{ij}^{(TS)}$ of the molecule corresponding to the transition state (as well as to any critical point of the molecule's potential energy surface), although, stretching the molecule while maintaining its transition-state configuration does not correspond to any experimental scenario. This stiffness can be estimated again from Eq. 2.18 by using the Hessian matrix corresponding

to the transition state. Note that, while $k_{ij}^{(0)}$ is always positive, $k_{ij}^{(TS)}$ may be either positive or negative.

The stiffness k_{ij} (and its inverse, the compliance χ_{ij}) of the molecule in its reactant and the transition state configurations determines how the reactant or transition-state conformation is deformed by the force. Indeed, using Eqs. 2.15 and 2.16, we find:

$$R_{ij}^{(0,TS)} = R_{ij}^{(0,TS)}(0) + F / k_{ij}^{(0,TS)} = R_{ij}^{(0,TS)}(0) + \chi_{ij}^{(0,TS)} F \,, \tag{2.19}$$

an equivalent of Eqs. 2.4 and 2.7. Furthermore, the difference between the compliances in the transition and reactant state configurations determines the second-order response of the reaction barrier to the force. Indeed, the EBT formula for the force-dependent rate (Eq. 2.9) can be conveniently rewritten in a one-dimensional form similar to Eq. 2.5[13, 14]:

$$V^{\neq}(F) = V^{\neq}(0) - F\left(R_{ij}^{(TS)} - R_{ij}^{(0)}\right) - (\chi_{ij}^{(TS)} - \chi_{ij}^{(0)})F^2 / 2 \,, \tag{2.20}$$

which can be derived by substituting Eqs. 2.16 and 2.19 into Eq. 2.14. This result shows that, while the extension or contraction of the distance R_{ij} determines the first-order effect of the force on the barrier, the curvature of the dependence $V^{\neq}(F)$ is controlled by the difference in the compliances of the transition and reactant states. The latter effect accounts for the change in the elastic energy stored by the molecule when going from the reactant state to the transition state.

The relative importance of the second-order correction thus depends on the compliance of the molecule in the reactant and the transitions state. More precisely, the second-order term in Eq. 2.20 is negligible when $F \ll \left|R_{ij}^{(TS)} - R_{ij}^{(0)}\right| / \left|\chi_{ij}^{(TS)} - \chi_{ij}^{(0)}\right|$. In the

same range of forces, therefore, stiffer molecules will be better described by Bell's formula than more compliant ones. For example, the *trans*-isomer of 1,2-dimethylbenzocyclobutene is fairly stiff in both the reactant and transition states ($k^{(0)} \approx 48.5$ N/m, $k^{(TS)} \approx 67.8$ N/m) as compared to the *cis*-isomer ($k^{(0)} \approx 34.0$ N/m, $k^{(TS)} \approx 11.6$ N/m), which exhibits a much softer transition state. This explains the relative success of Bell's theory in the former case given comparable values of the stretching force. Indeed, a stiffer molecule stretched by a force undergoes a smaller deformation, resulting in a smaller overall elastic energy; this elastic energy can be altogether neglected for sufficiently stiff molecules.

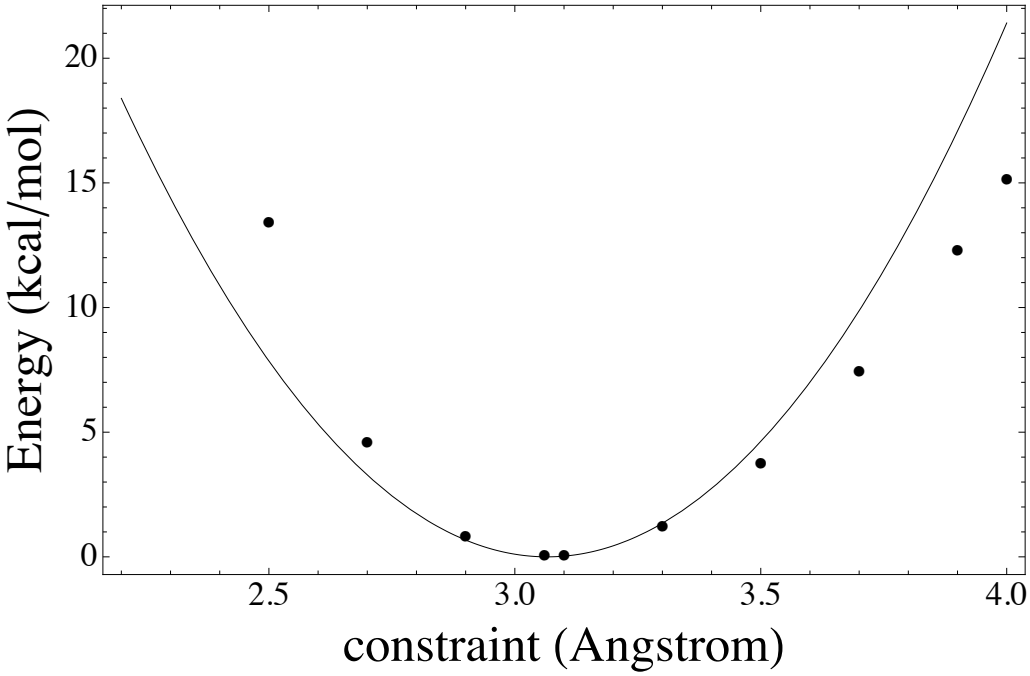

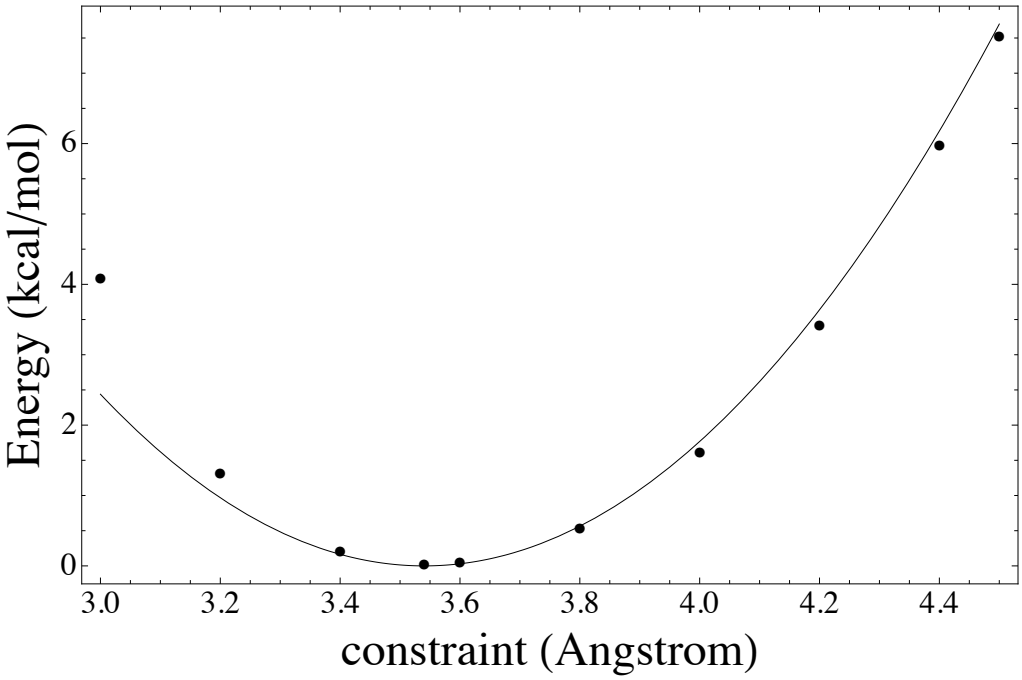

Figure 2.5: The reactant (a) and transition-state (b) energies of *cis*-1,2-dimehtylbenzocyclobutene as a function of the extension R_{ij}. The energy in each case is measured relative to its respective minimum value. Solid lines show the harmonic approximation (Eqs. 2.16, 2.18) while the solid symbols represent results of constrained optimization.

The quality of the harmonic approximation (Eq. 2.18), when applied to the same model systems as in Section 3, is examined in Figures 2.5 and 2.6. Using Eq. 2.16 and 2.18, we calculate a harmonic estimate of $U^{(0,TS)}(R_{ij})$ and compare it with the "exact" result obtained via constrained optimization of the reactant and transition states, as described in Section 3. While the harmonic approximation is exact for small extensions, nonlinear effects become significant for larger extensions. In the case of the *cis* isomer, the harmonic approximation is seen to work better for the transition state than for the reactant. For the *trans*-isomer, we see an opposite trend: Significant deviations from the harmonic approximation are observed in the transition state for rather small deformations (~0.1Å). Nevertheless, because the stiffness of the molecule (i.e., the curvature of the dependence seen in Fig. 2.6b) is much higher in this case than for the *cis*-isomer, the resulting elastic energy is very small, only fractions of kcal/mol (given the same value of the force), and so the elastic energy term is essentially negligible in the force dependence of the activation barrier observed in Fig. 2.4b.

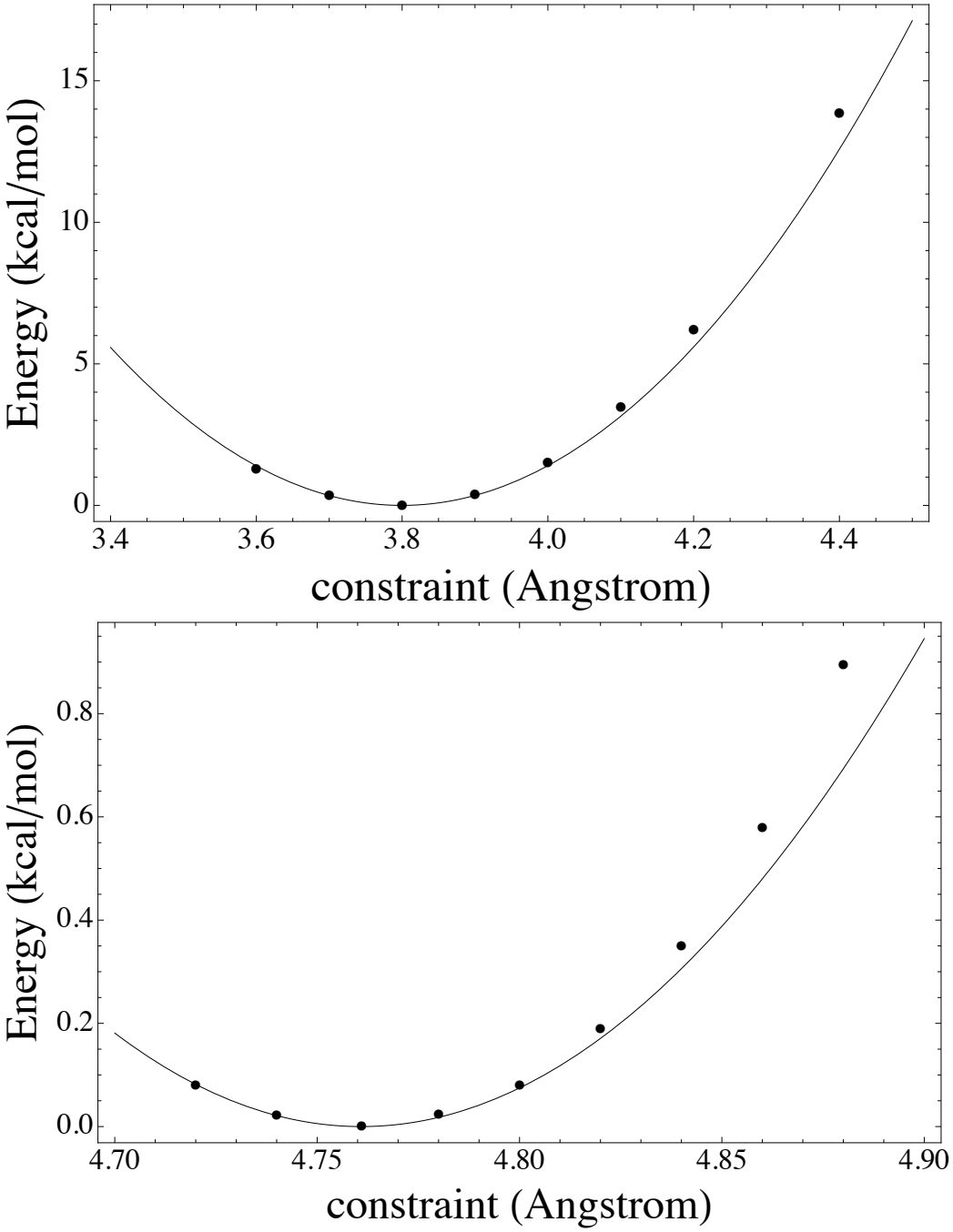

Figure 2.6: The reactant (a) and transition-state (b) energies of *trans*-1,2-dimehtylbenzocyclobutene as a function of the extension R_{ij}. The energy in each case is measured relative to its respective minimum value. Solid lines show the harmonic approximation (Eqs. 2.16, 2.18) while the solid symbols represent results of constrained optimization.

Finally, it is instructive to compare EBT to the phenomenological cusp-shaped potential model (CSPM)[56, 104], which is perhaps the simplest model that can account for experimentally observed deviations from Bell's theory [71]. Similarly to EBT, CSPM assumes the effective potential along the pulling coordinate R_{ij} to be a harmonic reactant well. In contrast, the cusp-shaped barrier implies that the location of the CSPM transition state does not depend on the force. Formally, this corresponds to setting $\chi_{ij}^{(TS)} = 0$ in EBT, or, equivalently, to dropping the term containing the transition-state Hessian in Eq. 2.9. Both CSPM and EBT predict that the reaction barrier $V^{\neq}(F)$ is a second-degree polynomial of F. However, in the multidimensional case, there is qualitative difference between the CSPM and EBT predictions regarding the curvature of the $V^{\neq}(F)$ dependence. Specifically, CSPM always predicts the last term in Eq. 2.20 to be positive so that the overall force dependence of the reaction barrier $V^{\neq}(F)$ is weaker than in Bell's theory. As discussed in Section 2, this is not necessarily the case for EBT: While $\chi_{ij}^{(0)}$ is always positive, the sign of $\chi_{ij}^{(TS)}$ can be variable, and the resulting force dependence of the reaction barrier can be either stronger (cf. Fig. 2.4a) or weaker than that predicted by Bell's formula.

CONCLUDING REMARKS

In this chapter, we have examined an extension of Bell's theory that includes second-order corrections in the dependence of the reaction barrier on the mechanical force. Our approach is exact (inasmuch as the energies predicted by electronic structure

calculations are viewed as exact) in the limit of sufficiently weak force. Like the original formulation developed by Bell, the extended Bell theory requires only zero-force information about the structures and the energies of the molecule in the transition and the reactant state. Therefore, this approach allows one to predict the effect of a mechanical force, applied to any atoms of the molecule, without explicitly incorporating stress or strain into electronic structure calculations. Our numerical example shows that EBT is considerably more accurate than the standard formula due to Bell. Moreover, EBT provides a convenient way of characterizing the sensitivity of any reaction pathway to a mechanical force using two parameters, namely the change in distance, ΔR, and the change in the compliance, $\Delta\chi$, between the initial and transition states. The sign and magnitude of these two quantities allow one to quickly predict the force dependence of the reaction rate.

This substantial computational gain offered by EBT over explicit calculations involving force comes at a cost: First, while the second-order correction is sufficient in the examples considered in Section 3, there is no guarantee that this is always the case for any value of the force that is relevant in practice. Second, our theory assumes that the force continuously transforms the transition state without changing its underlying properties. At sufficiently high forces, however, the topography of the underlying potential surface may change and the saddle point – and the corresponding reaction channel – may, for example, disappear altogether. When this happens, then one has no other choice but to explicitly include the force in the calculations[86]. An example of this behavior is readily seen in the example studied in Section 3, where EBT provides no

warning signs that the conrotatory reaction channel would disappear[86] for forces higher than ~1nN.

While the above caveats certainly cannot be disregarded, we note that the validity of our approach for any given reaction is straightforward to verify by comparing the EBT prediction with a calculation that explicitly includes a force that corresponds to the maximum relevant force. Such a test is relatively inexpensive because it involves a single transition state search. Moreover, even in the regime where the accuracy of EBT is not satisfactory, using the EBT estimate for the force-induced transition-state distortion (Eq. 2.7) as the initial guess may help speed up the search for the correct transition state.

Chapter 3: Regiochemical Effects on Molecular Stability: A Mechanochemical Evaluation of 1,4- and 1,5-Disubstituted Triazoles

ABSTRACT

Mechanochemistry or the modulation of chemical reactivity using mechanical forces has shown great promise in directing chemical transformations in otherwise prohibitive pathways. A recent study has shown that the highly inert 1,2,3-triazole molecule is susceptible to cycloreversion in the presence of ultrasound[8]. This work is extended to the case where polymer chains of varying molecular weight were grown from 1,4- and 1,5-disubstituted triazoles. Experimental evidence suggests that the rate constant for the cycloreversion of the 1,5-disubstituted triazoles was 1.2 times larger than that of the 1,4-disubstituted congener[7]. The difference was attributed to the increase mechanical deformability of the 1,5-regioisomer as compared to the 1,4-isomer. This interpretation was supported by computational studies, which employed the extended Bell theory to predict the force dependence of the activation barriers for the cycloreversions of both isomers.

INTRODUCTION

The burgeoning field of polymer mechanochemistry, wherein exogenous forces are directed to chemical functionalities in a locally anisotropic manner through polymer actuators, presents the opportunity to precisely direct chemical reactivity down specific pathways[3, 15]. As a result, mechanical forces have been shown to facilitate a number of intriguing, and often novel, transformations[6, 8, 11, 123-125]. For example, a recent study has shown that mechanochemical approaches could effect the formal [3+2] cycloreversion of

1,4-disubstituted 1,2,3-triazoles, a process that currently cannot be accessed through any other stimuli (thermal, photochemical, etc.)[8]. We hypothesized that the 1,5-disubstitued isomers[126] of 1,2,3-triazoles, might also be susceptible to cycloreversion under mechanical activation (Figure. 3.1). Furthermore, we reasoned that 1,4- and 1,5-disubstituted triazole mechanophores presented a unique opportunity to explore regiochemical effects on molecular stability using polymer mechanochemistry. Although stereochemistry has been shown to influence mechanochemical transformations[11, 89, 127], there have been no reports demonstrating how mechanical processes are influenced by the regiochemistry of the polymer attachments on the mechanophore. Beyond enriching the field of mechanochemistry[13, 128], such an endeavor was envisioned to provide insight that would be beneficial for the rational design of new mechanophores as well as force-responsive materials.

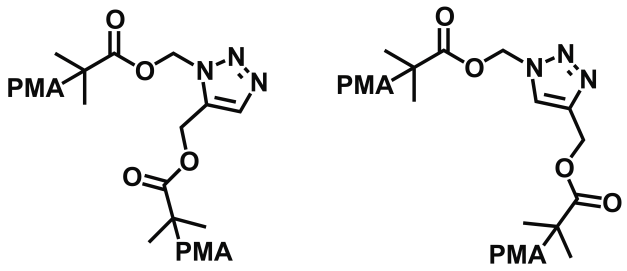

Figure 3.1: Structures of 1,5-disubstituted (left) and 1,4-disubstituted (right) triazoles contained within a poly(methyl acrylate) (PMA).

MODEL

Following ref.[83], the reaction barrier, as a function of force F, was computed according to the formula:

$$V^{\neq}(F) = V^{\neq}(0) - \mathbf{f}\left[\mathbf{r}^{(TS)}(0) - \mathbf{r}^{(0)}(0)\right] - \frac{1}{2}\mathbf{f}^T\left[\left(\mathbf{h}^{(TS)}\right)^{-1} - \left(\mathbf{h}^{(0)}\right)^{-1}\right]\mathbf{f}$$
$$\equiv V^{\neq}(0) + \Delta V_1^{\neq}(F) + \Delta V_2^{\neq}(F) \tag{3.1}$$

Here $\mathbf{f} = (f_{x1}, f_{y1}, f_{z1}, ..., f_{xN}, f_{yN}, f_{zN})$ is a 3*N*-dimensional force vector, whose components are given by the equations

$$\begin{aligned} &f_{xi} = -FE_x, f_{yi} = -FE_y, f_{zi} = -FE_z, \\ &f_{xj} = FE_x, f_{yj} = FE_y, f_{zj} = FE_z, \quad , \\ &f_{xk} = f_{yk} = f_{zk} = 0, \text{ for } k \neq i, j \end{aligned} \tag{3.2}$$

assuming that the pulling force is applied to atoms *i* and *j* such that it is aligned along the vector

$$(E_x, E_y, E_z) \equiv \mathbf{E} = \frac{\mathbf{R}_j - \mathbf{R}_i}{\left|\mathbf{R}_j - \mathbf{R}_i\right|} \tag{3.3}$$

connecting those atoms. The matrices $\mathbf{h}^{(0)}$ and $\mathbf{h}^{(TS)}$ in Eq. 3.1 are the Hessian matrices corresponding to the zero-force reactant and transition states and $\left(\mathbf{h}^{(0,TS)}\right)^{-1}$ is regarded as a generalized inverse that suppresses the terms corresponding to rigid body motion in the spectral expansion of the matrix.

The first- and second-order contributions can also be written, respectively, as

$$V_1^{\neq}(F) = -F\left(R_{ij}^{(TS)} - R_{ij}^{(0)}\right) \tag{3.4}$$

and

$$V_2^{\neq}(F) = -(\chi_{ij}^{(TS)} - \chi_{ij}^{(0)})F^2 / 2 \tag{3.5}$$

Here $R_{ij}^{(0,TS)}$ is the distance between the atoms in the reactant or transition state and $\chi_{ij}^{(0,TS)}$ is the corresponding molecular compliance (which is positive for the reactant state but can be either positive or negative for the transition state). The explicit expression for the compliances in terms of the Hessian matrices is given in ref. [83].

According to Eqs. 3.4 and 3.5, the first-order effect of the force on the reaction barrier is determined by the change in the distance R_{ij}, while the curvature of the dependence $V^{\neq}(F)$ is controlled by the difference in the compliances of the transition and reactant states.

RESULTS

Experimental evidence suggests that the rate constant for the cycloreversion of 1,5-triazole ($k_{1,5} = 3.22 \times 10^{-5}\ \text{min}^{-1}$) to be 1.2 times larger than that of the 1,4-isomer ($k_{1,4} = 2.76 \times 10^{-5}\ \text{min}^{-1}$)[7]. In an effort to explain the aforementioned rate differences, we first reasoned that the 1,5-triazole was more responsive to mechanical activation in part because the vicinal polymer attachments were localizing the mechanical forces generated under ultrasound to a smaller region of the triazole (i.e. the N1-C5 bond). In contrast, the polymers attached to the 1,4-regioisomer would translate mechanical energy across the heterocyclic scaffold, effectively requiring additional force to facilitate the cycloreversion process. We also reasoned that (1) the N1-C5 bond should be more susceptible to mechanical deformation than the N3-C4 bond (due to the rigidity imposed by the π-

character in the N2-N3 bond) and (2) the N1-C5 bond of the 1,5-regioisomer should be slightly weakened as a consequence of steric congestion.

To explore these viewpoints more quantitatively, we employed electronic structure calculations to probe the mechanically induced cycloreversion processes. Specifically, we used the recently described extended Bell theory (EBT)[83], which offers a computationally inexpensive alternative to methods that explicitly include the effect of mechanical stress[6, 86, 87] or strain[4] on molecular potential energy surfaces. Regardless, EBT accurately predicts mechanochemical reactivity using standard geometry optimizations and saddle point searches performed for mechanically unperturbed molecules[83]. The method also determines the force dependence of the activation barrier for a given transformation using only two parameters. The first parameter is the change in distance between the two atoms to which the force is applied in going from the reactant state to the transition state (TS). If this distance increases, then applying an elongational force across those two atoms should lower the overall reaction barrier.[24] Conversely, if the distance between these atoms decreases at the TS, then applying an elongational force should retard activation. The second parameter is the difference in the molecular compliance between the TS and the reactant state, which determines the curvature of the force dependence of the activation barrier. Thus, EBT generalizes the classic Bell model[101], which assumes that the barrier is linearly dependent on the force. While this method requires that the applied force not be too large, the amount of information that can be extracted from such a relatively simple set of calculations makes EBT attractive for the evaluation of mechanochemical phenomena.

EBT calculations for the triazole cycloreversions were performed with the NWChem package[115] using density functional theory[116], employing the 6-31G* basis set[117] and the B3LYP exchange-correlation energy functional[118]. Triazoles featuring 1,4- and 1,5-dimethyl substituents (TA1 and TA2, respectively; Figure 3.2) were initially chosen for the in silico evaluation of the cycloreversion process. In the case of TA1, the N1 and C4 atoms were considered to be the points to which the pulling forces were applied, as we reasoned that these nuclei would simulate the translation of mechanical force to the triazole moeity. Similarly, the N1 and C5 atoms were treated as the pulling points for EBT analysis of TA2. To determine which set of pulling points would more readily facilitate the triazole cycloreversion, the internuclear distances between the aforementioned atoms in TA1 and TA2 were calculated in the reactant and transition state geometries. As expected, the change in distance between the pulling points in TA2 was larger than the corresponding change between the pulling points in TA1 (0.93 Å for TA2 vs 0.62 Å for TA1). As such, TA2 was predicted to be more susceptible to mechanical activation than TA1 (vide infra; Figure 3.2). By extension, 1,5-disubstituted triazoles should respond to mechanical forces (i.e. undergo mechanical cycloreversion) more readily than their 1,4-disubstituted congeners, which was consistent with the experimental observations previously discussed.

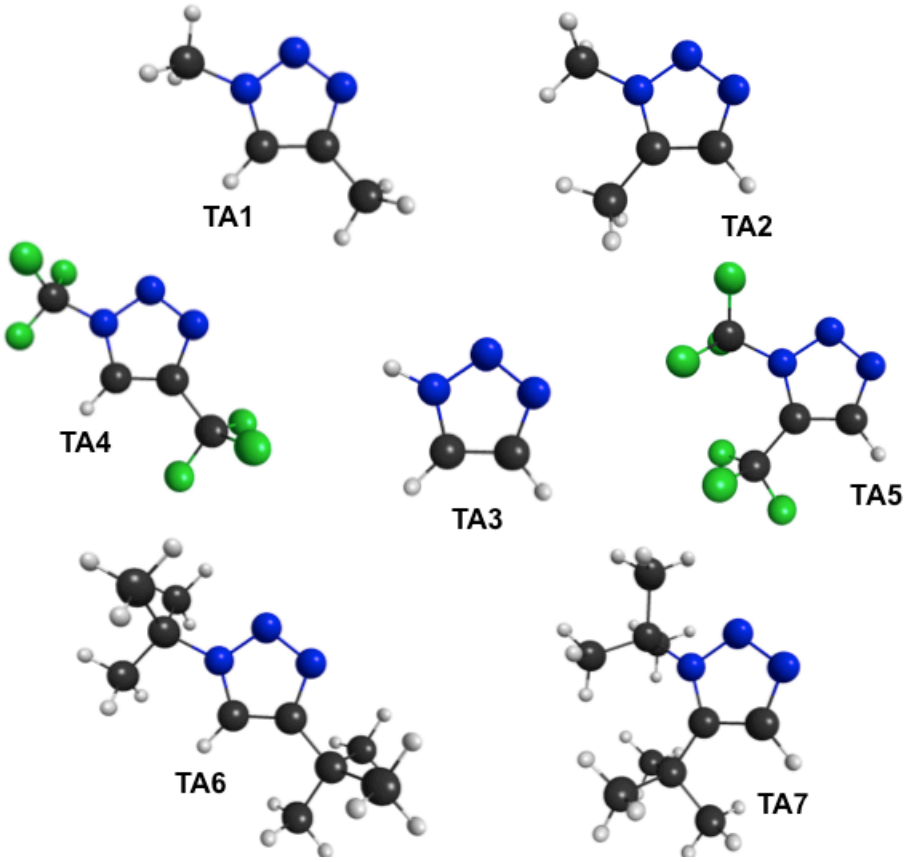

Figure 3.2: Reactant state geometries of **TA1**-**TA7**. Legend: C, black; H, white; F, green; N, blue.

The intrinsic reactivity of the 1,2,3-triazole was explored through evaluation of an analogue bearing only hydrogen substituents, and therefore devoid of steric bulk or highly perturbing electronic effects (**TA3**; Figure 3.2). As in the aforementioned calculations, the change in the N_1-C_5 internuclear distance from the reactant state to the transition state was larger than the corresponding change in the N_1-C_4 distance (0.85 Å vs 0.60 Å), consistent with the hypothesis that direct bond activation in the 1,5-regioisomer (in contrast to force translation across the 1,4-regioisomer) facilitates the cycloreversion

process by pulling the triazole into a TS geometry for the retro-[3+2] reaction. Since stereoelectronic effects were negligible in **TA3**, this result also suggested that the N_1-C_5 bond is inherently more susceptible to mechanical deformation than the N_3-C_4 bond, which could result from the rigidity imposed by the N_2-N_3 bond (*vide supra*). Collectively, these results further supported the conclusion that 1,5-disubstituted triazoles were intrinsically more susceptible to mechanical activation than the corresponding 1,4-regioisomers.

Having explored the intrinsic susceptibility of 1,4- and 1,5-disbustituted triazoles to mechanical activation, the response of the cycloreversion energy barrier to exogenous forces was probed using EBT. Figure 3.3 shows the predicted changes in the reaction barriers for the cycloreversions of **TA1** (black) and **TA2** (blue) as a function of force, hereafter referred to as force curves (FCs). A series of functionalized triazole analogues (**TA4-TA7**, Figure 3.2) were also evaluated computationally in the manner previously discussed (*vide supra*) to elucidate electronic or steric effects on the cycloreversion process. Importantly, the zero force barriers corresponding to cycloreversions of the 1,5-regioisomers were lower than those of the analogous 1,4-regioisomers in all cases. Building on this result, we sought to draw a comparison between predicted trends in cycloreversion and known triazole reactivity. We reasoned that electron deficient triazoles should be predicted to undergo cycloreversion more readily than electron rich analogues, as electron deficient triazoles are known to participate in the Dimroth rearrangement[129]. Toward this end, the zero force barriers to cycloreversion for bis(trifluoromethyl) substituted triazoles (**TA4** and **TA5**) and dimethyl substituted

triazoles (**TA1** and **TA2**) were compared. As expected, the activation energies for the cycloreversions involving the dimethylated isomers (E_a = 90.7 kcal/mol for **TA1**; E_a = 88.9 kcal/mol for **TA2**) were found to be larger than those for the analogous trifluoromethyl congeners (E_a = 85.0 kcal/mol for **TA4**; E_a = 68.7 kcal/mol for **TA5**). Since this result conformed to our prediction, we turned our attention to an evaluation of steric effects on the cycloreversion processes.

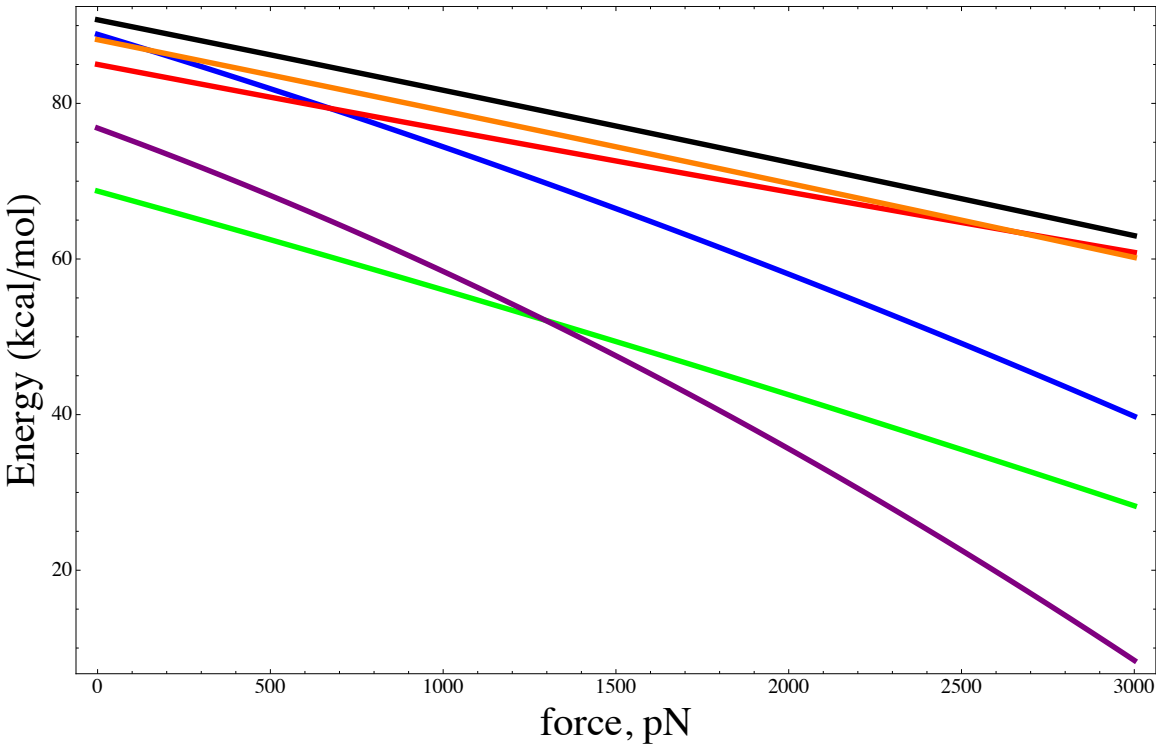

Figure 3.3: Force curves for **TA1** (black), **TA2** (blue), **TA4** (red), **TA5** (green), **TA6** (orange), and **TA7** (violet). Energy barrier refers to the predicted activation energy for the cycloreversion of the triazole analogue.

To explore the role of sterics, the cycloreversions of dimethyl substituted triazoles were compared to bis(t-butyl) analogues (**TA6** and **TA7**). We reasoned that the relative

differences between the zero force energy barriers for each set of analogues would reveal the extent to which steric congestion influenced the cycloreversion processes. In accord with this assessment, the difference between the aforementioned barriers for the cycloreversions of **TA1** and **TA2** (ΔE_a= 1.87 kcal/mol) was calculated to be smaller than that of **TA6** and **TA7** (ΔE_a= 11.37 kcal/mol). This result also demonstrated that steric interactions present in 1,5-disubstituted triazoles were increasing the overall molecular compliances, as evidenced by the appreciable curvature of the FC for **TA7**. Indeed, the FCs for all of the 1,5-analogues exhibited greater curvature than those of the corresponding 1,4-isomers. It should also be noted that **TA7** exhibited the largest force dependence of all the small molecule analogues that were analyzed using EBT, as evidenced by the precipitous decrease in activation energy for the cycloreversion of this analogue under increasing force (Figure 3.3). Collectively, these results indicated that, in combination with the intrinsic deformability of the N_1-C_5 bond, steric congestion rendered the 1,5-regioisomer more susceptible to mechanical activation than the 1,4-regioisomer.

CONCLUSIONS

In summary, we provide computational evidence for the mechanically facilitated cycloreversion of 1,5-disubstituted triazoles to afford azide and terminal alkyne moieties. In agreement with experimental data, the difference in the rate of cycloreversion between the 1,5- and 1,4-isomer was explained computationally by a combination of increased molecular compliance and direct bond activation in the case of the former. In a broader

context, these results indicate that the relative regiochemistry of the polymer attachments on a mechanophore must be considered when evaluating or designing mechanochemical systems.

Chapter 4: Molecular Catch Bonds and the Anti-Hammond Effect in Polymer Mechanochemistry

ABSTRACT

While the field of polymer mechanochemistry has traditionally focused on the use of mechanical forces to accelerate chemical processes, theoretical considerations predict an underexplored alternative: the suppression of reactivity through mechanical perturbation. Here, we use electronic structure calculations to analyze the mechanical reactivity of six mechanophores, or chemical functionalities that respond to mechanical stress in a controlled manner. Our computational results indicate that appropriately directed tensile forces could attenuate (as opposed to facilitate) mechanochemical phenomena. Accompanying experimental studies supported the theoretical predictions and suggested that relatively simple computational models may be used to design new classes of mechanically responsive materials. In addition, our computational studies and theoretical considerations implicated the prevalence of the anti-Hammond (as opposed to Hammond) effect (*i.e.*, the increased structural dissimilarity between the reactant and transition state upon lowering of the reaction barrier) in the mechanical activation of polyatomic molecules.

INTRODUCTION

The use of mechanical forces to bias chemical reactions, commonly referred to as mechanochemistry[3, 15, 16], has increasingly found applications in the synthetic and materials science communities. Within this field, polymer mechanochemistry, or the mechanical manipulation of reactive functional groups (termed mechanophores)

embedded within polymeric matrices, has attracted considerable attention due to its ability to facilitate a number of otherwise kinetically inaccessible processes[7-12, 127]. While theoretical models have been shown to successfully account for these experimental observations[13, 69, 81-83, 85, 86, 89, 130], such models are typically used as post-experimental rationalizations. Here, we show that theoretical analysis may be used to guide the rational design of mechanophores that exhibit novel, force induced reactivity. Moreover, our results uncovered general trends in the mechanical response of polyatomic molecules that have significant implications for the design of new mechanophores and force responsive materials. These trends stem from the inherent multidimensionality of mechanochemical processes and, therefore, cannot be accounted for by one-dimensional models commonly used to explain mechanical activation[100, 101]. Indeed, while the one-dimensional approximation necessitates that force acts in the direction of the reaction coordinate (RC), thereby lowering the transition state (TS) barrier and accelerating the associated transformation, we will show that such an alignment between the force and a typical RC is extremely improbable in the high-dimensional configuration space of a typical mechanophore.

THEORETICAL DISCUSSION

Misalignment between mechanical stress and the targeted reaction pathway can result in a number of distinct scenarios. Figure 4.1 illustrates some of these activation motifs using a model two-dimensional potential energy surface (PES) that exhibits a single minimum (which corresponds to the reactant) and a saddle-point (which

corresponds to the TS). Of the two coordinates that specify the molecular configuration, R quantifies the mechanical strain (which, in most experimental studies, corresponds to the distance between a pair of atoms on which the applied force is exerted), and X represents the remaining molecular degrees of freedom. While similar scenarios to those depicted in Figure 4.1 have been explored[108, 109, 131], we emphasize that the reduction to two degrees of freedom is an oversimplification in the present context and is only used for illustrative purposes.

A force F acting along the mechanical coordinate R performs mechanical work ($W = F\Delta R$) as the molecule evolves toward the TS, where ΔR is the change in the mechanical pulling coordinate. The activation energy is effectively lowered by W and the transition rate $k(F)$ is enhanced by a factor of $e^{W/k_BT} = e^{F\Delta R/k_BT}$. This result, commonly referred to in the literature as the "Bell formula" [10, 11], however, does not account for the force induced displacement of the reactant and transition states. If the true RC (*i.e.*, the steepest descent path connecting the TS saddle point to the reactant state minimum on the PES) coincides with the mechanical coordinate (Fig. 4.1A) then a stretching force pushes the TS toward the reactant. This phenomenon is usually referred to as the Hammond effect, which posits that the reactant and TS structures are driven toward each other as the barrier separating them is lowered[13, 48]. As the Hammond effect reduces the molecular distortion (*i.e.*, ΔR), it weakens the force dependence of the reaction rate.

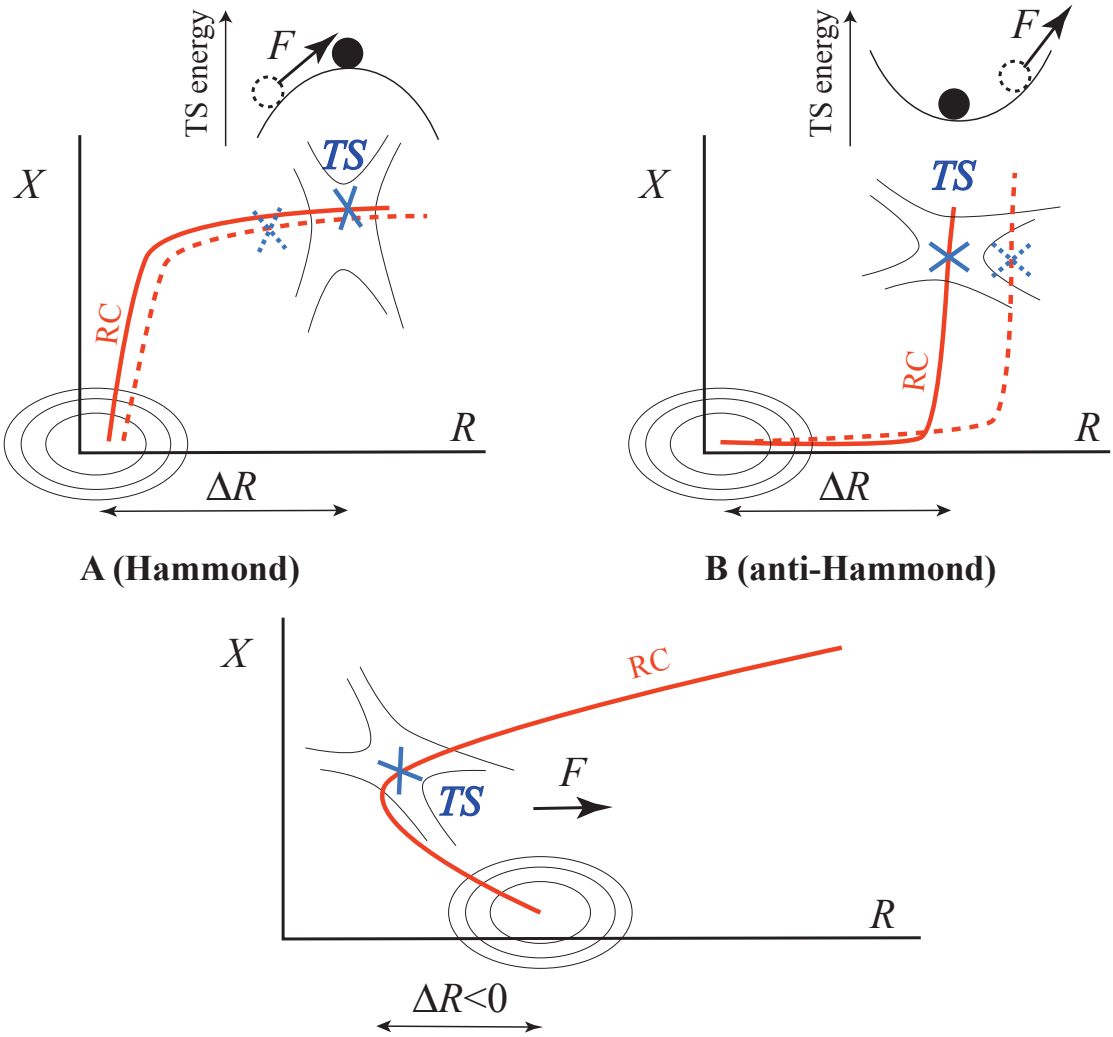

Figure 4.1: Force induced changes on a reaction pathway. (A) The Hammond effect, where the "true" reaction coordinate (RC, red line) is aligned with the mechanical coordinate (R). Mechanical equilibrium necessitates that a pulling force (F) shifts the TS toward the reactant state minimum (because the TS energy exhibits a maximum along R). The shifted RC and the new TS are shown as a dashed red line and a blue "X", respectively. (B) The anti-Hammond effect, where there is misalignment between RC and R (so that the TS exhibits a minimum as a function of R) and the TS is more compliant than the reactant. (C) Catch bond behavior, where molecular distortion along R initially decreases but later increases along the RC.

A very different scenario is shown in Fig. 4.1B, where the mechanical coordinate is misaligned with the RC in the vicinity of the TS saddle such that the TS energy exhibits a minimum (rather than a maximum) when R is varied. Consequently, a pulling force F may *increase* the separation between the TS and the reactant, thus resulting in "anti-Hammond" behavior. In this case, the structural separation between the reactant and the TS increases, but the energy barrier between these two states decreases. As the anti-Hammond effect increases the work done by the force, it provides an additional acceleration of the reaction rate.

These considerations are quantified in the recently reported Extended Bell Theory (EBT)[69, 83, 85], which accounts for the force induced shifts of the TS and reactant states along a given reaction pathway in the 3N-dimensional (where N is the number of atoms) configuration space of the molecular system of interest. To second order in the applied force, the reaction rate $k(F)$ is given by[56]:

$$\ln k(F)/k(0) = \left(k_B T\right)^{-1}\left(F\Delta R + F^2\Delta\chi/2\right) \tag{4.1}$$

The $F\Delta R$ term in Eq. 4.1 is identical to Bell's formula. The quadratic term results from the interplay of two effects: (1) the elastic energy stored in the molecule as a result of mechanical deformation and (2) the additional work done by the applied force as a result of the Hammond or anti-Hammond shift in ΔR. This shift is described by the formula:

$$\Delta\Delta R = \Delta R_{TS} - \Delta R_r = \chi_{TS}F - \chi_r F = \Delta\chi F \tag{4.2}$$

where χ_r and χ_{TS} are, respectively, the compliances of the reactant state and TS in response to pulling along R. These compliances can be computed from the molecule's (

$3N \times 3N$) Hessians in the reactant and TS configurations[56] as described below. A key departure from one-dimensional theories[10, 11] is that the TS compliance (χ_{TS}) can be either positive or negative[56]. As a result, both anti-Hammond ($\Delta R > 0; \Delta\chi > 0$) and Hammond ($\Delta R > 0; \Delta\chi < 0$) behavior is possible. We emphasize that the Hammond or anti-Hammond behavior is controlled by $\Delta\Delta R$, which is the shift in the reactant-to-TS distortion in response to force.

COMPUTATIONAL RESULTS AND DISCUSSION

To explore the correlation between mechanical activation and the direction along which the pulling force is exerted, we have performed a comprehensive survey of all possible pulling scenarios in the context of six previously reported mechanically induced transformations: the conrotatory electrocyclic ring opening of *cis* and *trans*-disubstituted benzocyclobutene[11], the formal [3+2] cycloreversion of 1,2,3-triazoles[7, 8], the formal [4+2] cycloreversions of a furan/maleimide Diels-Alder adduct and a maleimide/anthracene Diels-Alder adduct[10], and the isomerization of a spiropyran derivative[12] (Figure 4.2).

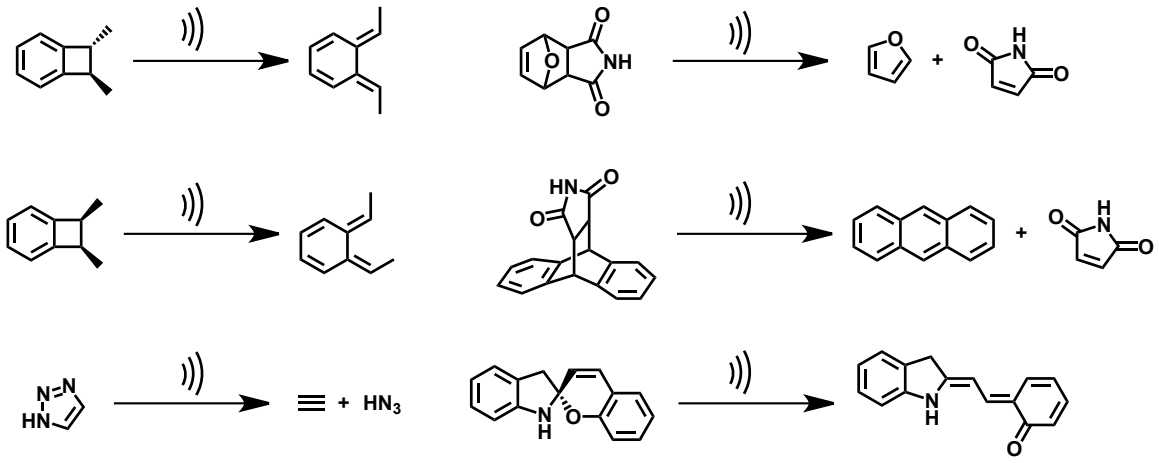

Figure 4.2: Mechanophore models.

In order to probe the intrinsic reactivity of each mechanophore in the absence of strongly perturbing steric or electronic environments, we employed truncated analogues bearing only hydrogen substituents (although methyl substituents were used to account for stereochemistry when necessary). For the same reason, polymeric handles, while important[70, 82], were not included in the calculations. In other words, the force in Eq. 4.1 is assumed to be exerted directly on a pair of atoms belonging to the mechanophore. The mechanism through which the force is transmitted to the mechanophore and its dependence on, *e.g.*, experimental design or the structure of the polymer backbone, is not considered here. Instead, we sought to demonstrate that the qualitative trends one obtains from our simplified model can aid in the experimental design of new systems (even though some pulling scenarios are strictly "thought" experiments).

EBT calculations were performed with the NWChem package[115] using density functional theory[116], employing the 6-31G* basis set[117] and the B3LYP exchange-correlation energy functional[118]. To verify the insensitivity of our results to the choice of

the density functional and the basis set, we also repeated calculations using the M05-2X hybrid meta exchange-correlation functional[132] and the 6-31++G**/6-31G* basis sets (see the Appendix for details). The nature of the stationary points was confirmed by a vibrational frequency analysis. In addition, each TS was confirmed by following the reaction coordinate from the TS to the reactant and the product using the intrinsic reaction coordinate (IRC) method[133, 134]. The force dependence of the reaction rate was estimated using Eq. 1, where $\Delta R = R_{TS} - R_r$ was computed from optimized reactant and TS geometries. To compute $\Delta\chi = \chi_{TS} - \chi_r$ we used the identity[83] $\chi_{r,TS} = 2/\lambda$, where λ is the nonzero eigenvalue of the 6x6 matrix

$$\bar{\mathbf{h}}_{11} = \mathbf{h}_{11} - \mathbf{h}_{12}\left(\mathbf{h}_{22}\right)^{-1}\mathbf{h}_{21} \tag{4.3}$$

computed, respectively, from the reactant or TS Hessian matrix

$$\mathbf{h} = \begin{pmatrix} \mathbf{h}_{11} & \mathbf{h}_{12} \\ \mathbf{h}_{21} & \mathbf{h}_{22} \end{pmatrix} \tag{4.4}$$

In Eq. 4.4, this matrix is written in block-form in terms of, respectively, 6×6, 6×(3N-6), (3N-6)×6 and (3N-6)×(3N-6) matrices $\mathbf{h}_{11}$, $\mathbf{h}_{12}$, $\mathbf{h}_{21}$, and $\mathbf{h}_{22}$[83]. Eq. 4.4 further assumes that the atoms are renumbered such that one always pulls on atoms 1 and 2. In contrast to the experimental and earlier computational studies, we evaluated all $N(N-1)/2$ possible pulling points for each mechanophore scaffold of *N* atoms, thus resulting in a total of 1456 simulated pulling experiments. The use of the EBT approximation allows one to accomplish this seemingly formidable task at modest computational expense.

We systematically determined $\Delta\chi$ ($i.e., \chi_{TS} - \chi_r$) and ΔR ($i.e., R_{TS} - R_r$) for each atom pair, and the corresponding results are summarized in Fig 4.3. Surprisingly, a comparable number of instances of reaction suppression ($\Delta R < 0$) and enhancement ($\Delta R > 0$) were observed. This finding is counterintuitive, as is apparent from the thought experiment involving the application of forces to the two atoms belonging to a diatomic molecule. Suppressing bond scission would require that the forces push the atoms toward each other, but such an arrangement of atoms leads to mechanical instability akin to that experienced by a pencil balanced on its tip. Direct bond compression, therefore, cannot account for reaction suppression, which, instead, must require an indirect mechanism involving coupled distortions of multiple bonds. A cartoon depiction of this suppression mechanism is given in Fig. 4.1C, where a RC in the multidimensional configuration space diverges from the mechanical coordinate such that the stretching force pushes the molecule away from its energetically favorable pathway.

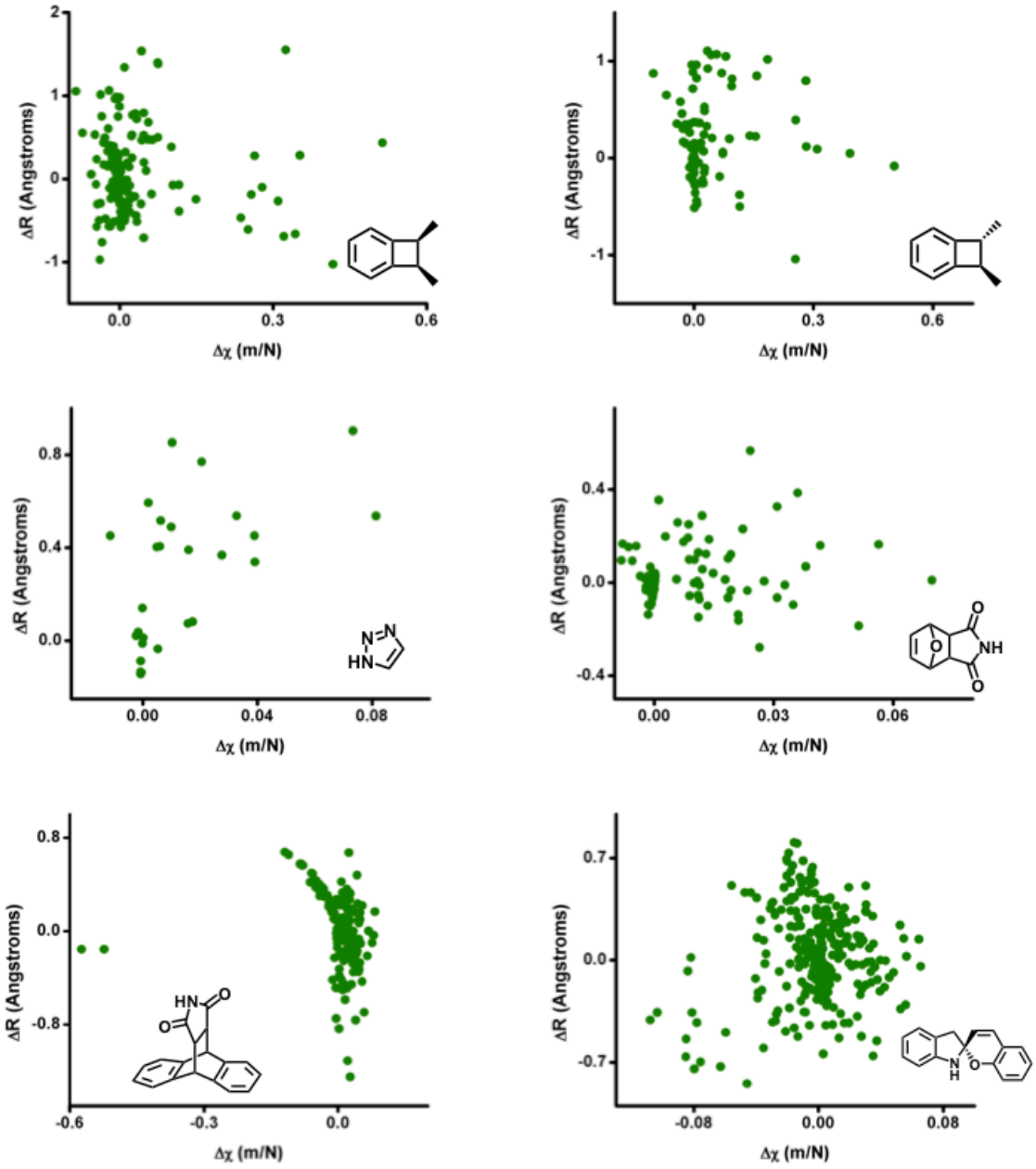

Figure 4.3: Computed values of ΔR and $\Delta\chi$ for all possible combinations of pulling points for the indicated mechanophores. Nearly all combinations result in a positive value of $\Delta\chi$; however, both signs of ΔR are present with almost equal frequency.

A similar phenomenon has been observed for the forced dissociation of biomolecular adhesion complexes[135], where mechanical suppression of dissociation is known as the "catch bond" or "molecular jamming" effect[55, 61]. While theoretically predicted[81, 85, 108, 109, 131], catch bonds are fairly atypical; conversely, "slip bonds", whose dissociation is promoted by force, are more common[136]. Only recently have catch bond effects (*i.e.*, the apparent strengthening of a covalent bond under mechanical stress) been implicated in mechanochemical transformations involving non-biological chemical systems. In particular, Boulatov and colleagues reported the kinetic stabilization of esters toward hydrolysis under tension[137], and Marx *et al*. showed that disulfide bonds are less susceptible to nucleophilic attack under the action of mechanical force[138]. Our results, however, suggest that catch bonds may be common in a variety of chemical transformations. A few salient examples are presented in Fig. 4.4, which show that even a subtle change in mechanophore design may result in a switch from slip bond to catch bond behavior. Moreover, a "rollover" phenomenon similar to that predicted for biomolecular catch bonds[81, 108, 109, 131] is observed (*i.e.*, a catch bond at low forces that becomes superseded by a slip bond at higher forces; for further details, see Figs. 4.7 - 4.9). The ability to selectively suppress a chemical transformation through the application of mechanical stress could have important design implications, particularly in the context of molecular machines or force responsive materials[139]. For example, mechanical degradation of such systems could be attenuated by directing external loads to mechanically labile bonds in a manner that would suppress bond scission. Furthermore,

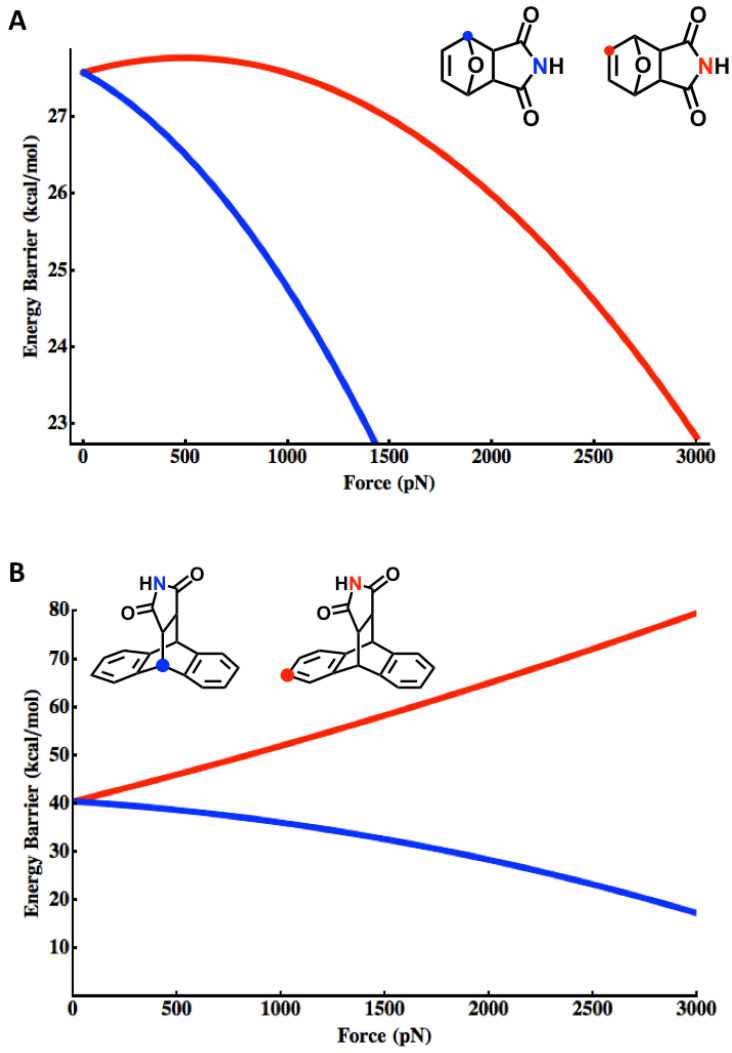

Figure 4.4: Examples of mechanically accelerated and mechanically suppressed reactivity. (A) Computed changes in the activation energy (equal to $U_{TS} - U_R - F\Delta R$, where $U_{r(TS)}$ is the reactant (or TS) energy on the force-modified potential energy surface) for the cycloreversion of a Diels-Alder adduct using pulling points for reaction acceleration (blue) and pulling points for reaction suppression (red). Note the rollover behavior: a catch bond at low forces is superseded by a slip bond at a higher force. (B) Computed changes in the activation energy for the cycloreversion of a Diels-Alder adduct using the pulling points for reaction acceleration (blue) and the pulling points for reaction suppression (red).

catch bond effects could potentially be harnessed to access materials that become more mechanically robust under stress.

A separate but equally intriguing trend observed in Fig. 4.3 is the predominantly positive sign of $\Delta\chi$, which underscores the prevalence of the anti-Hammond effect in this study. While puzzling at first glance, this result stems from the multidimensional character of the underlying PES. A negative sign for the TS compliance (χ_{TS}), which would lead to a negative $\Delta\chi$, becomes statistically unlikely for systems of high dimensionality. Indeed, as shown in Fig. 4.1A, χ_{TS} is negative only when the RC is sufficiently aligned with the mechanical coordinate R such that strain causes the TS energy to decrease. Since the TS configuration corresponds to a first-order saddle, there is only one normal mode along which the energy decreases, while there are $3N$-1 modes along which the energy increases (or remains constant). Thus, the probability of favorable alignment between R and the RC becomes vanishingly small with increasing number of atoms, N. If, for example, the pulling direction is a random vector in the $3N$-dimensional space, then this probability is shown (Appendix) to decrease exponentially with N, thereby rendering a negative value of χ_{TS} highly improbable even for systems of modest size. Indeed, for all cases displayed in Fig. 4.3, χ_{TS} was found to have a positive value (Fig. 4.5). Note, however, that symmetry requirements may lead to perfect alignment between R and RC in certain pulling arrangements. Such cases would be exceptions to the trend observed here.

Of course, a positive sign for χ_{TS} does not guarantee anti-Hammond behavior, since $\Delta\chi$ could still be negative if $\chi_{TS} < \chi_r$. This scenario, while explaining the few instances of negative $\Delta\chi$ observed in Fig. 4.3, should be rare, considering that the TS of a reaction involving bond scission is expected to be more mechanically labile than the relatively stable reactant state.

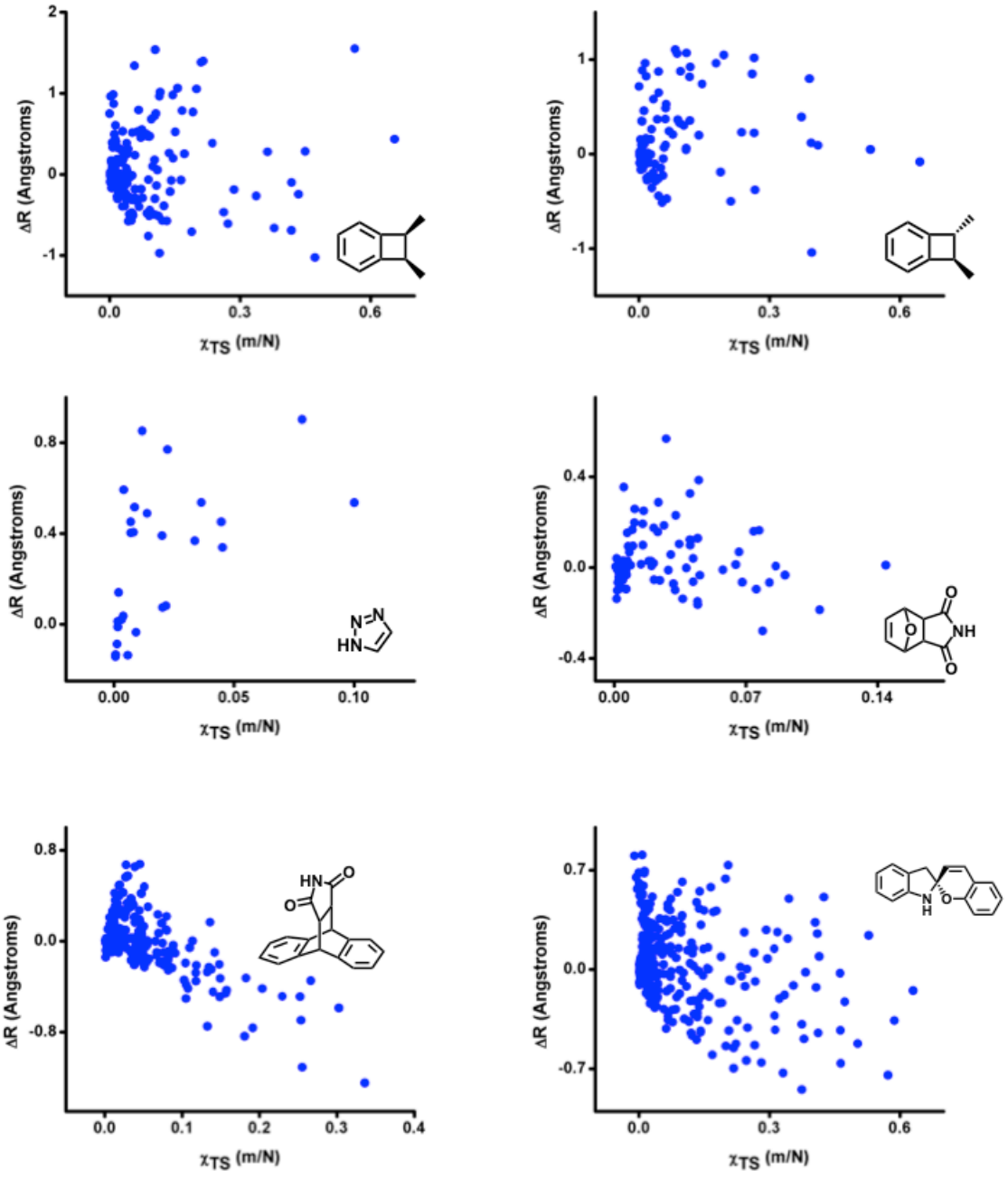

Figure 4.5: Computed values of ΔR and χ_{TS} calculated at the B3LYP/6-31G* level of theory for all possible pulling points in the indicated mechanophores.

Although our findings are based on calculations that employ the EBT approximation (whose limitations have been discussed in the literature[83, 85, 140]), the above general considerations indicate that our conclusions are, in fact, not critically dependent on the underlying EBT assumptions. For example, recent studies[70, 140] highlight the effect of the statistical-mechanical properties of the polymer backbone attached to the mechanophore on the overall mechanochemical reactivity. It would appear that multiple polymer conformations would invalidate the EBT assumption of a single TS. This situation is, however, common in condensed phase rate theory, where the assumption of a single PES saddle is inevitably incorrect. Coarse graining is the standard way of treating this problem, where nonreactive degrees of freedom (such as those of the polymer backbone or a solvent) are removed; as a result, the PES becomes replaced by a (typically smoother) effective *free* energy surface (FES)[141]. Within this framework, the EBT formula (4.1) can be derived from Kramers' type theory or its multidimensional generalization due to Langer (see, *e.g.*, Hanggi et al.[103]), provided that the extension ΔR is replaced by the *statistically averaged* extension and the susceptibilities χ_r and χ_{TS} are computed from the Hessian matrices of the FES[108, 142]. While the computation of a FES is a nontrivial task, the above arguments show that the anti-Hammond effect is caused not by some specific properties of the underlying PES but simply by its inherent multi-dimensionality. As such, this argument equally applies to any multidimensional FES. In support of this coarse-grained view of mechanochemical phenomena, studies of a two-dimensional FES led to the prediction of anti-Hammond behavior in force-induced protein unfolding[131], a finding supported by kinetic studies[143].

CONCLUSIONS

In sum, theoretical analysis revealed that anti-Hammond (rather than Hammond) behavior should be prevalent in the mechanically induced changes of molecular energy landscapes. In addition, our computational model predicted that mechanical forces may facilitate or suppress a given chemical transformation, depending on how they are applied. Experimental results supported the theoretically predicted reactivity trends and demonstrated that subtle changes in mechanophore design can lead to dramatic (and even counterintuitive) changes in mechanically induced reactivity[84]. Moreover, the work reported here constitutes the first example of utilizing a theoretical model in the *a priori* design and development of a novel mechanophore. Beyond its fundamental importance, the ability to mechanically suppress chemical reactivity is expected to find applications in materials science (*e.g.*, materials that resist mechanical degradation under stress) and facilitate future studies of force-induced biochemical phenomena[79].

APPENDIX

Computational details: Benchmark studies

DFT with the B3LYP functional was previously used for several mechanochemical studies involving the COGEF and EFEI methods for simulating mechanical stress[11, 86, 89]. B3LYP with the 6-31G* basis set was proven to provide excellent geometries for reactants and transition states involving pericyclic reactions[144]. To verify that our results were insensitive to the choice of the functional, we have also repeated calculations using the M05-2X functional, which was shown to compare well

with the more expensive and accurate electronic structure methods[145, 146]. Specifically, we compared the results from B3LYP/6-31G* with M05-2X/6-31++G**/6-31G* for 5 distinct mechanochemical processes: the conrotatory electrocyclic ring opening of a *cis*- and *trans*-disubstituted benzocyclobutene, the formal [3+2] cycloreversion of a 1,2,3-triazole, and the formal [4+2] cycloreversions of a furan/maleimide Diels-Alder adduct and a maleimide/anthracene Diels-Alder adduct. Results from B3LYP/6-31G* were compared with M05-2X/6-31G* for the maleimide/anthracene Diels-Alder adduct owing to the size of the mechanophore. We determined $\Delta\chi$ (*i.e.*, $\chi_{TS} - \chi_r$) and ΔR (*i.e.*, $R_{TS} - R_r$) for each atom pair using EBT (Eq. 4.1 from main text), and plotted the results from M05-2X/6-31++G**/6-31G* in comparison to B3LYP/6-31G* in Fig. 4.6.

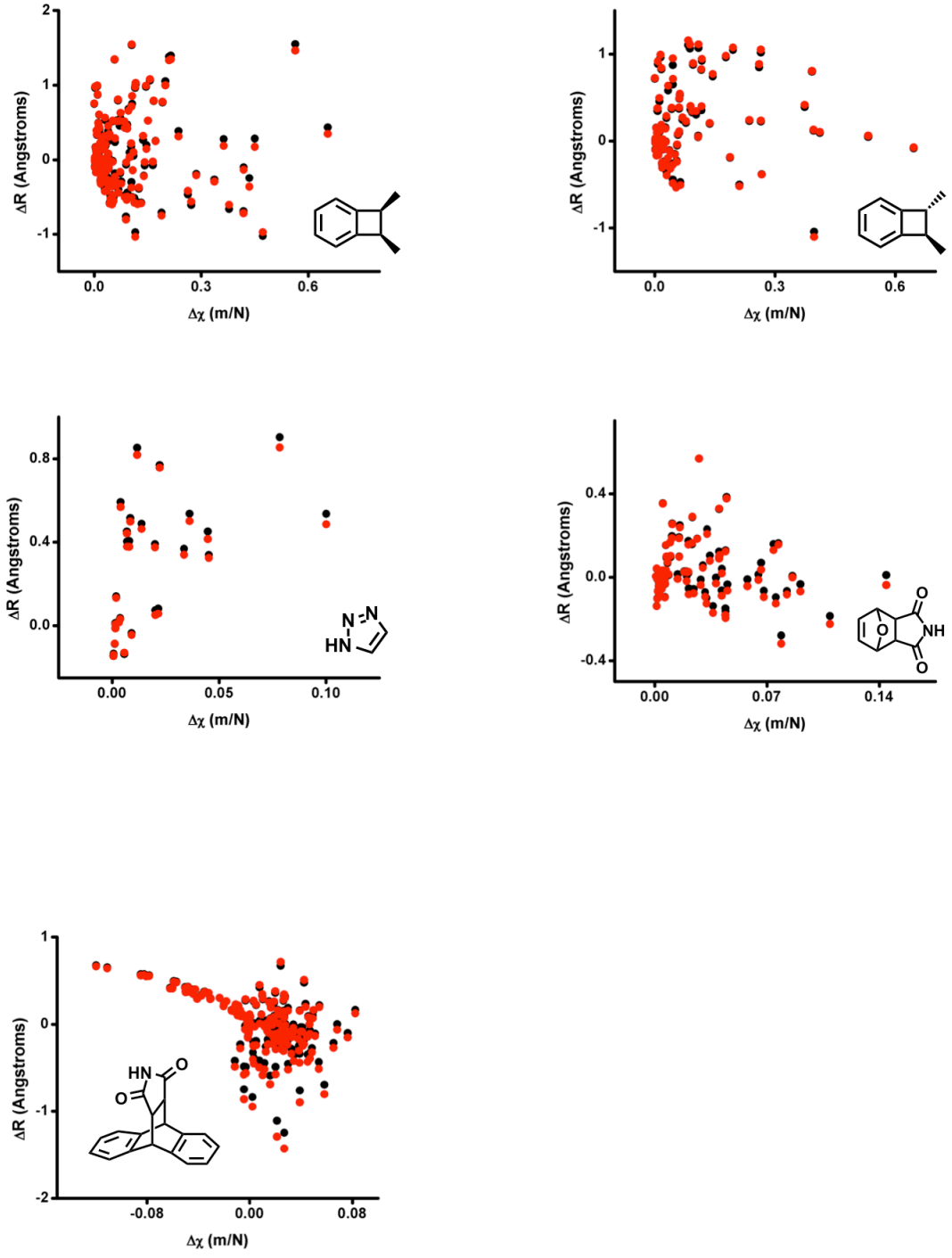

Figure 4.6: Comparison plots of ΔR and $\Delta\chi$ calculated using B3LYP/6-31G* (black) and M05-2X/6-31++G**/6-31G* (red) functionals.

Prevalence of the anti-Hammond effect on multidimensional energy landscapes: Probability considerations

Here we estimate the probability that "random" strain will decrease the energy of the molecule at the TS saddle resulting in $\chi_{TS} < 0$. In the vicinity of a TS saddle-point, the energy of the molecule (relative to that of the saddle) can be written in terms of appropriately chosen normal coordinates as

$$U = -k_1 u_1^2/2 + \sum_{i=2}^{n} k_i u_i^2/2 \ ,$$

where $n = 3N\text{-}6$ is the total number of degrees of freedom, excluding the translations and rotations. The first term accounts for the displacement along the unstable barrier mode. For simplicity, we will further assume that all k_i's are the same. Whenever the molecule's atoms are subjected to a small displacement, this sets a directional unit vector $\mathbf{u} = (u_1,....,u_n)$ in the n-dimensional space of the molecule's internal degrees of freedom. The ends of all such vectors lie on an n-dimensional sphere of unit radius. The susceptibility χ_{TS} is negative if $-u_1^2/2 + \sum_{i=2}^{n} u_i^2/2 < 0$. Assuming random direction of the vector, the probability of this is given by

$$P_n = S_{n-1}^{-1} \int ds_{n-1} \theta(u_1^2 - \sum_{i=2}^{n} u_i^2) \Big/ \int ds_{n-1} = S_{n-1}^{-1} \int ds_{n-1} \theta(2u_1^2 - 1) \ , \qquad (4.5)$$

where $\theta(x)$ is the Heaviside step function, $S_{n-1} \equiv \int ds_{n-1} = 2\pi^{n/2}/\Gamma(n/2)$ is the surface area of the sphere, and ds_{n-1} indicates integration over the (n-1)-dimensional surface of the sphere. Using the spherical coordinates

$$u_1 = \cos\varphi_1$$
$$u_2 = \sin\varphi_1 \cos\varphi_2$$
$$u_3 = \sin\varphi_1 \sin\varphi_2 \cos\varphi_3$$
...
$$u_{n-1} = \sin\varphi_1 \sin\varphi_2 ... \sin\varphi_{n-2} \cos\varphi_{n-1}$$
$$u_n = \sin\varphi_1 \sin\varphi_2 ... \sin\varphi_{n-2} \sin\varphi_{n-1}$$

and

$$ds_{n-1} = \sin^{n-2}\varphi_1 \sin^{n-3}\varphi_2 ... \sin\varphi_{n-2} d\varphi_1 d\varphi_2 .. d\varphi_{n-1} \ ,$$

we observe that integration over φ_1 decouples from that over the rest of the variables; therefore, the ratio of the two surface integrals in Eq. 4.5 can be written in terms of one-dimensional integrals:

$$P_n = \frac{\int_0^{\pi} d\varphi_1 \sin^{n-2}\varphi_1 \theta(2\cos^2\varphi_1 - 1)}{\int_0^{\pi} d\varphi_1 \sin^{n-2}\varphi_1} = 1 - \frac{\int_{\pi/4}^{3\pi/4} d\varphi_1 \sin^{n-2}\varphi_1}{\int_0^{\pi} d\varphi_1 \sin^{n-2}\varphi_1} = 1 - \frac{\int_{-1/\sqrt{2}}^{1/\sqrt{2}} dx (1-x^2)^{(n-3)/2}}{\int_{-1}^{1} dx (1-x^2)^{(n-3)/2}}$$

where $x = \cos\varphi_1$. For large *n* values, both integrals are dominated by the values of *x* that are close to 0; thus, their ratio is close to 1 and P_n becomes vanishingly small. In fact, P_n decreases exponentially with increasing *n*. Since the number of possible pulling directions (3*N*)(3*N*-1)/2 increases quadratically with the number of atoms, the probability that one of them will align with the unstable direction to result in a negative χ_{TS} becomes vanishingly small as *N* increases.

Illustrative Examples of Catch Bond Behavior

The formal [4+2] cycloreversions of a furan/maleimide and a maleimide/ anthracene Diels-Alder adduct were investigated for possible catch-bond scenarios using EBT. As shown in Figs. 4.4A and 4.7, the application of a mechanical force leads to initial reaction suppression at low forces and a rollover at high forces. The experimental pulling points correspond to atoms (bridgehead C_7 and the imide N_{17}; Fig. 4.7) that are further apart in the transition state than in the reactant configuration, which leads to an acceleration of the reaction. However, EBT calculations suggest that pulling on atoms C_3 and N_{17} (which move closer together in the transition state; Fig. 4.7) leads to a "jamming effect". This scenario is depicted in Fig. 4.1C where the mechanical pulling coordinate, R, first decreases but eventually increases at higher forces. An alternative explanation for the "jamming effect" is that the application of a stretching force at atoms C_3 and N_{17} prevents the necessary motion/mode to access the transition state. Specifically, a stretching force exerted on these atoms could promote a "slipping" motion, as opposed to the necessary pseudo-butterfly motion, that prevents cycloreversion. This effect can be overcome at sufficiently high forces, which results in the dissociation of the furan/maleimide fragments. A similar scenario can be seen in Figs. 4.4B and 4.8, where pulling on the mechanical coordinate leads to reaction suppression with no rollover at high forces. The experimental pulling points correspond to the atom pair (anthracene C_5 and imide N_{31}) that facilitates the reaction, whereas pulling on atoms C_8 and N_{31} leads to suppression of chemical reactivity. The absence of rollover at high forces results from a greater contribution of the first order term ($F\Delta R$) as compared to the second order term (

$F^2\Delta\chi/2$) and from the overall convexity of the energy barrier plotted as a function of the force (Fig. 4.4B), which, in turn, is a consequence of the negative sign of $\Delta\chi$.

Previous theoretical accounts have explored mechanochemical reactivity using hydrogen atoms as the pulling points[85, 147]. Consequently, we have investigated the mechanical suppression of reactivity in the maleimide/anthracene Diels-Alder adduct using the hydrogen atom substituents on C_5, C_8 and imide N_{31} as the pulling points (Fig. 4.9). Consistent with the trends shown in Fig. 4.4B, employing the hydrogen atoms as pulling points results in suppression of reactivity when pulling on the C_8 and N_{31} hydrogen atom substituents; conversely, the selection of the hydrogen atom substituents on C_5 and N_{31} as the pulling points results in an acceleration of mechanochemical reactivity.

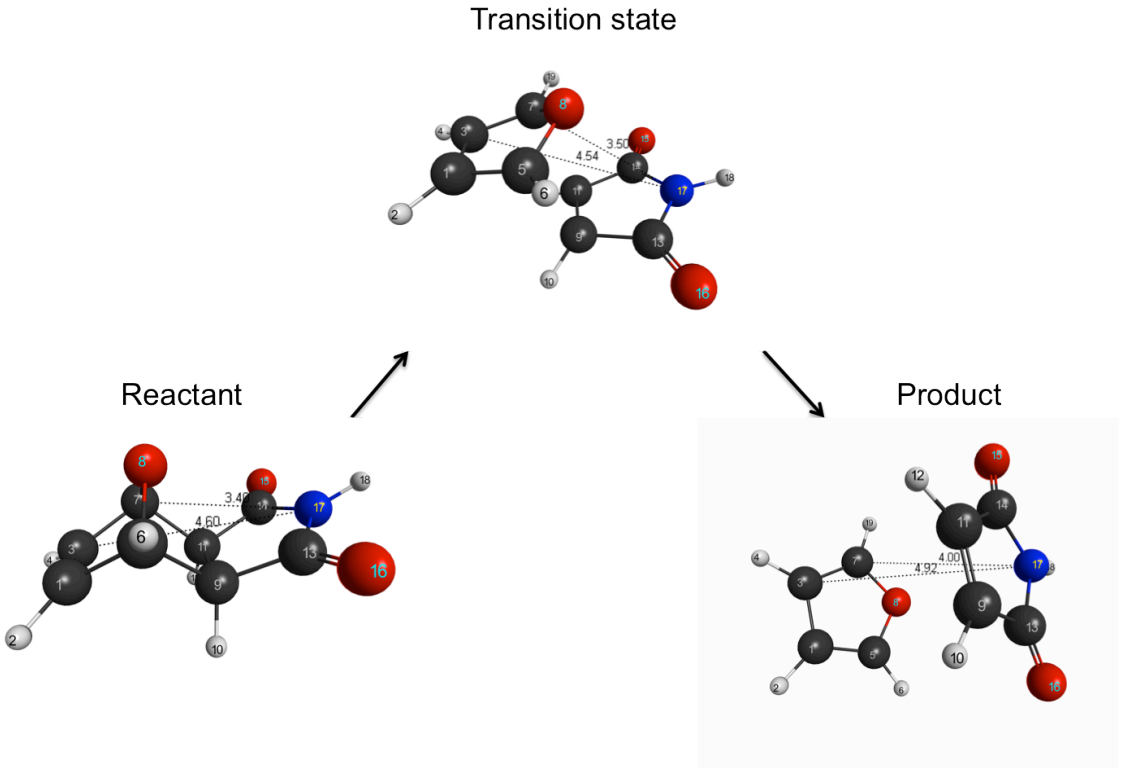

Figure 4.7: Computed values of ΔR at the B3LYP/6-31G* level of theory for the formal cycloreversion of a furan/maleimide Diels-Alder adduct. According to our theoretical predictions, pulling on the bridgehead C_7 and the imide N_{17} facilitates the reaction. In contrast, pulling on the methine C_3 and N_{17} suppresses the same transformation. Internuclear distances are indicated in Angstroms. Atom code: C (Black), H (White), N (Blue), O (Red).

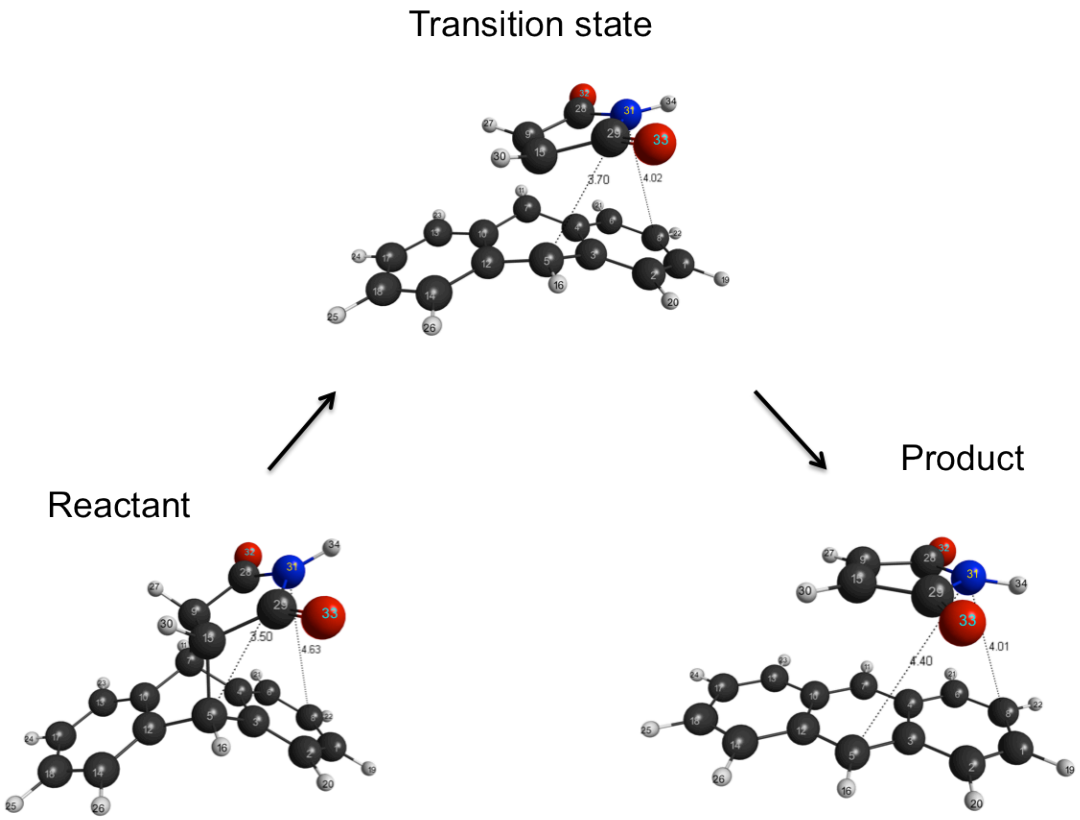

Figure 4.8: Computed values of ΔR at the B3LYP/6-31G* level of theory for the formal cycloreversion of a maleimide/anthracene Diels-Alder adduct. According to our theoretical predictions, pulling on the imide N_{31} and the anthracene C_5 facilitates the reaction. In contrast, pulling on the imide N_{31} and the anthracene C_8 suppresses the cycloreversion reaction. Internuclear distances are indicated in Angstroms. Atom code: C (Black), H (White), N (Blue), O (Red).

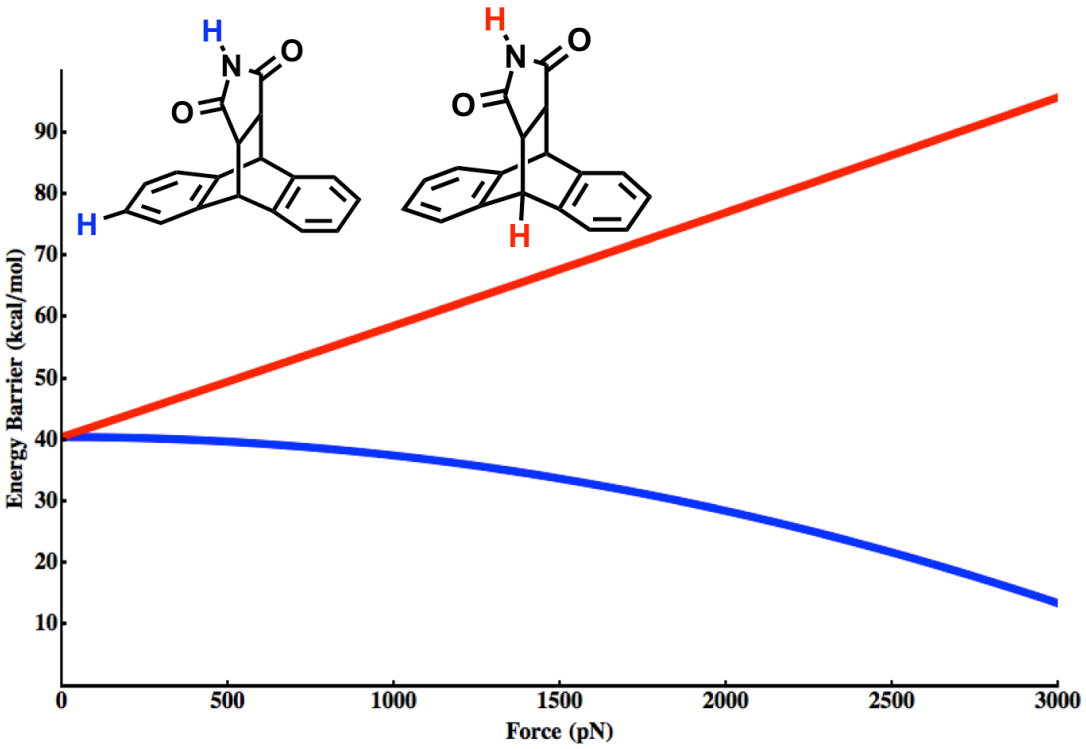

Figure 4.9: Computed changes in the activation energy (B3LYP/6-31G* level of theory) for the cycloreversion of a maleimide/anthracene Diels-Alder adduct using the hydrogen atom substituents on the N/C centers (as opposed to the ring N/C atoms; *cf* Fig. 4.4B) as pulling points for reaction acceleration (blue) and suppression (red).

Chapter 5: Exploring the topography of the stress-modified energy landscapes of mechanosensitive molecules

ABSTRACT

We propose a method for computing the activation barrier for chemical reactions involving molecules subjected to mechanical stress. The method avoids reactant and transition-state saddle optimizations at every force by, instead, solving the differential equations governing the force dependence of the critical points (i.e. minima and saddles) on the system's potential energy surface (PES). As a result, only zero-force geometry optimization (or, more generally, optimization performed at a single force value) is required by the method. In many cases, minima and transition-state saddles only exist within a range of forces and disappear beyond a certain critical point. Our method identifies such force-induced instabilities as points at which one of the Hessian eigenvalues vanishes. We elucidate the nature of those instabilities as fold and cusp catastrophes, where two or three critical points on the force-modified PES coalesce, and provide a classification of various physically distinct instability scenarios, each illustrated with a concrete chemical example.

INTRODUCTION

Control of chemical reactivity by mechanical forces has been the subject of many theoretical and experimental activities over the last several years. The coupling between chemical and mechanical processes has been explored, for example, in the context of single-molecule pulling studies of biomolecules[20, 30-64], DNA and protein transport across pores[25, 71-77], molecular motors[65-67], and materials chemistry[3, 5-8, 11, 13-15, 80-89]. Unlike

thermodynamic variables such as temperature or pressure, a mechanical force is a vector, a property that enables its use to drive chemical reactions along specific, desirable pathways. Rate calculations employing *ab initio* potential energy surfaces offer insights into the force effect on the reaction rates[3-7, 13, 14, 69, 81-89, 148] and, recently[84], have been employed for first principles design of mechanophores (i.e., mechanoresponsive molecules). The starting point of most such studies is the expression for the force-dependent reaction rate,

$$k(\mathbf{f}) = \nu \exp\left(-\frac{\Delta E(\mathbf{f})}{k_B T}\right), \tag{5.1}$$

where $\Delta E(\mathbf{f})$ is the force-dependent activation barrier. Here, the force $\mathbf{f}$ is viewed as a vector in the $3N$-dimensional space of the N-atomic molecular system. In other words, any combination of forces applied to each individual atom is, in principle, allowed, as long as the total force and the total torque on then molecule are zero, ensuring its mechanical stability. The most common pulling scenario involving a pair of opposing forces applied to two atoms then corresponds to a more restrictive choice of the force $\mathbf{f}$.

The activation barrier is computed as the energy difference between the transition-state (TS) saddle and the reactant-state (RS) minimum on the force-deformed potential energy surface (PES):

$$V_{\mathbf{f}}(\mathbf{r}) = V(\mathbf{r}) - \mathbf{fr} \ . \tag{5.2}$$

Here $V(\mathbf{r})$ is the zero-force potential energy viewed as a function of the $3N$-dimensional configuration vector $\mathbf{r}$, whose components are the x, y, and z coordinates of each atom. If

$\mathbf{r}_{RS}(\mathbf{f})$ and $\mathbf{r}_{TS}(\mathbf{f})$ are the force-dependent positions of the RS minimum and the saddle, then we have

$$\Delta E(\mathbf{f}) \equiv V\left[\mathbf{r}_{TS}(\mathbf{f})\right] - V\left[\mathbf{r}_{RS}(\mathbf{f})\right] - \mathbf{f}\left[\mathbf{r}_{TS}(\mathbf{f}) - \mathbf{r}_{RS}(\mathbf{f})\right] \tag{5.3}$$

Two types of approaches have been proposed to estimate the activation barrier of Eq. 5.3. The first one is "exact"[82, 86] (inasmuch as the computed underlying potential energy and transition-state theory expression of Eq. 5.1 are deemed exact). For any value of the applied force, it seeks, numerically, the minimum and the saddle configurations $\mathbf{r}_{RS}(\mathbf{f})$ and $\mathbf{r}_{TS}(\mathbf{f})$ corresponding to the force-modified potential $V_{\mathbf{f}}(\mathbf{r})$. Equivalently, the same result can be obtained from minimum and saddle-searches on a strain-modified PES, where appropriate distance constraints are applied to the pulling points[3, 4, 89]. These brute-force approaches are costly because a saddle-point search, for any force, requires evaluation of the electronic energies for multiple molecular structures. In response to this challenge, approximate methods were sought that estimate the force dependence of the activation barrier using electronic energies and molecular configurations at zero-force. The simplest one neglects the force dependence of the configurations $\mathbf{r}_{RS}(\mathbf{f})$ and $\mathbf{r}_{TS}(\mathbf{f})$ thus resulting in a linear force dependence of the barrier in Eq.3. This result is commonly referred as the "Bell formula"[101] although it was proposed earlier in different contexts[19, 100].

A simple extension of the Bell formula[69, 83, 85, 88] accounts for the displacements in $\mathbf{r}_{RS}(\mathbf{f})$ and $\mathbf{r}_{TS}(\mathbf{f})$ to first order, and for the change in the reaction barrier to second order in the force **f**. Perhaps somewhat inaccurately, we termed this approach the extended Bell

theory (EBT)[83]. Like Bell's formula, EBT does not require any information other than the TS and RS configurations, energies, and Hessians evaluated at zero force, thus providing considerable computational savings as compared to the brute-force approaches. EBT can also be extended to include quantum mechanical effects[149]. The disadvantage of the EBT approximation is that it is just that: an approximation. Its most glaring deficiency is that it fails to account for the changes in the reaction mechanism that may occur at high forces. That is, the particular TS may disappear at a certain value of the force, resulting in a switch to an alternative reaction mechanism[150] or even to a barrierless, downhill process. EBT, in contrast, assumes that the TS configuration evolves continuously with the force and, therefore, exists regardless of the value of the force[83, 85]. Although chemical insight combined with calculations may allow one to discover such reaction mechanism switches even within the EBT framework[85], a more automated way of detecting those phenomena is desirable.

A switch in a reaction mechanism presents a difficulty even for brute-force calculations. In practice, disappearance of a particular TS at a certain force is manifested by the failure of the optimization routine to find a saddle point[85]. But such a failure could also be blamed on an inadequate saddle search routine or impatience of the researcher. Moreover, finding the exact force at which the TS disappears by analyzing the code's failures is both problematic and inefficient.

The purpose of this chapter is to describe and validate an exact method that tracks the evolution of any given PES critical point (RS or TS) as a function of the applied force. Depending on both the pulling geometry and the energetics of the reaction, the

force-induced evolution of a critical point may come to an end at a certain force, above which this critical point no longer exists. Our method automatically detects such force-induced instabilities. We further classify possible types of instabilities encountered as the PES topology evolves with the force. By adapting results from differential geometry and catastrophe theory to the specific case of force-modified PES, we thus provide a systematic mathematical framework for describing mechanochemical phenomena.

EVOLUTION OF PES SADDLES AND MINIMA IN RESPONSE TO AN EXTERNAL FORCE

Consider a one-dimensional particle subjected to a potential $V(x)$ and an external force f. The critical points of the force-modified potential, $V_f(x) = V(x) - fx$, are given by $(d/dx)\left[V(x) - fx\right] = 0$ or

$$V'(x) = f \ . \tag{5.4}$$

If the force is increased by df then the change in the critical point position can be found from the equation

$$V'(x + dx) = V'(x) + V''(x)dx = f + df \ ,$$

or

$$dx = df / V''[x(f)] \ , \tag{5.5}$$

where $x(f)$ describes the "trajectory" spanned by the critical point when the force is varied. Eqs. 5.4 - 5.5 are easily generalized to the multidimensional potential of Eq. 5.2. The molecular configurations corresponding to its critical points (i.e., minima, saddles and maxima) satisfy the equation

$$\nabla V = \mathbf{f}\,, \tag{5.6}$$

where ∇V is the PES gradient. The multidimensional equivalent of Eq. 5.5 is then

$$d\mathbf{r} = \mathbf{h}^{-1}[\mathbf{r}(\mathbf{f})]\mathbf{df}\,, \tag{5.7}$$

where $\mathbf{h}(\mathbf{r})$ is the Hessian matrix corresponding to the PES $V(\mathbf{r})$. In most of the pulling studies, the direction of the force vector is constant, so we can write $\mathbf{f} = F\mathbf{l}$, where F is the absolute value of the force and $\mathbf{l}$ is a vector that specifies its direction. Integrating Eq. 5.7, we now obtain

$$\mathbf{r}(F) = \mathbf{r}(0) + \int_0^F \mathbf{h}^{-1}[\mathbf{r}(F')]\mathbf{l}\,dF' \tag{5.8}$$

The approach presented here is based on Eq. 5.8. Starting with a zero-force TS saddle or RS minimum, we propagate Eq. 5.8 numerically using a finite difference method. Thus, the method requires only a single saddle search performed at zero force, just like in EBT. At the same time, uncontrolled approximations inherent to EBT are no longer made.

The reaction barrier is now computed using Eq. 5.3, or, equivalently

$$\Delta E(F) \equiv V\left[\mathbf{r}_{TS}(F)\right] - V\left[\mathbf{r}_{RS}(F)\right] - F\mathbf{l}\left[\mathbf{r}_{TS}(F) - \mathbf{r}_{RS}(F)\right] \tag{5.9}$$

It is also possible to write an equation analogous to Eq. 5.8 for the barrier itself (see refs.[83, 108, 109]):

$$\Delta E(F) = \Delta E(0) - \int_0^F dF'[\mathbf{r}_{TS}(F') - \mathbf{r}_{RS}(F')]\mathbf{l} \tag{5.10}$$

In practice, we do not need to integrate Eq. 5.10 since we can estimate the barrier directly from Eq. 5.9.

Eqs. 5.5 and 5.7 assume that the PES is locally quadratic. This assumption breaks down if the Hessian matrix becomes singular and thus non-invertible. In 1D, this happens at the inflection points of $V(x)$, where $V''(x)=0$. In an M-dimensional molecular space, such offending points occupy (M-1)-dimensional surfaces and so instances where a curve $\mathbf{r}(F)$ hits such a surface are common. Such events are not merely numerical nuisance: they signify qualitative changes in the reaction mechanism, where, for example, a particular TS saddle ceases to exist. The calculation, therefore, must be terminated and alternative reaction mechanisms have to be considered. The points where Hessian singularities are encountered, or the "catastrophes" in the language of catastrophe theory[151, 152], are the force-induced instabilities previously discussed in the context of mechanochemistry[85] Similar phenomena are well known in the theory of phase transitions. In the next Section we will provide both a classification of possible catastrophes relevant for the calculation of force-dependent reaction rates and illustrate them with chemical examples. Before doing so, we close this Section with two comments. First, unless internal coordinates are used to specify the molecular configuration $\mathbf{r}$, $\mathbf{h}(\mathbf{r})$ is already singular, with at least 3 eigenvalues corresponding to rigid-body translations (see Section 5 for further discussion of the precise number of zero modes and its dependence on the pulling setup). This complication can be avoided by replacing the inverses appearing in Eqs. 5.7 – 5.8 with the generalized inverse[83], where

the zero eigenmodes are explicitly eliminated from the spectral expansion of $\mathbf{h}^{-1}(\mathbf{r})$. The use of the generalized inverse is justified because the requirement of mechanical equilibrium necessitates that any physically acceptable force **f** must be orthogonal to the null-space corresponding to rigid-body motions.

Second, for the specific pulling scenario where a pair of opposing forces, *F* and -*F*, are exerted on two atoms, we note that Eqs. 5.7 - 5.10 can also be rewritten in a one-dimensional-like form. Let $R_{TS(RS)}$ be the distance between the pulling points in the transition or reactant state. The evolution of this distance with the magnitude of the pulling force *F* is then given by

$$dR_{TS(RS)}/dF = \chi_{TS(RS)}(R_{TS(RS)}), \tag{5.11}$$

where the TS(RS) compliance $\chi_{TS(RS)}$ can be computed from the corresponding Hessians as described in refs.[83, 84]. This equation is further supplemented by the equation describing the evolution of the TS or RS energy[83, 84, 108],

$$dE_{TS(RS)}/dF = -R_{TS(RS)}, \tag{5.12}$$

resulting in

$$\frac{d^2R_{TS(RS)}}{dF^2} + \chi_{TS(RS)}(R_{TS(RS)}) = 0 \tag{5.13}$$

These equations yield the EBT approximation if the compliances $\chi_{TS(RS)}$ are taken to be constant. On the other hand, force-induced instabilities, or catastrophes, occur when the distance between the pulling points attains a value such that $\chi_{TS(RS)}(R_{TS(RS)}) = \infty$.

COMPUTATIONAL DETAILS AND SYSTEMS OF INTEREST

To test the approach of the previous Section, we have applied it to the ring-opening reactions of *trans* 1,2-dimethylbenzocyclobutene (DBC) and 1,3-cyclohexadiene (CHD)[83, 85, 86]. This choice was largely guided by the availability of an earlier study by Bailey and Mosey[85], to which our results can be compared.

All calculations were performed with an in-house python script embedded in the NWCHEM package[115]. The calculations reported in the main text employ density functional theory with the B3LYP exchange-correlation functional[118]. The analytical hessian implementation available for the B3LYP exchange-correlation functional was found to significantly reduce numerical errors and computational expense required for the eigenvalue analysis, which is reported in the Results section in order to elucidate the precise nature of force-induced instabilities. However in order to compare our results to those of Bailey and Mosey[85], we have also performed calculations using CASSCF(6,6)/6-31G** (same level of theory as in ref. [85]) and found that our predictions for the force dependence of activation barriers are virtually indistinguishable from those of ref.[85]. See Appendix for further details.

Electronic structure calculations were performed at the B3LYP/6-31G* and B3LYP/6-31G** level of theory for DBC and CHD, respectively. Eq. 5.8 was integrated with Heun's predictor-corrector algorithm[153] using, respectively, a force step of 4.1 pN and 0.8 pN for DBC and CHD. The activation barrier was then computed, as a function of the force, using Eq. 5.9.

RESULTS: ANALYSIS OF REACTANT- AND TRANSITION-STATE INSTABILITIES OCCURRING IN WELL STUDIED MECHANOPHORES

When applied to the evolution of a molecular PES, catastrophe theory makes a general prediction[151]. If only a single parameter is varied (force) and in the absence of any special symmetries of the underlying PES, the only possible force-induced instability is of the fold-catastrophe type, where two critical points disappear via coalescence with one another. This prediction is explicitly proven, for a two-dimensional PES, in Appendix A. This type of instability has been studied quite extensively for one-dimensional potentials[40, 105-107, 154], where the RS minimum and the TS maximum merge with one another resulting is the disappearance of the activation barrier.

When, however, the force-modified PES has certain symmetry, another type of instability is possible, where two equivalent critical points merge with a third one, resulting in a single critical point. Known as the cusp catastrophe, this type of instability is also well known in the context of second-order phase transitions.

Because the minima and rank 1 saddles have special physical significance as reactant and transition states, the above two mathematical possibilities result in several physically distinct scenarios shown in Figure 5.1. In what follows, these scenarios are described and illustrated with specific chemical examples.

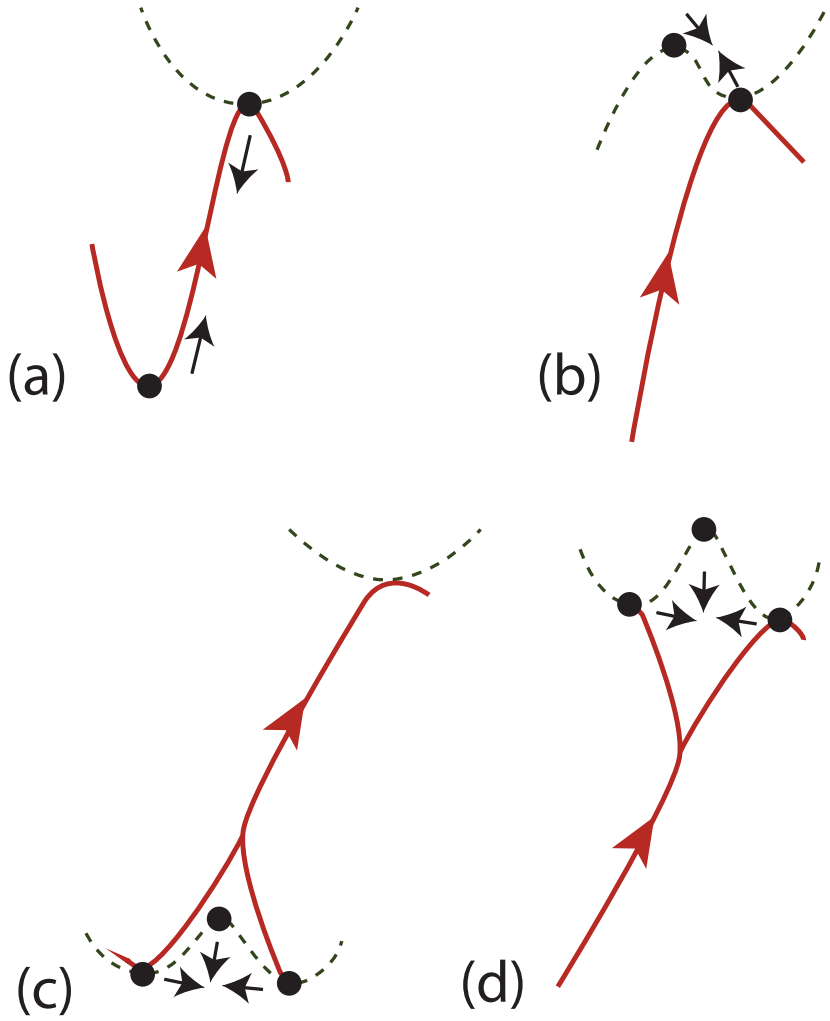

Figure 5.1: Cartoon representation of various instabilities occurring when the molecular PES is deformed by the application of a force. The red line shows the change in potential energy as the system evolves along its (local) reaction coordinate while the dashed line shows the energy variation along a transverse degree of freedom. Black arrows show relative movement of the PES critical points as the force approaches a critical value corresponding to the instability.

Case 1: A TS saddle coalesces with a RS minimum. The barrier between the two vanishes.

The scenario where the barrier separating the RS and the TS disappears when the RS minimum and the TS saddle merge (Fig. 5.1a) is illustrated by the conrotatory ring-opening of DBC (Fig. 5.2), with a pair of opposing forces applied to the substituent carbon atoms (C1 and C2) as in earlier studies[83, 86]. As the magnitude of the pulling force is increased, the barrier between the RS and the TS disappears (Fig. 5.3a), and, at the same time, the negative eigenvalue of the TS Hessian matrix approaches zero from below while one of the positive eigenvalues of the RS Hessian approaches zero from above (Fig. 5.3b). Use of EBT in this case does not lead to qualitative errors because the EBT calculation should, of course, be stopped whenever the barrier it predicts vanishes. Nevertheless, EBT significantly underestimates the precise value of the force at which this happens (see the dashed line in Fig. 5.3a).

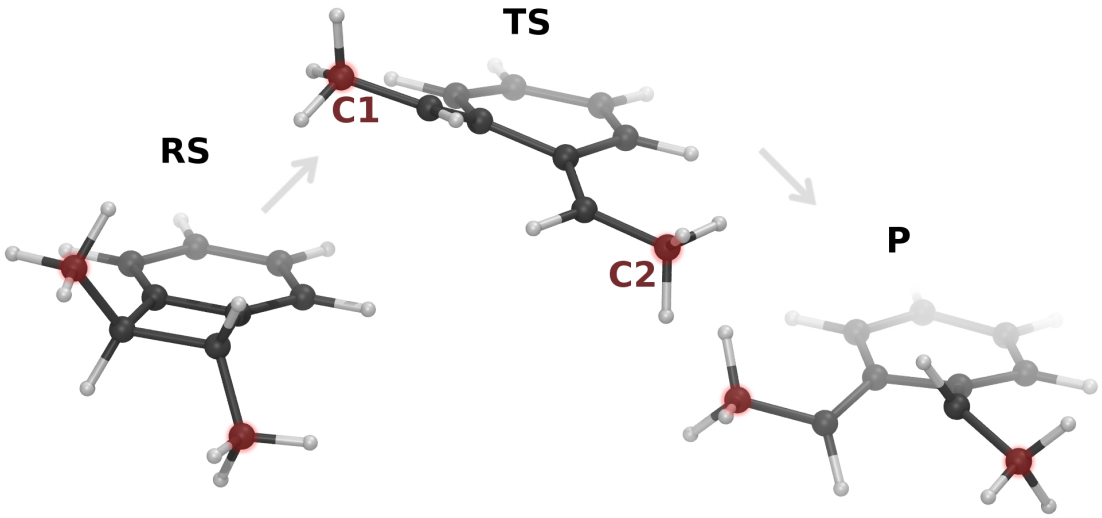

Figure 5.2: Reaction pathway for ring-opening of DBC. The pulling points are shown in red.

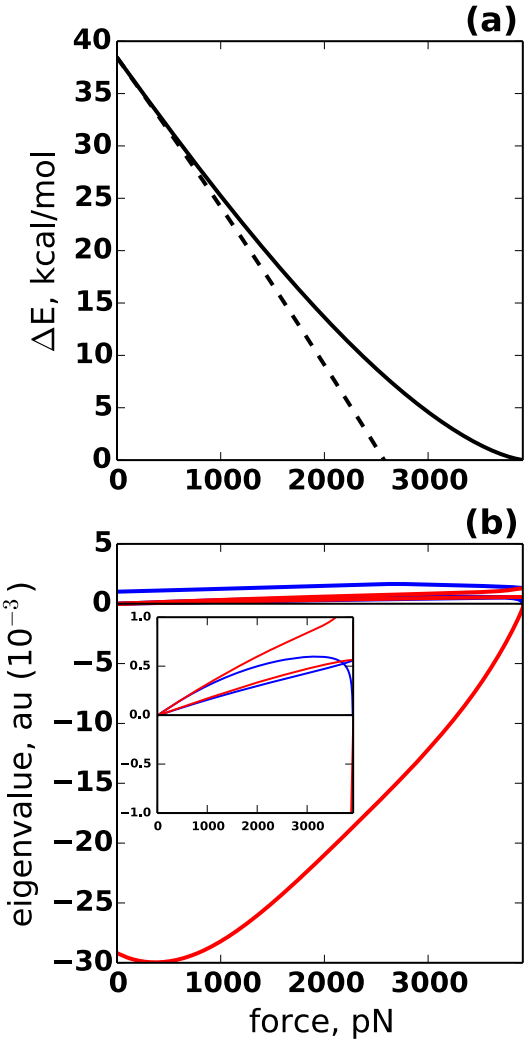

Figure 5.3: Fold catastrophe on the DBC potential energy surface (Case 1): (a) The activation barrier for ring-opening reaction of DBC as a function of the pulling force applied between the C1 and C2 atoms, as shown in Fig. 2. The EBT estimate is shown as a dashed line. (b) Force dependence of the lowest three non-zero eigenvalues of the TS and RS Hessians. Red: TS modes. Blue: RS modes. Horizontal black line denotes a zero- frequency baseline. Inset shows a magnified image of the low eigenvalue range where the negative TS mode and the positive RS mode simultaneously approach the zero-baseline at a critical force.

Case 2: A TS saddle coalesces with a rank 2 saddle.

The case where the TS saddle coalesces with a rank 2 saddle (Fig. 5.1b) is exemplified by the conrotatory ring-opening of CHD (RS1 $\rightarrow$ TS1 $\rightarrow$ P1 in Fig. 5.4) while a pair of opposing forces are applied to the H1 and H2 atoms, as shown in Fig. 5.4. Note that the same pulling points are labeled differently (H5-H6) in ref.[85]. The pulling force lowers the reaction barrier until a critical force of ~ 1585 pN is reached, beyond which the conrotatory transition state (labeled TS1 in Fig. 5.4) disappears. In contrast to Case 1, however, the reactant state RS1 undergoes no instability and so the energy difference between TS1 and RS1 does not vanish (Fig. 5.5a). Consequently, EBT calculations provide no immediate means for detecting this type of instability and erroneously predict the existence of the conrotatory pathway beyond the critical force. The coalescence of TS1 with a rank 2 saddle is evident from the analysis of the transition state Hessian spectrum (Figs. 5.5b), with its *positive* eigenvalue approaching zero from above. At the same time, the nature of the minimum, RS1, does not change and the corresponding eigenvalues remain finite (except for those that are always identically equal to zero due to the translational and rotational invariance). We note that this scenario was previously found in ref.[85], where the disappearance of the conrotatory transition state TS1 was deduced from the failure of the optimization routine to converge to a saddle beyond a critical force. Our method both allows one to precisely locate this instability and clarifies the changes in the PES topology that lead to this type of scenario.

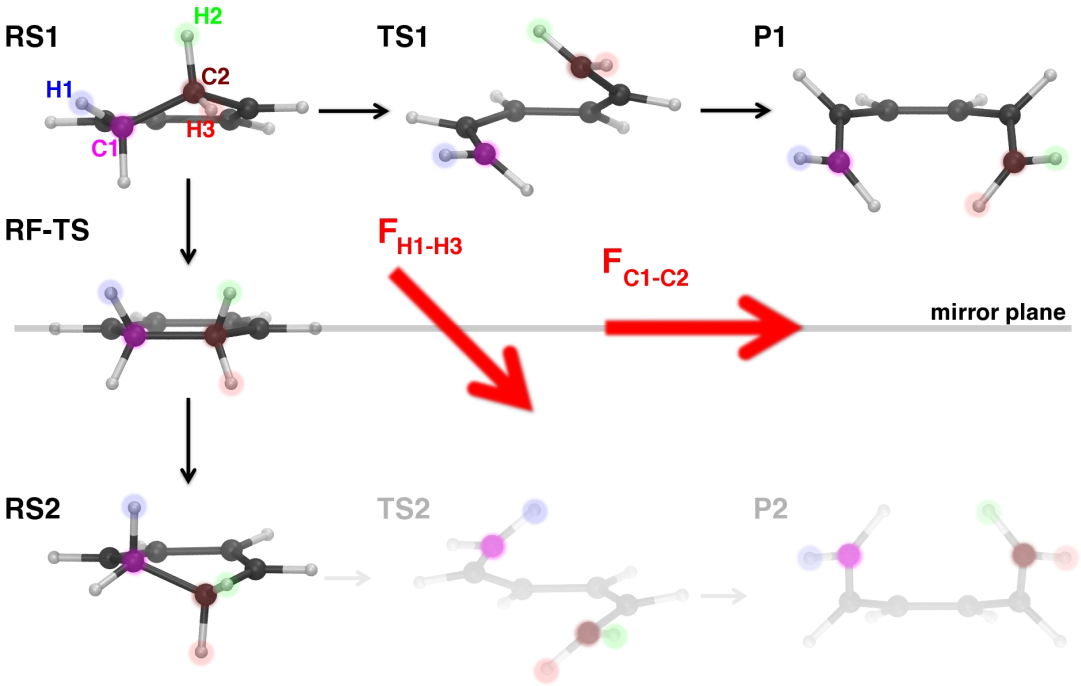

Figure 5.4: Possible reactant and transition-state structures of CHD encountered in the conrotatory ring-opening (RS1 → TS1 → P1) and ring-flip (RS1 → RF-TS → RS2) reactions. Red arrows schematically show the force vectors orientation with respect to mirror-plane of RF-TS structure. The symmetry-related structures shown in light gray are not explicitly considered in our calculations.

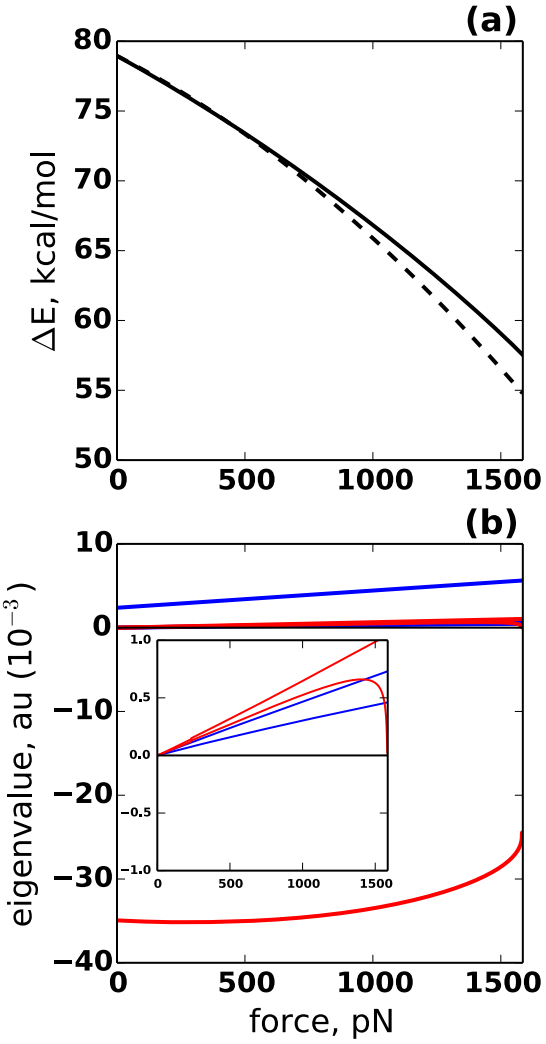

Figure 5.5: Fold catastrophe on the CHD potential energy surface (Case 2): (a) Ring-opening activation barrier for CHD plotted as a function of an external force applied between the H1 and H2 atoms, as shown in Fig. 5.4. The EBT estimate is shown as a dashed line. (b) Force dependence of the lowest three non-zero eigenvalues for TS1 and RS1. Red: TS1 modes. Blue: RS1 modes. Horizontal black line denotes a zero- frequency baseline. Inset shows a magnified image of the low eigenvalue range where one of the positive TS1 modes is approaching the zero-baseline at a critical force.

Case 3: A RS minimum is destabilized by the force.

A RS can be destabilized by a force when it coalesces with a rank 1 saddle. Although, fundamentally, this mechanism is identical to that of Case 1, its practical implications are different in that the saddle involved in the RS destabilization is different from the TS of the reaction under study. The same reaction as in Case 2, the conrotatory ring-opening of CHD, provides an example of this scenario when a pair of opposing forces are applied to H1 and H3 (Fig. 5.4). At zero force, the reactant RS1 is separated from the (symmetrically equivalent) RS2 and interconversion between RS1 and RS2 involves a ring-flip reaction through a saddle that we denote RF-TS.

At nonzero force, this symmetry is broken and, as the force is increased, RS1 merges with RF-TS at a force of about ~ 675 pN (Fig. 5.6a). At forces above this critical value, only RS2 exists. As in Case 1, one positive eigenvalue of the RS1 Hessian matrix and the negative eigenvalue of the RF-TS Hessian matrix approach zero, respectively, from above and below (Fig. 5.6b). An upshot of this instability is that the reaction pathway RS1 $\rightarrow$ TS1 $\rightarrow$ P1 ceases to exist above 675 pN, in agreement with the findings of ref.[85].

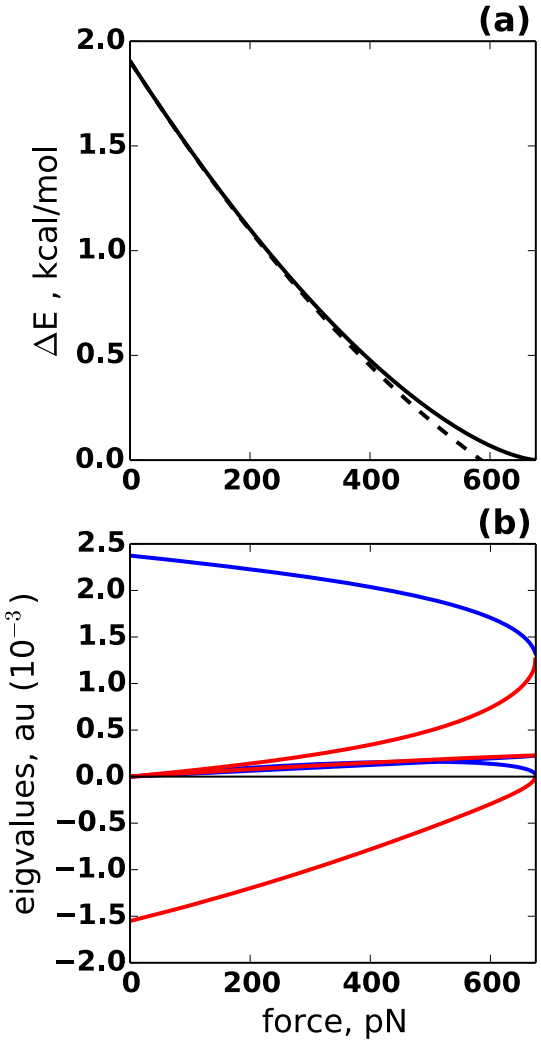

Figure 5.6**:** Fold catastrophe on the CHD potential energy surface (Case 3): (a) The activation barrier for the ring-flip reaction (i.e. the one from RS1 to RS2 in Fig. 5.4) plotted as a function of a force applied between the H1 and H3, as shown in Fig. 4. The EBT estimate is shown as a dashed line. (b) Force dependence of the lowest three non-zero eigenvalues for the RF-TS and RS1 Hessians. Red: RF-TS modes. Blue: RS1 modes.

Case 4: Cusp catastrophe

In Case 3, application of a force between the H1 and H3 atoms breaks the symmetry of the two states, RS1 and RS2, which are symmetrically equivalent at zero force. As a result, when the force is increased RS1 merges with RF-TS, while RS2 survives. If, in contrast, the C1 and C2 atoms in CHD are used as the pulling points (Fig. 5.4) the symmetry between RS1 and its mirror image RS2 is preserved even at a finite force. When the force is increased, the barrier to the ring-flip reaction disappears through a cusp catastrophe, where the three critical points, RS1, RS2, and RF-TS merge simultaneously into a single minimum (Figs. 5.7a,b). Since RS1 and RS2 are the mirror images of one another, the eigenvalue spectra of the RS1 and RS2 hessians are identical, with one positive eigenvalue approaching zero from above at the instability point (Fig. 5.7b), while the negative eigenvalue of the RF-TS hessian approaches zero from below.

Of course, such a choice of pulling points is unreasonable if acceleration of the ring-opening of CHD is desired, as the force is not aligned with the desired reaction pathway. Moreover, the instability we observe here occurs at a force so high that other mechanically induced bond rupture processes will likely take place. Nevertheless, the point of the exercise reported here is to point the possibility of a cusp-catastrophe instabilities in systems of high symmetry, regardless of their relevance for the particular reaction studied here. Figures 5.1c,d further elaborates on various scenarios where cusp catastrophes may be encountered. Specifically, the spatial location of the cusp catastrophe corresponds to a point where the reaction pathway bifurcates via the splitting of either a saddle or a reactant minimum into two.

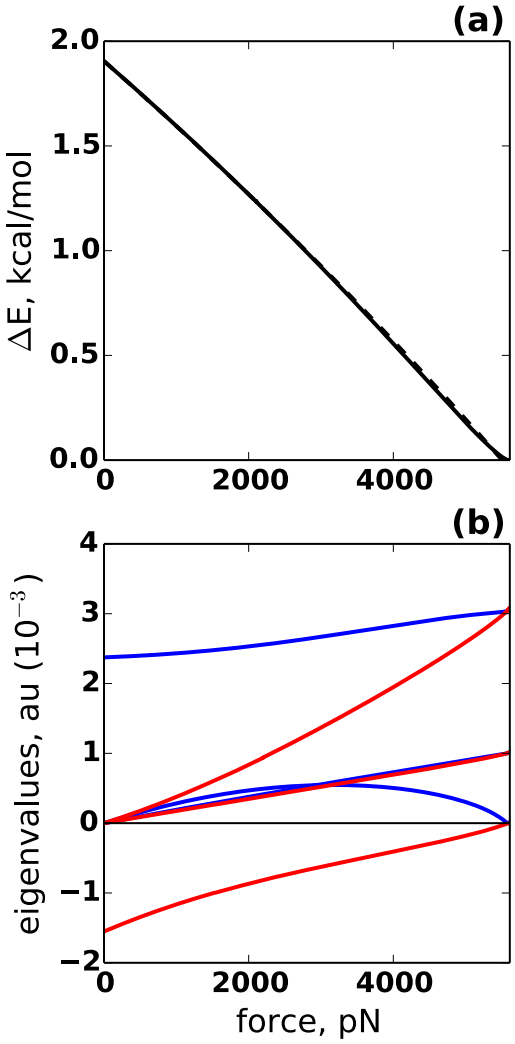

Figure 5.7: Cusp catastrophe on the CHD potential energy surface (Case 4): (a) The activation barrier for the ring-flip reaction (i.e. the one from RS1 to RS2 in Fig. 5.4) as a function of a force applied between the C1 and C2 atoms. The EBT estimate is shown as a dashed line. (b) Force dependence of the lowest three non-zero eigenvalues of the RF-TS and RS1 (or, equivalently, RS2) Hessians. Red: RF-TS modes. Blue: RS1 (RS2) modes. Horizontal black line denotes a zero- frequency baseline.

CONCLUDING REMARKS

Mechanochemistry holds promise to guide chemical transformation along otherwise inaccessible pathways and/or to mechanically stabilize transient molecular structures. There are, however, fundamental limitations on the type of PES transformations that can be achieved by subjecting molecules to constant forces. In particular, since the force-modified potential of Eq. 5.2 is linear in the force **f**, the molecule's Hessian, which determines the stability of any molecular configuration **r** in the presence of a force, depends on the configuration only and not (explicitly) on the force.

To illustrate this point, consider a two-dimensional PES $U(x,y)$ (Fig. 5.8) and its force-modified counterpart $U_{\mathbf{f}}(x,y)=U(x,y)-f_x x-f_y y$. Application of an appropriate force $(f_x,f_y)=\nabla U(x_0,y_0)$ ensures that the configuration (x_0,y_0) is a critical point of $U_{\mathbf{f}}(x,y)$, but the type of this critical point is entirely determined by the properties of the zero-force PES, since both $U(x,y)$ and $U_{\mathbf{f}}(x,y)$ have identical Hessians. As a result, the configurational space (*x*,*y*) is divided into three distinct regions (Fig. 5.8): Elliptic points (colored red in Fig. 5.8), where both eigenvalues of the Hessian $\mathbf{h}(x,y)$ are positive, become stable minima when an appropriate force is applied. Hyperbolic points, where $\mathbf{h}(x,y)$ has a positive and a negative eigenvalue (green), become rank-1 saddles when an appropriate force is applied. A hyperbolic point cannot correspond to a stable molecular structure under any constant force. Finally, configurations corresponding to the elliptic points (blue) where both eigenvalues of $\mathbf{h}(x,y)$ are negative can only be maxima on the

force-modified PES. The mechanical instabilities studied in this paper occur at the parabolic points belonging to the lines that separate the regions of elliptic and hyperbolic points. Therefore, the configurations corresponding to these instabilities are implicitly determined by the equation

$$\det \mathbf{h}(x, y) = 0$$

This argument, when extended to spaces of higher dimensionality, leads to the conclusion that molecular configurations $\mathbf{r}$ corresponding to mechanical instabilities must lie on the hypersurfaces (lines in 2D) that satisfy the equation

$$\det' \mathbf{h}(\mathbf{r}) = 0 \,, \tag{5.14}$$

where the prime indicates that the zero eigenvalues corresponding to the translations and, where appropriate, rotations (see below) are omitted from the determinant.

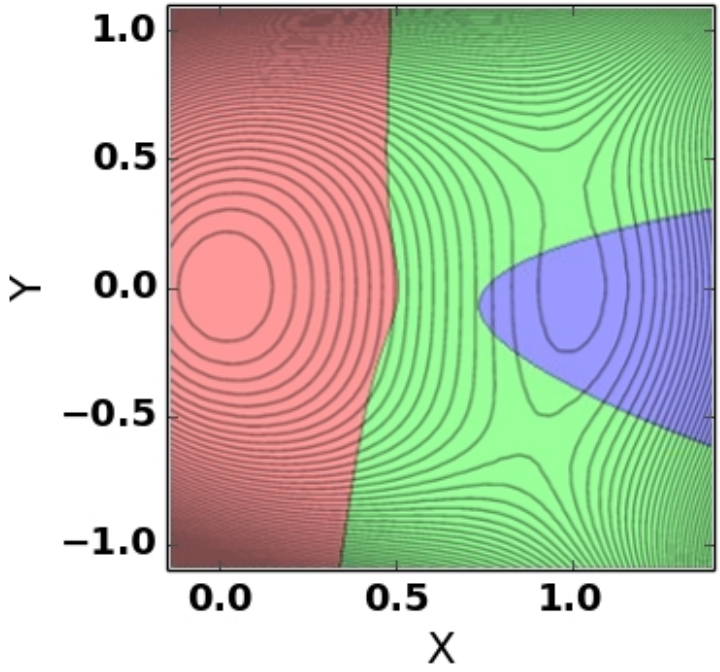

Figure 5.8: Any configuration (x,y) can be made a critical point on a force-modified PES by applying an appropriate force, but its properties (i.e. whether the critical point is a minimum, saddle, or a maximum) are entirely determined by the zero-force PES $U(x,y)$, whose contour plot is shown here. In 2D, the (x,y) plane is then divided into the regions of elliptic points (red, blue) corresponding, respectively, to the minima and the maxima of the force-modified PES, and hyperbolic points (green), which are saddles. The parabolic points belonging to the lines that separate these regions are where the force-induced instabilities take place. The specific PES used to make this plot is given by $U(x,y) = x^2/2 - x^3/3 + (1/2)\left[y^4/4 + y^2(0.75 - x)/2\right] + 0.2xy^3/3$.

Determination of the number of zero modes that are to be omitted from Eq. (5.14) is subtle. Recall that the $3N$ components of the force vector **f** are the x, y, and z components of the forces acting on each atom. If **f** is subject to the physically sensible requirement that the sum of all the forces acting on the molecule's atoms is zero, then the resulting force-modified PES is invariant with respect to arbitrary translations but –

generally – not rotations. Thus, in contrast to the equilibrium zero-force RS or TS configuration, whose Hessian has 6 zero eigenvalues (5 for linear molecules), for "most" configurations $\mathbf{h}(\mathbf{r})$ has only three zero eigenvalues corresponding to translations. However, in the more specific case where opposing forces act on a pair of atoms, the force-modified PES retains a symmetry with respect to rotations around the axis connecting the two atoms and so the Hessian has 4 zero eigenvalues. Note that the condition $\mathbf{f}=0$ may itself be viewed as an instability point, since the rotational symmetry of the zero-force PES is (fully or partially) destroyed by application of an arbitrarily small force and, as a result, one or more Hessian eigenvalues vanish when the force approaches zero. This behavior is, indeed, observed in Figs. 5.3, 5.5 - 5.7.

Since, in addition to offering a general framework for understanding mechanical instabilities, this paper purports to provide a numerical approach to computing force-dependent activation barriers, comments concerning the numerical efficiency of the method are in order. The anecdotal experience provided by the calculations we have performed so far is that, away from the instabilities, the force dependence of the activation barrier, $\Delta E(F)$, converges quickly to the exact curve as the finite-difference force step is decreased. This is not surprising since the EBT result may be viewed as a single-step finite-difference approximation to Eqs. 5.8 - 5.9, where the RS and TS hessians are taken to be constant matrices evaluated at zero force. Since in most cases EBT is already a good approximation, further reduction of the force step is likely to lead to quick improvement. However, if the precise identification of the instability points and/or hessian eigenvalue analysis in the vicinity of those points is desired, the numerical

demands are found to increase rapidly. The reason is, again, not surprising since the inverse $\mathbf{h}^{-1}$ needed in Eqs. 5.7 – 5.8 diverges as $|F - F_c|^{-1/2}$ in the vicinity of the force $F \approx F_c$ where the instability takes place (see Appendix). Adaptive finite-difference schemes with a force step that decreases in the vicinity of the instability point may be useful in this case. In addition, accurate solution of Eqs. 5.7 – 5.8 in the vicinity of F_c places an increased demand on the accuracy of the hessian matrix **h** itself. This should be kept in mind in situations where the matrix **h** cannot be evaluated analytically and finite-difference approximations are used instead.

APPENDIX

Fold catastrophe on a 2D PES

To examine the behavior of a PES in the vicinity of a catastrophe, consider the force-modified PES of the form

$$V_F(x,y) = V(x,y) - F(l_x x + l_y y),$$

where the vector $\mathbf{l} = (l_x, l_y)$ specifies the direction of the force, whose magnitude is given by F. Suppose the Hessian,

$$\mathbf{h} = \begin{bmatrix} V_{xx} & V_{xy} \\ V_{yx} & V_{yy} \end{bmatrix}$$

becomes singular at some critical value of the force, $F = F_c$. We then consider the variation of the PES in vicinity $F = F_c$, viewing

$$\varphi = F - F_c$$

as a small parameter. Let us further assume that, at $\varphi = 0$, the critical point (minimum, saddle, or a maximum) of the potential $V_{F_c}(x,y)$ is located at $x = y = 0$. Since one of the Hessian eigenvalues must vanish at this point, the Taylor expansion of the PES near this point, to third order, can be written in the form

$$V_{F_c}(x,y) = ky^2/2 + \sum_{n=0}^{3} C_{n,3-n} x^n y^{3-n} \qquad \text{(A5.1)}$$

Here the coordinate *y* is chosen to coincide with the eigenvector of **h** that has a nonzero eigenvalue *k*. Since the other eigenvalue must be zero, the term quadratic in *x* is absent in this expansion. At $F \neq F_c$, we can write

$$V_F(x,y) = ky^2/2 + \sum_{n=0}^{3} C_{n,3-n} x^n y^{3-n} - (F - F_c)(l_x x + l_y y) = ky^2/2 + \sum_{n=0}^{3} C_{n,3-n} x^n y^{3-n} - \varphi(x+y), \quad \text{(A5.2)}$$

where we can always chose $l_x = l_y = 1$ by rescaling the coordinates. Our goal is to find the fate of the critical point when the force is changed from F_c to $F = F_c + \varphi$, where φ is small. By setting the first derivatives of the potential to zero, we obtain the equations satisfied by the critical point:

$$-\varphi + \sum_{n=1}^{3} C_{n,3-n} n x^{n-1} y^{3-n} = 0 \qquad \text{(A5.3)}$$

$$ky - \varphi + \sum_{n=1}^{3} C_{3-n,n} n y^{n-1} x^{3-n} = 0 \qquad \text{(A5.4)}$$

We will allow φ to be of either sign and look for the solution in the form of a power law:

$$x = \alpha |\varphi|^a, y = \beta |\varphi|^b \qquad \text{(A5.5)}$$

It can be shown that, if $a>b$, equations A5.3 – 5.4 cannot be satisfied. Assuming then $a<b$, we write Eq. A5.3, to lowest order in φ:

$$-\varphi + 3C_{3,0}x^2 = -\varphi + 3C_{3,0}\alpha^2|\varphi|^{2\alpha} = 0 \qquad \text{(A5.6)},$$

which gives $a = 1/2$ and

$$\alpha^2 = \frac{sign(\varphi)}{3C_{3,0}} \qquad \text{(A5.7)}$$

Importantly, a pair of real-valued solutions to Eq. A5.7, $\pm|\alpha|$, exists only for a negative φ if $C_{3,0} < 0$ and vice versa. Therefore, the corresponding pair of critical points of the force-modified PES disappears as the force approaches F_c from below or above, depending on the sign of the anharmonic coefficient $C_{3,0}$.

Substituting Eq. A5.7 into A5.4 one obtains, to lowest order in φ,

$$k\beta|\varphi|^b - \varphi + C_{2,1}\alpha^2|\varphi|^{2a} = 0,$$

resulting in b=1.

Do the nontrivial critical points obtained at nonzero φ correspond to minima, saddles, or maxima? To answer this question, we need to examine the sign of the determinant of the hessian calculated at this point. Evaluating the second derivatives of the potential to lowest order in φ, we obtain

$$\mathbf{h} \approx \begin{bmatrix} \pm 6C_{3,0}|\alpha||\varphi|^{1/2} & \pm 2C_{2,1}|\alpha||\varphi|^{1/2} \\ \pm 2C_{2,1}|\alpha||\varphi|^{1/2} & k \end{bmatrix}$$

and

$$\det \mathbf{h} = \pm 6kC_{3,0}|\alpha||\varphi|^{1/2} \qquad \text{(A5.8)}$$

Since, according to Eq. A5.8, det **h** has opposite signs for the two critical points, one of them must be a saddle and the other a minimum or a maximum.

Two important observations that are used in the main body of this article are as follows:

1. A pair of critical points that differ in their saddle rank by 1, e.g. a maximum and a saddle or a minimum or a saddle, coalesce and vanish when the force approaches a critical value from above or from below (depending on the local PES details near the critical point).
2. This is accompanied by the vanishing of one of the eigenvalues of the Hessian **h**. From Eq. A5.8 we also see that the vanishing eigenvalue approaches zero as $|\varphi|^{1/2} = |F - F_c|^{1/2}$.

Comparison to previous work: An illustrative example

To provide a comparison with previously published data, here we focus on the example of the previously studied ring-opening of CHD[85] using the H4 - H5 and H6 - H7 atom pairs as the pulling points (Fig. 5.9). Note that the same pulling points were referred to as H2-H3 and H1-H4 in ref. [85]. In contrast to the processes discussed in the main text, regardless of its magnitude, a force applied between these pulling points does not destabilize the reactant minimum. As discussed in ref. [85], the ring-opening reaction may proceed through the conrotatory and disrotatory transition states (RS → C-TS → P and RS → D-TS → P, respectively, in Fig. 5.9). The electronic structure calculations were

performed at the same level of theory (CASSCF(6,6)/6-31G**) as in ref. [85] and a force increment of ~ 4.1 pN was used to integrate Eq. 5.8. The force dependences of the reaction barrier obtained for each pathway are visually indistinguishable from the barrier vs. force plots reported by Bailey and Mosey[85] (Fig. 5.10). Consistent with their observations, a pulling force applied between the H4 - H5 atoms suppresses the reaction along the disrotatory pathway (blue line in Fig. 5.10a) and promotes the reaction along the conrotatory pathway (red line in Fig. 5.10a). The case of the H6-H7 pulling points (Fig. 5.10b) is an example, where EBT predictions significantly diverge from the exact result at high forces. Again, our approach in this case yields results that are virtually indistinguishable from the calculations reported in ref.[85].

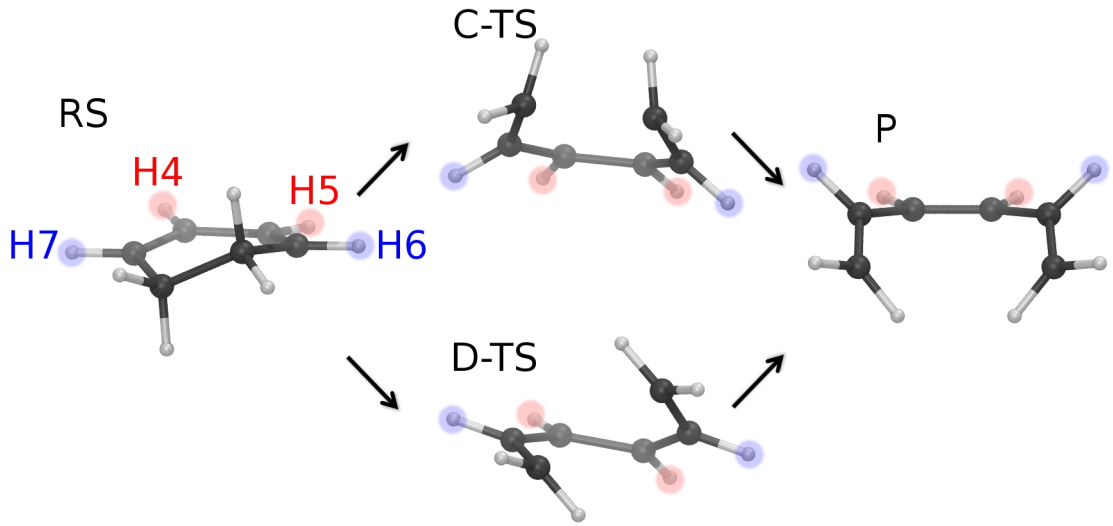

Figure 5.9: Ring-opening of CHD through the conrotatory (C-TS) and disrotatory (D-TS) transition states. The pulling points used in the calculation are shown in color.

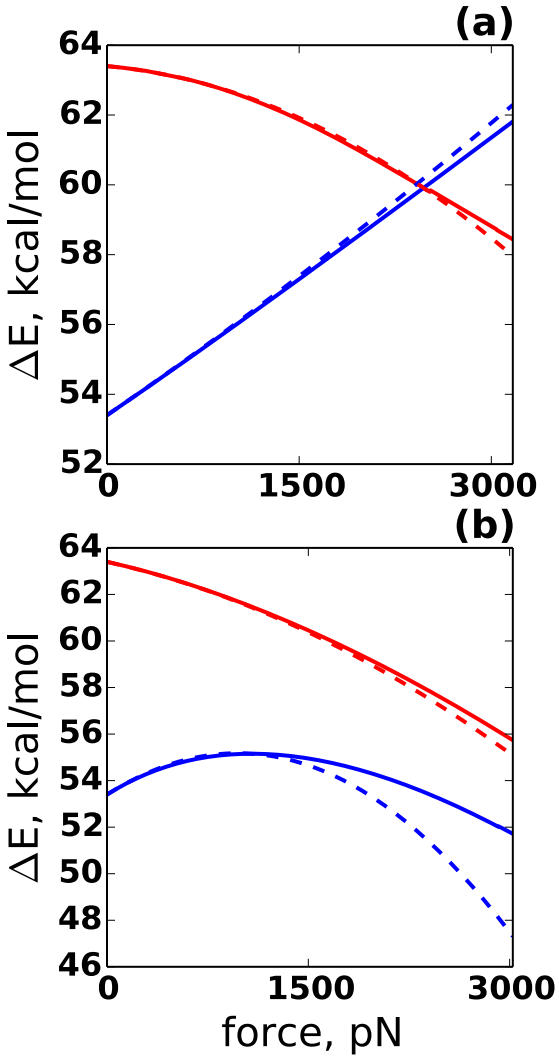

Figure 5.10: Activation energy for ring-opening of CHD plotted as a function of a pulling force applied between (a) H4-H5 and (b) H6-H7 atom pairs for conrotatory (red) and disrotatory (blue) reaction pathways. Solid line: Numerical results using Eqs. 5.8 and 5.9. Dashed line: EBT.

References

1. D. Chandler, *Introduction to Modern Statistical Mechanics*. (Oxford University Press, Oxford, 1987).
2. M. E. Tuckerman, *Statistical Mechanics: Theory and Molecular Simulation*. (Oxford University Press, Oxford, 2010).
3. M. M. Caruso, D. A. Davis, Q. Shen, S. A. Odom, N. R. Sottos, S. R. White and J. S. Moore, Chemical Reviews **109** (11), 5755-5798 (2009).
4. M. K. Beyer, Journal of Chemical Physics **112** (17), 7307-7312 (2000).
5. M. K. Beyer and H. Clausen-Schaumann, Chemical Reviews **105** (8), 2921-2948 (2005).
6. J. M. Lenhardt, M. T. Ong, R. Choe, C. R. Evenhuis, T. J. Martinez and S. L. Craig, Science **329** (5995), 1057-1060 (2010).
7. J. N. Brantley, S. S. M. Konda, D. E. Makarov and C. W. Bielawski, J Am Chem Soc **134** (24), 9882-9885 (2012).
8. J. N. Brantley, K. M. Wiggins and C. W. Bielawski, Science **333**, 1606 (2011).
9. K. M. Wiggins and C. W. Bielawski, Angew. Chem., Int. Ed. **51**, 1640-1643, S1640/1641-S1640/1611 (2012).
10. K. M. Wiggins, J. A. Syrett, D. M. Haddleton and C. W. Bielawski, J Am Chem Soc **133** (18), 7180-7189 (2011).
11. C. R. Hickenboth, J. S. Moore, S. R. White, N. R. Sottos, J. Baudry and S. R. Wilson, Nature **446** (7134), 423-427 (2007).
12. D. A. Davis, A. Hamilton, J. Yang, L. D. Cremar, G. D. Van, S. L. Potisek, M. T. Ong, P. V. Braun, T. J. Martinez, S. R. White, J. S. Moore and N. R. Sottos, Nature **459**, 68-72 (2009).
13. R. Boulatov and T. J. Kucharski, Journal of Materials Chemistry **21** (23), 8237-8255 (2011).
14. Z. Huang and R. Boulatov, Chemical Society reviews **40** (5), 2359-2384 (2011).
15. A. L. Black, J. M. Lenhardt and S. L. Craig, J. Mater. Chem. **21**, 1655-1663 (2011).
16. J. N. Brantley, K. M. Wiggins and C. W. Bielawski, Polym. Int. (2012).
17. K. M. Wiggins, J. N. Brantley and C. W. Bielawski, Chemical Society Reviews **42** (17), 7130-7147 (2013).
18. H. Eyring, J Chem Phys **3**, 107 (1935).

19. H. Eyring, J. Chem. Phys. **4**, 283 (1936).

20. A. Minajeva, M. Kulke, J. M. Fernandez and W. A. Linke, Biophysical Journal **80**, 1442 (2001).

21. N. Becker, E. Oroudjev, S. Mutz, J. P. Cleveland, P. K. Hansma, C. Y. Hayashi, D. E. Makarov and H. G. Hansma, Nature Materials **2**, 278 (2003).

22. G. E. Fantner, E. Oroudjev, G. Schitter, l. S. Golde, P. Thumer, M. M. Finch, P. Turner, T. Gutsmann, D. E. Morse, H. Hansma and P. K. Hansma, Biophysical Journal **90**, 1411-1418 (2006).

23. B. L. Smith, T. E. Schaffer, M. Viani, J. B. Thompson, N. A. Frederick, J. Kindt, A. Belcher, G. D. Stucky, D. E. Morse and P. K. Hansma, Nature **399**, 761 (1999).

24. C. Lee, M. P. Schwartz, S. Prakash, M. Iwakura and A. Matouschek, Mol. Cell **7**, 627-637 (2001).

25. D. E. Makarov, Acc Chem Res **42** (2), 281-289 (2009).

26. A. Matouschek, Current Opinion in Structural Biology **13**, 98-109 (2003).

27. A. Matouschek and C. Bustamante, Nat Struct Biol **10** (9), 674-676 (2003).

28. S. Prakash and A. Matouschek, Trends in Biochemical Sciences **29** (11), 593-600 (2004).

29. K. Shariff, S. Ghosal and A. Matouschek, Biophysical Journal **86**, 3647-3652 (2004).

30. J. Alegre-Cebollada, R. Perez-Jimenez, P. Kosuri and J. M. Fernandez, Journal of Biological Chemistry **285**, 18961-18966 (2010).

31. P. E. Marsalek, H. Lu, H. Li, M. Carrion-Vazquez, A. F. Oberhauser, K. Schulten and J. Fernandez, Nature **402**, 100 (1999).

32. E. Paci and M. Karplus, J. Mol. Biol. **288**, 441-459 (1999).

33. D. K. Klimov and D. Thirumalai, Proc. Natl. Acad. Sci. USA **97** (13), 7254 (2000).

34. D. E. Makarov, P. K. Hansma and H. Metiu, J. Chem. Physics **114**, 9663 (2001).

35. A. F. Oberhauser, P. K. Hansma, M. Carrion-Vazquez and J. M. Fernandez, Proc. Natl. Acad. Sci USA **98** (2), 468-472 (2001).

36. M. Rief, J. M. Fernandez and H. E. Gaub, Phys. Rev. Lett. **81**, 4764 (1998).

37. M. Rief, M. Gautel, F. Oesterhelt, J. M. Fernandez and H. E. Gaub, Science **276**, 1109-1112 (1997).

38. M. Schlierf, H. Li and J. M. Fernandez, Proc. Natl. Acad. Sci USA **101**, 7299 (2004).

39. S. Kirmizialtin, L. Huang and D. E. Makarov, J. Chem. Phys. **122**, 234915 (2005).

40. D. J. Lacks, Biophysical Journal **88**, 3493-3501 (2005).

41. B. Isralewitz, M. Gao and K. Schulten, Current Opinion in Structural Biology **11**, 224-230 (2001).

42. S. Izrailev, S. Stepaniants, M. Balsera, Y. Oono and K. Schulten, Biophysical Journal **72** (4), 1568-1581 (1997).

43. H. Lu, B. Isralewitz, A. Krammer, V. Vogel and K. Schulten, Biophysical Journal **75**, 662 (1998).

44. H. Lu and K. Schulten, Chemical Physics **247**, 141 (1999).

45. C. Bustamante, Y. R. Chemla, N. R. Forde and D. Izhaky, Ann. Rev. Biochem **73**, 705-748 (2004).

46. E. Evans and K. Ritchie, Biophysical Journal **72**, 1541-1555 (1997).

47. E. Evans and K. Ritchie, Biophysical Journal **76**, 2439 (1999).

48. C. Hyeon and D. Thirumalai, Biophysical journal **90** (10), 3410-3427 (2006).

49. C. Hyeon, G. Morrison and D. Thirumalai, Proc. Natl. Acad. Sci. U. S. A. **105** (28), 9604-9609 (2008).

50. C. Hyeon and D. Thirumalai, Proc. Natl. Acad. Sci. U. S. A. **102** (19), 6789-6794 (2005).

51. D. E. Makarov, Biophys J **92** (12), 4135-4136 (2007).

52. D. J. Brockwell, E. Paci, R. C. Zinober, G. S. Beddard, P. D. Olmsted, D. A. Smith, R. N. Perham and S. E. Radford, Nature structural biology **10** (9), 731-737 (2003).

53. P.-C. Li and D. E. Makarov, J. Chem. Phys. **119**, 9260 (2003).

54. V. Barsegov, G. Morrison and D. Thirumalai, Phys Rev Lett **100** (24), 248102 (2008).

55. V. Barsegov and D. Thirumalai, Proc. Natl. Acad. Sci. U. S. A. **102** (6), 1835-1839 (2005).

56. O. K. Dudko, G. Hummer and A. Szabo, Phys Rev Lett **96** (10), 108101 (2006).

57. M. Sotomayor and K. Schulten, Science **316** (5828), 1144-1148 (2007).

58. O. K. Dudko, G. Hummer and A. Szabo, Proc. Natl. Acad. Sci. U. S. A. **105** (41), 15755-15760 (2008).

59. D. J. Brockwell, G. S. Beddard, E. Paci, D. K. West, P. D. Olmsted, D. A. Smith and S. E. Radford, Biophysical Journal **89** (1), 506-519 (2005).

60. R. B. Best, E. Paci, G. Hummer and O. K. Dudko, J. Phys. Chem. B **112**, 5968-5976 (2008).

61. O. V. Prezhdo and Y. V. Pereverzev, Acc Chem Res **42** (6), 693-703 (2009).

62. D. E. Makarov, in *Single-molecule studies of protein structure and function*, edited by A. Oberhauser (Springer, New York, 2012), pp. 235.

63. I. Franco, C. B. George, G. C. Solomon, G. C. Schatz and M. A. Ratner, J Am Chem Soc **133** (7), 2242-2249 (2011).

64. M. McCullagh, I. Franco, M. A. Ratner and G. C. Schatz, J Am Chem Soc **133** (10), 3452-3459 (2011).

65. M. E. Fisher and A. B. Kolomeisky, Proc. Natl. Acad. Sci. U. S. A. **96** (12), 6597-6602 (1999).

66. M. E. Fisher and A. B. Kolomeisky, Proc. Natl. Acad. Sci. U. S. A. **98** (14), 7748-7753 (2001).

67. A. B. Kolomeisky, J Phys Condens Matter **25** (37), 370301 (2013).

68. Q.-Z. Yang, Z. Huang, T. J. Kucharski, D. Khvostichenko, J. Chen and R. Boulatov, Nature Nano **4** (5), 302-306 (2009).

69. Z. Huang and R. Boulatov, Pure App. Chem. **82** (4), 931-951 (2010).

70. Y. Tian and R. Boulatov, Chemphyschem **13** (9), 2277-2281 (2012).

71. O. K. Dudko, J. Mathe, A. Szabo, A. Meller and G. Hummer, Biophys J **92** (12), 4188-4195 (2007).

72. S. Matysiak, A. Montesi, M. Pasquali, A. B. Kolomeisky and C. Clementi, Phys Rev Lett **96** (11), 118103 (2006).

73. L. Huang, S. Kirmizialtin and D. E. Makarov, J. Chem. Phys. **123**, 124903 (2005).

74. D. K. West, D. J. Brockwell and E. Paci, Biophysical Journal **91**, L51-L53 (2006).

75. L. Huang and D. E. Makarov, J Chem Phys **129** (12), 121107 (2008).

76. D. Panja, G. T. Barkema and A. B. Kolomeisky, J Phys Condens Matter **25** (41), 413101 (2013).

77. P. Tian and I. Andricioaei, J Mol Biol **350** (5), 1017-1034 (2005).

78. D. E. Makarov, Protein and Peptide Letters **21** (3), 217-226 (2014).

79. A. T. Hawk, S. S. M. Konda and D. E. Makarov, J. Chem. Phys. **139** (6), 064101 (2012).

80. J. N. Brantley, K. M. Wiggins and C. W. Bielawski, Polym Int **62**, 2 (2013).

81. P. Dopieralski, P. Anjukandi, M. Ruckert, M. Shiga, J. Ribas-Arino and D. Marx, J. Mater. Chem. **21** (23), 8309-8316 (2011).

82. J. Ribas-Arino and D. Marx, Chem. Rev. **112** (10), 5412-5487 (2012).

83. S. S. M. Konda, J. N. Brantley, C. W. Bielawski and D. E. Makarov, J. Chem. Phys. **135**, 164103 (2011).

84. S. S. M. Konda, J. N. Brantley, B. T. Varghese, K. M. Wiggins, C. W. Bielawski and D. E. Makarov, J Am Chem Soc **135** (34), 12722-12729 (2013).

85. A. Bailey and N. J. Mosey, J Chem Phys **136**, 044102 (2012).

86. J. Ribas-Arino, M. Shiga and D. Marx, Angewandte Chemie-International Edition **48** (23), 4190-4193 (2009).

87. G. S. Kochhar, A. Bailey and N. J. Mosey, Angewandte Chemie-International Edition **49** (41), 7452-7455 (2010).

88. R. Boulatov, Pure and Applied Chemistry **83** (1), 25-41 (2011).

89. M. J. Kryger, A. M. Munaretto and J. S. Moore, J. Am. Chem. Soc. **133**, 18992-18998 (2011).

90. K. S. Suslick and G. J. Price, Annual Review of Materials Science **29** (1), 295-326 (1999).

91. K. S. Suslick, Science **247** (4949), 1439-1445 (1990).

92. K. S. Suslick and D. J. Flannigan, Annual Review of Physical Chemistry **59** (1), 659-683 (2008).

93. B. Schuler, Chemphyschem **6** (7), 1206-1220 (2005).

94. B. Schuler, E. A. Lipman and W. A. Eaton, Nature **419** (6908), 743-747 (2002).

95. O. Bilsel and C. R. Matthews, Current Opinion in Structural Biology **16** (1), 86-93 (2006).

96. A. A. Deniz, T. A. Laurence, G. S. Beligere, M. Dahan, A. B. Martin, D. S. Chemla, P. E. Dawson, P. G. Schultz and S. Weiss, Proceedings of the National Academy of Sciences **97** (10), 5179-5184 (2000).

97. X. Michalet, S. Weiss and M. J√§ger, Chemical Reviews **106** (5), 1785-1813 (2006).

98. M. Grandbois, M. Beyer, M. Rief, H. Clausen-Schaumann and H. E. Gaub, Science **283** (5408), 1727-1730 (1999).

99. A. Borgia, P. M. Williams and J. Clarke, Annual Review of Biochemistry **77** (1), 101-125 (2008).

100. S. N. Zhurkov, International Journal of Fracture Mechanics **1** (4), 311-322 (1965).

101. G. I. Bell, Science **200**, 618-627 (1978).

102. S. S. M. Konda, S. M. Avdoshenko and D. E. Makarov, J. Chem. Phys. **140** (10), 104114 (2014).

103. P. Hanggi, P. Talkner and M. Borkovec, Rev. Mod. Phys. **62**, 251 (1990).

104. G. Hummer and A. Szabo, Biophysical Journal **85** (1), 5 (2003).

105. O. K. Dudko, A. E. Filippov, J. Klafter and M. Urbakh, Proc Natl Acad Sci U S A **100** (20), 11378-11381 (2003).

106. C. E. Maloney and D. J. Lacks, Phys Rev E Stat Nonlin Soft Matter Phys **73** (6 Pt 1), 061106 (2006).

107. D. J. Lacks, J. Willis and M.-P. Robinson, The Journal of Physical Chemistry B **114** (33), 10821-10825 (2010).

108. Y. Suzuki and O. K. Dudko, Phys Rev Lett **104** (4), 048101 (2010).

109. Y. Suzuki and O. K. Dudko, Journal of Chemical Physics **134** (6), 065102 (2011).

110. D. K. West, E. Paci and P. D. Olmsted, Phys Rev E Stat Nonlin Soft Matter Phys **74** (6 Pt 1), 061912 (2006).

111. Z. T. Yew, M. Schlierf, M. Rief and E. Paci, Phys Rev E Stat Nonlin Soft Matter Phys **81** (3 Pt 1), 031923 (2010).

112. D. J. Brockwell, E. Paci, R. C. Zinober, G. S. Beddard, P. D. Olmsted, D. A. Smith, R. N. Perham and S. E. Radford, Nature Structural Biology **10** (9), 731 (2003).

113. P.-C. Li and D. E. Makarov, J. Chem. Phys. **121**, 4826 (2004).

114. R. B. Woodward and R. Hoffmann, Angew. Chem. Int. Ed. Engl. **8**, 781-853 (1969).

115. M. Valiev, E. J. Bylaska, N. Govind, K. Kowalski, T. P. Straatsma, H. J. J. Van Dam, D. Wang, J. Nieplocha, E. Apra, T. L. Windus and W. A. de Jong, Comp. Phys. Comm. **181** (9), 1477-1489 (2010).

116. R. G. Parr and W. Yang, *Density-functional theory of atoms and molecules*. (Oxford University Press, New York 1989).

117. M. S. Gordon, J. S. Binkley, J. A. Pople, W. J. Pietro and W. J. Hehre, J Am Chem Soc **104** (10), 2797-2803 (1982).

118. A. D. Becke, Journal of Chemical Physics **98** (2), 1372 (1993).

119. B. M. Bode and M. S. Gordon, Journal of Molecular Graphics and Modelling **16** (3), 133-138 (1998).

120. K. Eom, S. C. Baek, J. H. Ahn and S. Na, Journal of computational chemistry **28** (8), 1400-1410 (2007).

121. R. J. Guyan, AIAA Journal **3** (2), 380 (1965).

122. R. Soheilifard, D. E. Makarov and G. J. Rodin, J. Chem. Phys. **135** (5), 054107 (2011).

123. A. G. Tennyson, K. M. Wiggins and C. W. Bielawski, J. Am. Chem. Soc. **132** (Copyright (C) 2012 American Chemical Society (ACS). All Rights Reserved.), 16631-16636 (2010).

124. K. M. Wiggins, T. W. Hudnall, A. G. Tennyson and C. W. Bielawski, J. Mater. Chem. **21** (Copyright (C) 2012 American Chemical Society (ACS). All Rights Reserved.), 8355-8359 (2011).

125. K. M. Wiggins, J. A. Syrett, D. M. Haddleton and C. W. Bielawski, J. Am. Chem. Soc. **133**, 7180-7189 (2011).

126. B. C. Boren, S. Narayan, L. K. Rasmussen, L. Zhang, H. Zhao, Z. Lin, G. Jia and V. V. Fokin, J Am Chem Soc **130** (28), 8923-8930 (2008).

127. J. M. Lenhardt, A. L. Black and S. L. Craig, J. Am. Chem. Soc. **131** (Copyright (C) 2012 American Chemical Society (ACS). All Rights Reserved.), 10818-10819 (2009).

128. C. R. Hickenboth, J. D. Rule and J. S. Moore, Tetrahedron **64** (36), 8435-8448 (2008).

129. T. Horneff, S. Chuprakov, N. Chernyak, V. Gevorgyan and V. V. Fokin, J Am Chem Soc **130** (45), 14972-14974 (2008).

130. I. Franco, G. C. Schatz and M. A. Ratner, J Chem Phys **131** (12), 124902 (2009).

131. O. K. Dudko, T. G. Graham and R. B. Best, Phys Rev Lett **107** (20), 208301 (2011).

132. Y. Zhao, N. E. Schultz and D. G. Truhlar, Journal of Chemical Theory and Computation **2** (2), 364-382 (2006).

133. C. Gonzalez and H. B. Schlegel, J Chem Phys **90** (4), 2154-2161 (1989).

134. C. Gonzalez and H. B. Schlegel, The Journal of Physical Chemistry **94** (14), 5523-5527 (1990).

135. B. T. Marshall, M. Long, J. W. Piper, T. Yago, R. P. McEver and C. Zhu, Nature **423** (6936), 190-193 (2003).

136. H. Li and Y. Cao, Acc. Chem. Rev. **43** (10), 1331-1341 (2010).

137. S. Akbulatov, Y. Tian, E. Kapustin and R. Boulatov, Angewandte Chemie International Edition **52** (27), 6992-6995 (2013).

138. P. Dopieralski, J. Ribas-Arino, P. Anjukandi, M. Krupicka, J. Kiss and D. Marx, Nat Chem **5** (8), 685-691 (2013).

139. W. R. Browne and B. L. Feringa, Nat. Nano. **1** (1), 1748-3387 (2006).

140. Y. Tian and R. Boulatov, Chemical Communications **49** (39), 4187-4189 (2013).

141. G. A. Voth and R. M. Hochstrasser, The Journal of Physical Chemistry **100** (31), 13034-13049 (1996).

142. D. E. Makarov, in *Single-molecule studies of proteins*, edited by A. F. Oberhauser (Springer, New York, 2013).

143. B. Jagannathan, P. J. Elms, C. Bustamante and S. Marqusee, Proceedings of the National Academy of Sciences (2012).

144. V. Guner, K. S. Khuong, A. G. Leach, P. S. Lee, M. D. Bartberger and K. N. Houk, The Journal of Physical Chemistry A **107** (51), 11445-11459 (2003).

145. E. R. Johnson, P. Mori-Sanchez, A. J. Cohen and W. Yang, J Chem Phys **129** (20), - (2008).

146. Y. Zhao and D. G. Truhlar, Journal of Chemical Theory and Computation **7** (3), 669-676 (2011).

147. M. T. Ong, J. Leiding, H. Tao, A. M. Virshup and T. J. MartiÃÅnez, J Am Chem Soc **131** (18), 6377-6379 (2009).

148. C. R. Hickenboth, J. S. Moore, S. R. White, N. R. Sottos, J. Baudry and S. R. Wilson, Nature **446**, 423-427 (2007).

149. D. E. Makarov, J Chem Phys **135** (19), 194112 (2011).

150. T. G. Graham and R. B. Best, J Phys Chem B **115** (6), 1546-1561 (2011).

151. R. Gilmore, *Catastrophe Theory for Scientists and Engineers* (John Wiley and Sons, New Yourk, Chichester, Brisbane, Toronto, 1981).

152. D. J. Wales, Science **293** (5537), 2067-2070 (2001).

153. S. Chapra and R. Canale, *Numerical Methods for Engineers*. (McGraw-Hill, 2009).

154. C. L. Dias, M. Dube, F. A. Oliveira and M. Grant, Phys Rev E Stat Nonlin Soft Matter Phys **72** (1 Pt 1), 011918 (2005).